STATE OF CALIFORNIA • DEPARTMENT OF TRANSPORTATION

Lock Form

TECHNICAL REPORT DOCUMENTATION PAGE

TR-0003 (REV 04/2024)

1. REPORT NUMBER	2. GOVERNMENT ASSOCIATION NUMBER	3. RECIPIENT'S CATALOG NUMBER
CA25-3677		

4. TITLE AND SUBTITLE	5. REPORT DATE
Caltrans Risk Based Seismic Design (RBSD) - Seismic Demand Parameters for Ordinary Bridge Columns in California	04/20/2025
	6. PERFORMING ORGANIZATION CODE UCI
7. AUTHOR Saurabh Singhal and Farzin Zareian	8. PERFORMING ORGANIZATION REPORT NO.
9. PERFORMING ORGANIZATION NAME AND ADDRESS The Regents of the University of California, Irvine.	10. WORK UNIT NUMBER
	11. CONTRACT OR GRANT NUMBER 65A0774 TO 003
12. SPONSORING AGENCY AND ADDRESS California Department of Transportation, Division of Research, Innovation and System Information, MS-83, P.O. Box 942873, Sacramento, CA 94273-0001.	13. TYPE OF REPORT AND PERIOD COVERED Final Report 03/03/2021 – 02/28/2023
	14. SPONSORING AGENCY CODE

15. SUPPLEMENTARY NOTES

Prepared in cooperation with the State of California Department of Transportation.

16. ABSTRACT

The Caltrans Risk-Based Seismic Design (CT-RBSD) framework is a performance-based bridge design methodology that uses reliability theory to assess the probability of seismic damage in bridge columns. Building on experimental fragility curves and statistical modeling, the approach enables engineers to design with explicit consideration of post-earthquake damage states. This study significantly enhances CT-RBSD by developing high-resolution seismic demand parameter maps across California and expanding the design basis to include a broader range of column geometries. It also integrates advanced ground motion simulations and recommends the adoption of updated seismic hazard models, offering engineers more precise tools for resilient and cost-effective bridge design in earthquake-prone regions.

17. KEY WORDS	18. DISTRIBUTION STATEMENT	
bridge, damage, earthquake, RBSD, probabilistic design, coefficient of variation, adjustment factor, reliability index, return period,		
19. SECURITY CLASSIFICATION *(of this report)*	20. NUMBER OF PAGES	21. COST OF REPORT CHARGED
Unclassified	112	

Caltrans Risk Based Seismic Design (RBSD) - Seismic Demand Parameters for Ordinary Bridge Columns in California

by

Saurabh Singhal
Graduate Student Researcher
University of California, Irvine

Farzin Zareian
Professor (Principal Investigator)
University of California, Irvine

DISCLAIMER STATEMENT

This document is disseminated in the interest of information exchange. The contents of this report reflect the views of the authors who are responsible for the facts and accuracy of the data presented herein. The contents do not necessarily reflect the official views or policies of the State of California or the Federal Highway Administration. This publication does not constitute a standard, specification or regulation. This report does not constitute an endorsement by the Department of any product described herein.

For individuals with sensory disabilities, this document is available in alternate formats. For information, call (916) 654-8899, TTY 711, or write to California Department of Transportation, Division of Research, Innovation and System Information, MS-83, P.O. Box 942873, Sacramento, CA 94273-0001.

ACKNOWLEDGMENTS

The authors would like to thank the Caltrans Technical Advisory Panel, including Amir Malek, Ashraf Ahmed, Mark Mahan, Sam Ataya, Sharon Yen, Tony Yoon, Toorak Zokaie, and Christian Unanwa for their input throughout the study. We would also like to thank Prof. Norman Abrahamson and Prof. Saiid Saiidi for providing their thoughtful comments, which formed the foundation of this study.

This research study was funded by Caltrans through the PEER Bridge program. The opinions, findings, conclusions, and recommendations expressed in this publication are those of the author(s). They do not necessarily reflect the view of Caltrans, Pacific Earthquake Engineering Research (PEER) Center, and the Regents of the University of California.

CONTENTS

LIST OF TABLES

LIST OF FIGURES

1 EXECUTIVE SUMMARY

The Caltrans Risk-Based Seismic Design (CT-RBSD) procedure, formerly known as the Probabilistic Damage Control Application (PDCA), is a bridge design and assessment methodology rooted in Performance-Based Earthquake Engineering (PBEE), developed by the Pacific Earthquake Engineering Research (PEER) Center. Initiated by Caltrans Structure Policy & Innovation (SP&I), CT-RBSD modernizes bridge column assessment and design by incorporating state-of-the-art PBEE principles (Porter, 2003). Originally introduced by Saini and Saiidi (2014), the approach evaluates bridge performance based on the seismic response of seismically critical columns, leveraging reliability theory to express performance in terms of damage state exceedance probabilities. This enables decision-makers to assess key performance metrics, such as repair time and costs.

CT-RBSD allows engineers to explicitly incorporate post-event target damage states in design calculations. The methodology is based on the damage state classifications established by Vosooghi and Saiidi (2010), which define six primary damage states (DS1–DS6) based on plastic region deterioration in columns. Saini and Saiidi further developed fragility curves, using Damage Index (DI) as the engineering demand parameter, derived from shake table tests at the University of Nevada, Reno (UNR) and the PEER Center at the University of California, Berkeley.

The CT-RBSD framework quantifies the probability of column failure (when demand exceeds capacity) using a reliability integral, assuming a lognormal distribution for both demand and capacity DIs. The reliability index (β) is computed and converted into failure probability via normal distribution function charts, with β dependent on the mean and coefficient of variation (COV) of both demand and capacity parameters. While Saini and Saiidi (2014) provided capacity parameters, Yoon et al. (2019) extended the methodology to incorporate seismic demand parameters for ordinary bridges in California, addressing hazard levels, ground motion simulation, scaling, and risk integration.

Building on prior research, this study developed seismic demand statistical parameter maps for ordinary bridges across California, focusing on demand coefficient of variation (COV) and the nonlinear adjustment factor for demand displacement. Analysis was conducted on a 25×25-mile grid statewide, with a finer 5×5-mile grid for the Bay Area and Southern California, providing illustrative applications for bridge column assessment and design. Recommendations were made for post-processing methods of DI demand in future CT-RBSD developments.

To address design uncertainties, a broad matrix of column geometrical properties was analyzed, expanding the CT-RBSD design basis to encompass columns with DI values between 0.3 and 0.4. Ground motion time histories were generated via a stochastic simulation model by Dabaghi et al. (2014), ensuring alignment with target spectral values and validation against recorded ground motions from the NGA West-2 database. Verification confirmed that peak ground velocity (PGV) is a critical secondary intensity measure (IM).

Key findings indicate that demand COV decreases with increasing hazard levels and varies across California, with lower values in high-seismicity regions. Shear wave velocity (V_{S30}) is directly correlated with demand COV, as seismicity decreases with higher V_{S30}. The nonlinear adjustment factor frequently exceeds 1, challenging the Equal Displacement Rule assumption. Additionally, discrepancies between the assumed lognormal distribution of DI and its actual observed distribution necessitate modifications to the CT-RBSD framework to improve exceedance probability estimates. The study also assessed the integration of near-fault and basin amplification factors into CT-RBSD, recommending the adoption of the 2018 USGS National Seismic Hazard Model (NSHM) for more accurate acceleration spectrum estimations, as it accounts for basin amplification effects.

CT-RBSD represents a significant advancement in seismic bridge design, integrating PBEE methodologies and reliability theory to provide engineers and decision-makers with clearer, more actionable performance metrics. Ongoing refinements and further research will continue to enhance its accuracy and applicability in earthquake-prone regions like California.

2 Introduction

2.1 Overview

The past decade has seen a dynamic shift in seismic design from prescriptive design methodologies to performance-based design methodologies, giving designers greater control over structural performance in ways that are clear and understandable for decision-makers. In the case of buildings and related structures, this shift has led to the development of comprehensive assessment tools such as FEMA P-58[1], which provides a complete methodology for seismic performance assessment of buildings. Although efforts are being made to replicate the same in the domain of highway bridges, such as by Mackie and Stojadinović (2007), there is still scope for a robust probabilistic-based methodology for highway bridges across California. To address this, the California Department of Transportation (Caltrans), in partnership with several research entities, introduced the Risk-Based Seismic Design or CT-RBSD, formerly known as Probabilistic Damage Control Assessment or PDCA (Saini and Saiidi, 2014; Yoon et al., 2019, Yoon et al., 2022) design and assessment method, based on the PEER's PBEE methodology. A stochastic process in nature, CT-RBSD streamlines the performance assessment of modern bridges by calculating the probability of bridge responses being more than the capacity in case of several possible seismic events while directly considering the damage states in the process.

The bridge's seismic response is a combined function of the site-specific seismicity and the bridge's dynamic and structural characteristics. The Caltrans Seismic Design Criteria version 2.0 (referred to as SDC2.0 hereon) provides linear (ex. Equivalent Static Analysis, ESA) and nonlinear (ex. Nonlinear Time-History Analysis, NTHA) methods that a bridge designer can use to evaluate the seismic demand for bridges. Although NTHA is the ideal method of demand evaluation, it is usually not implemented for ordinary bridge design due to its cumbersome implementation. Linear methods such as ESA are often used in place, assuming that the elastic demand can be a good approximation for the inelastic demand generated by the ground motion (equal displacement rule). However, numerous studies (Ruiz- García and Miranda, 2003) have shown the difference between the two demand estimates and suggested using inelastic demand as the expected demand of the structure. The study presented in this report aims to provide tools to help the designer establish a bridge's inelastic response probability distribution. The said tools are provided as a series of demand statistical parameters maps for the major regions of California, developed by analyzing a comprehensive set of locations and possible bridge column designs. The report provides all the important details pertaining to the map development process and the various checks that were undertaken to ensure the correctness of the statistical parameters.

[1] https://femap58.atcouncil.org/reports

2.2 Background

2.2.1 Current Design Practice

California Transportation Department (Caltrans) was among the first agencies to suggest using a performance-based design approach for bridges. The same approach was later adopted by the American Association of State Highway and Transportation Officials (AASHTO) in their Bridge Design Specification (AASHTO, 2017). The criteria first distinguish bridges based on their importance category - important, recovery, ordinary; and then identify their performance criteria per the seismic hazard level – Safety Evaluation Earthquake (SEE) represented by a 5% probability of exceedance in 50 years or a return period of 975 years, and Functionality Evaluation Earthquake (FEE) represented by a 20% probability of exceedance in 50 years or a return period of 225 years. The current Caltrans Seismic Design Criteria (SDC2.0) (Caltrans, 2019) set the performance criteria for Californian ordinary standard bridges as minimizing the probability of collapse against a 975-year return period ground motion (Figure 2-1). In other words, an ordinary bridge is expected to experience major damage during a 975-year return period seismic event but is expected to minimize the chances of collapse during the event. Post the seismic event, the bridge is expected to be closed for damage repairs.

The current design guidelines require the designer to estimate the bridge's displacement demand using one of the prescribed methods and compare it to the capacity displacement of the bridge. If the demand is less than the capacity, the design is considered to be acceptable. However, this deterministic approach results in a binary decision, which may not be suitable for the stakeholders or owners as it does not give any estimate on the real-time decision variables such as the expected repair cost or the expected downtime. Moreover, the current approach restricts the designer to the prescribed performance level as the target and does not allow them to consider any other target performance for design.

BRIDGE CATEGORY	SEISMIC HAZARD EVALUATION LEVEL	EXPECTED POST EARTHQUAKE DAMAGE STATE	EXPECTED POST EARTHQUAKE SERVICE LEVEL
Ordinary	SEE	Major	No Service
Recovery	SEE	Moderate	Limited Service-weeks
	FEE	Minimal	Full Service
Important	SEE	Minimal to Moderate	Limited Service-days
	FEE	None to Minimal	Full Service

Figure 2-1 Expected Performance and Seismic Hazard Evaluation Levels per SDC2.0

2.2.2 Suggested Future Design Practice

State-of-the-art probabilistic design approaches allow designers to set performance levels as targets and evaluate the design to meet those specific performance criteria. With this in backdrop, Caltrans has introduced the Risk-Based Seismic Design or CT-RBSD design and assessment method, based on the PEER's PBEE methodology. CT-RBSD considers the seismic demand and structural capacity as probabilistic variables and uses them to compute the probability of failure, defined by the likelihood of exceeding a damage state in a certain number of years (ex. DS5 in 75 years). CT-RBSD directly utilizes reliability theory (please see Nowak and Collins, 2000, for a detailed description), which was the foundation for developing the AASHTO LRFD bridge design specifications. The main objective of the approach is to estimate the probability of exceeding a damage state from the reliability index (β) using the two random variables of the form; capacity represented by μ_R and δ_R, and demand represented by μ_L and δ_L. The reliability index β can be determined using Equation 2.1 with an assumption that both capacity and demand distributions are lognormal.

$$\beta = \frac{\ln\left(\frac{\mu_R}{\mu_L}\sqrt{\frac{\delta_L^2+1}{\delta_R^2+1}}\right)}{\sqrt{\ln[(\delta_L^2+1)(\delta_R^2+1)]}} \tag{2.1}$$

$$Probability\ of\ exceedence = 1 - \Phi(\beta) \tag{2.2}$$

Where β is the reliability index, μ_R and δ_R are the mean and COV of capacity for a given damage state, and μ_L and δ_L are the mean and COV of demand.

2.2.3 Gaps to be Filled

The capacity distribution under the CT-RBSD method depends on the target damage level and is established beforehand using laboratory experiments. The demand distribution for the target hazard is estimated from nonlinear time history analyses (NTHA) conducted on the bridge model, with defining events derived from the Probabilistic Seismic Hazard Analysis (PSHA) of the location. Although both processes are computationally expensive, performing them in advance can provide crucial and improved capacity and demand information, making the design process more comprehensive and accessible for designers. Recognizing the importance of this task, Caltrans initiated a series of studies to establish the capacity and demand distributions for ordinary bridge columns across California.

Vosooghi and Saiidi (2010) and Saini and Saiidi (2014) conducted extensive lab experiments to establish the capacity distributions along with the important damage states (more in the upcoming chapter). This report extends Caltrans' work by establishing the ordinary bridge column demand parameters across the important regions of California. The study presented in this report undertakes an analysis framework, that adheres to the CT-RBSD methodology and conducts NTHA analyses on a host of ordinary bridge columns to establish demand parameters across

California. The work results in maps of the demand coefficient of variation (δ_L) and nonlinear displacement adjustment factor for two site classes – Site Class C (V_{S30} = 537 m/s) and Site Class D (V_{S30} = 259 m/s); and three hazard levels – 225 years, 975 years and 2475 years return period. The report also provides detailed information and examples on how these maps can be used for seismic design and assessment of current as well as future bridge column designs.

2.3 Report Outline

This report is organized into eight chapters following this introduction. Chapter 3 details the CT-RBSD methodology, focusing on its application in performance-based design and assessment. Chapter 4 elaborates on the use of CT-RBSD methodology in the development of the demand maps, with the complete analysis framework and data. Chapter 5 describes the column's structural model and the design philosophy that led to its construction. It also provides detailed steps of the procedures that form the column's demand assessment. Chapter 6 presents the ground motion simulation and scaling model used in this study, followed by Chapter 7 summarizing the validation study performed on the structural model and the ground motion model along with the recommendations for latter's use in the study. Finally, Chapter 8 presents the results of this study in terms of the target maps with examples of their application, followed by recommendations for further studies.

3 Performance-Based Seismic Design of Bridges

3.1 Background

The performance evaluation of structures under earthquake deformation demands is complicated by uncertainties across a wide range of models and variables, from seismic hazard characterization to structural capacity description. This complexity is further exacerbated by the variation in expected performance levels for the structure. To address these issues, the Pacific Earthquake Engineering Research Center (PEER) introduced a comprehensive method for the performance evaluation of structures termed Performance-Based Earthquake Engineering (PBEE) (please see Krawinkler and Miranda, 2006, for a comprehensive review). PBEE framework identifies and provides a methodology for the quantification of the four key variables of the process: Ground Motion Intensity Measure (IM), Engineering Demand Parameter (EDP), Damage Measure (DM), and Decision Variable (DV).

Each of these variables is defined along the process, starting with the ground motion intensity measure (IM), which is a parameter defining the ground motion features in a probabilistic sense. IM is typically defined by the annual probability of exceedance, which is specific for the location and the structure design. Next is the estimation of the Engineering Demand Parameter (EDP) as the response of the structure in terms of response quantities such as deformations, accelerations, or velocities due to the ground motion IM. From EDP an inference is made on the post-event condition of the structural components and is defined by the term Damage Measure (DM). Identification of damages translates into risk management decisions quantified by the Decision Variable (DV). These variables are expressed in terms of their conditional probability of exceedance, i.e., p[A|B]. These conditional probabilities are stringed together using the total probability theorem to arrive at the probability estimate for the Decision Variable. The schematic process is depicted by the mathematical representation provided by Equation 3.1. It is noteworthy to mention that the estimation of these variables is affected by uncertainties.

$$v(DV) = \iiint G\langle DV|DM\rangle \mid dG\langle DM|EDP\rangle \mid dG\langle EDP|IM\rangle \mid d\lambda(IM)\big) \tag{3.1}$$

3.2 Caltrans Risk-Based Seismic Design

3.2.1 Introduction

Caltrans's Risk-Based Seismic Design follows the PBEE approach with direct integration of damage measure (referred to as damage level hereon) in the calculation. The core idea of the approach lies in assuming the bridge response is a direct result of bent-column behavior, which

goes in conjunction with SDC2.0 identifying the column as the seismically critical member (SCM) of the bridge as the modern bridges are designed with large seats (see SDC2.0) to further reduce the probability of collapse. The modern bridge columns are well-confined and are designed to minimize shear failure during a seismic excitations. This leaves the column response, and in turn the bridge's response entirely dependent on the column's flexural behavior. Under lateral loading, the column is assumed to form a plastic hinge along the length of the column, with the total column displacement as the sum of the displacements of the plastic region and the elastic region. The area around the plastic hinge will observe flexural cracks, spalling and even bar buckling around the hinge.

Vosooghi and Saiidi (2010) and Saini and Saiidi (2014) conducted lab experiments and identified the major damage states associated with the bridge column's flexural behavior. There are six main Damage States (DSs), namely, DS1 through DS6, and define the level of various degrees of damage seen within the plastic region of a column (Figure 3-2). Each of these damage states can be a "Target Damage State" for design and assessment purposes as per CT-RBSD. To quantify the chances of observing a damage state, the bridge column's capacity is defined in terms of an EDP called Damage Index (DI), which is a function of the column's lateral displacement, as shown in Equation (3.2).

$$DI = \frac{\Delta_D - \Delta_y}{\Delta_u - \Delta_y} \tag{3.2}$$

In Equation (3.2), Δ_D is the displacement demand, Δ_y is the yield displacement when reinforcing steel strain reaches the yield strain and Δ_u is the displacement associated with ultimate capacity. More on how to estimate these values is discussed in the later chapters.

Vosooghi and Saiidi (2010) and Saini and Saiidi (2014) developed the capacity fragilities for DI for the six different damage states (Figure 3-1). These fragility curves are lognormal CDFs, except for DS1, where a CDF for normal distribution is employed. CT-RBSD can be used in conjunction with design criteria set by Caltrans SDC2.0. SDC2.0 sets a target DS (or target performance) for ordinary standard bridges against a 975 yr. return period ground motion as major spalling within the plastic hinge region of a column, which in CT-RBSD terminology is equivalent to damage state DS3. CT-RBSD procedure follows the same objective; however, it has a direct approach to achieving this target. The bridge designer can target a DI value that corresponds to the considered performance level. From the capacity fragilities of DS3, the median DI is 0.375 (0.35, taken conservatively) and can be used to design against a 975 yr. return period ground motion.

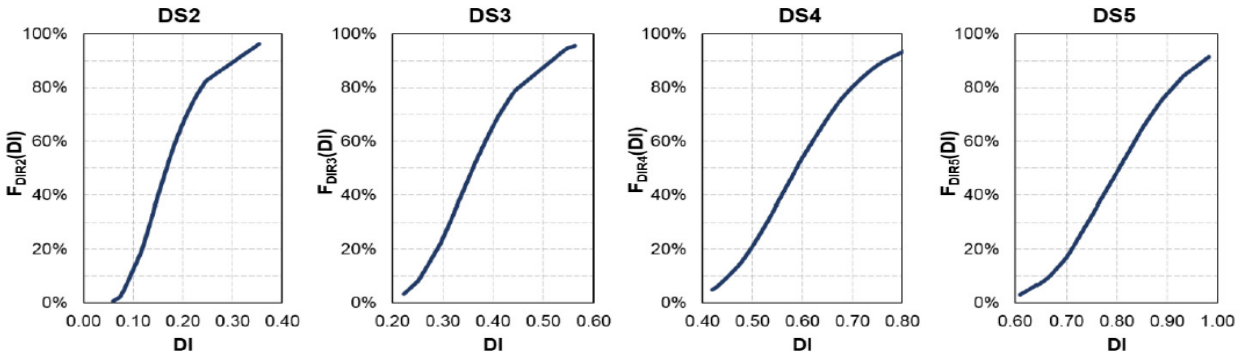

Figure 3-1 Cumulative Distribution Functions of DI_{Ri} (after Vosooghi and Saiidi, 2010)

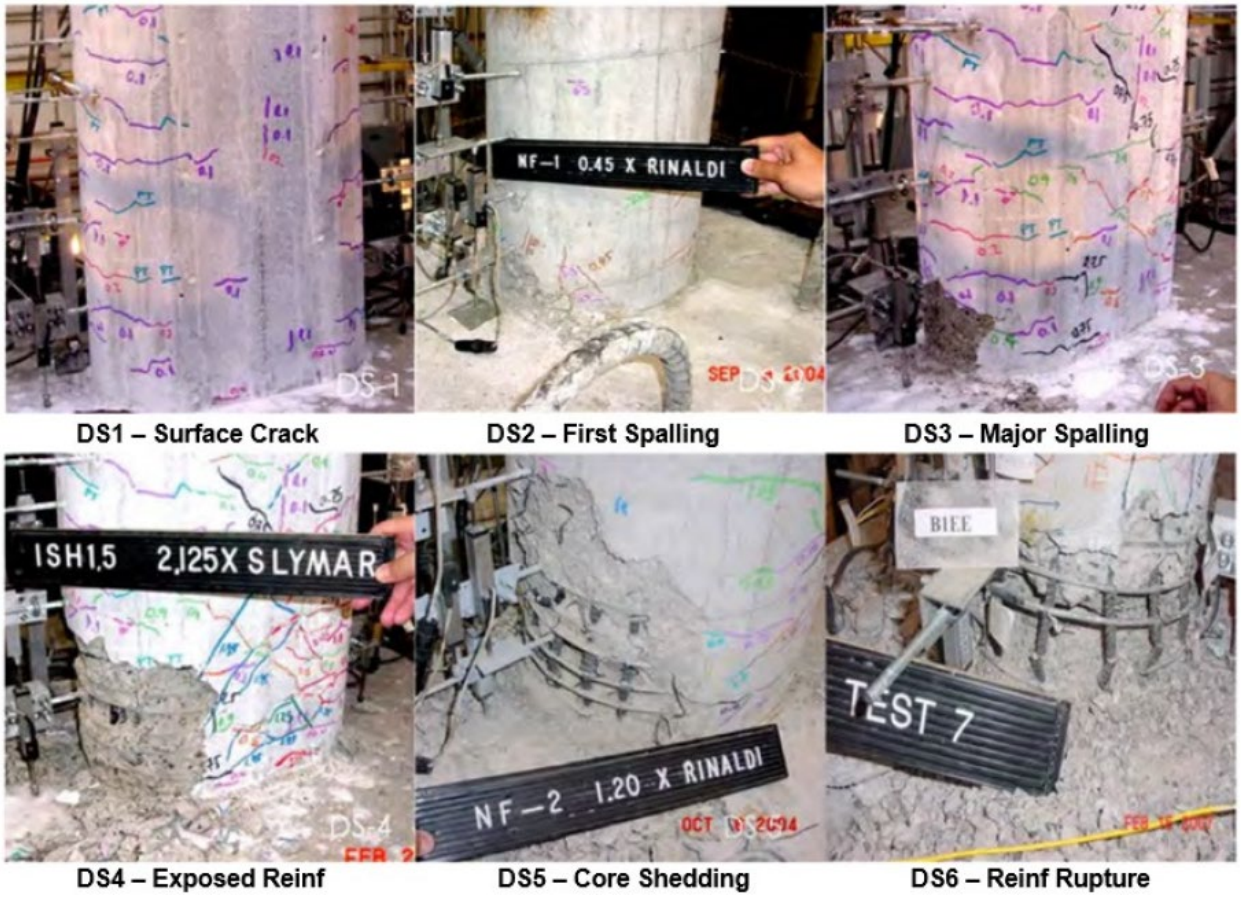

Figure 3-2 Damage States for Bridge Columns (Saini and Saiidi, 2014)

The prominence of CT-RBSD lies in its capability to analytically factor in both the variability in the estimation of demand and the capacity to arrive at an exceedance probability. CT-RBSD procedure employs the reliability theory (Nowak and Collins, 2000), which is also applied in developing the AASHTO LRFD bridge design specifications, to estimate the probability of exceeding each DS from the reliability index for each DS (β) using the two random variables of the DI form; capacity represented by DI_R and demand represented by DI_L. The reliability index β can be determined using Equation 3.3 with an assumption that both demand DI and capacity DI distributions are lognormal. In Equations 3.3 and 3.4, β is the reliability index, μ_R and δ_R are the

mean and COV of capacity DI (i.e., DI_R) for a given damage state, and μ_L and δ_L are the mean and COV of demand DI (i.e., DI_L). Note that COV is defined as the ratio of standard deviation to the mean (σ/μ).

$$\beta = \frac{\ln\left(\frac{\mu_R}{\mu_L}\sqrt{\frac{\delta_L^2+1}{\delta_R^2+1}}\right)}{\sqrt{\ln[(\delta_L^2+1)(\delta_R^2+1)]}} \tag{3.3}$$

$$Probability\ of\ exceedence = 1 - \Phi(\beta) \tag{3.4}$$

Table 3-1 Summary of μ_{Ri} and δ_{Ri} of DI_{Ri} (after Vosooghi and Saiidi, 2010)

	i = 3 for DS3	i = 4 for DS4	i = 5 for DS5	i = 6 for DS6
μ_{Ri}	0.375	0.6	0.822	1
δ_{Ri}	0.26	0.19	0.13	0

To exercise Equation (3.3), capacity information (μ_R and δ_R) is obtained from Vosooghi and Saiidi (2010) and Saini and Saiidi (2014). Demand DI information (μ_L and δ_L) are generated for the column based on its geometry and site characteristics for the target hazard level. The latter is a computationally intensive exercise, especially for the computation of δ_L. This project is intended to map δ_L across California, which designers can use for probability calculations as per the CT-RBSD framework and reduce the computational effort to arrive at β.

3.2.2 The Definition of Risk in CT-RBSD

The demand distribution parameters used for estimating β are specific to one hazard level and do not provide probability information for other hazard levels. For a more streamlined decision-making, the PBEE methodology suggests reporting a bridge's performance as a single value of exceedance risk probability of a damaged state over the bridge's lifespan (e.g., 75 years). This involves combining exceedance probabilities of the damage state at different hazard levels into a single curve, producing a damage state fragility curve. This fragility curve is then integrated over the hazard curve for the location to determine the exceedance probability of the damage state over the bridge's lifespan. Yoon et al. (2019) suggested using three representative hazard levels for different ranges of average return periods that can be combined per the total probability theorem to estimate the exceedance risk in the bridge's lifespan. The three hazard levels are – 225-yr for low intensity, 975-yr for high intensity, and 2475-yr for extreme intensity. Yoon et al. (2022) further refined the method by recommending fitting a lognormal distribution with exceedance probabilities as the representative cumulative densities and their respective hazard spectrum spectral accelerations as the quantiles (Figure 3-3). The fragility curve thus obtained represents the performance of a specific bridge geometry at the desired location, incorporating the bridge and location properties along the way. Integrating this fragility curve over the hazard curve (Equation

(3.6)) will yield the probability of exceeding a damage state in T years for the bridge, commonly known as 'Risk' under the PBEE framework.

$$\lambda_{DS_i} = \int G(DS_i|Sa)d\lambda_{Sa} \tag{3.6}$$

A logical interpretation suggests that a high-capacity bridge poses a lower risk than a low-capacity bridge at the same location. This is because the fragility curve for the high-capacity bridge will result in a lower probability of exceedance for the same ground motion intensity. Applying a similar perspective, a high-seismicity location inherently carries greater risk than a low-seismicity location. This concept is illustrated in Figure 3-3, where fragilities can vary based on either site seismicity—low seismic (LS) vs. high seismic (HS)—or bridge capacity—low capacity (LC) vs. high capacity (HC). The figure highlights the level of risk associated with each fragility scenario.

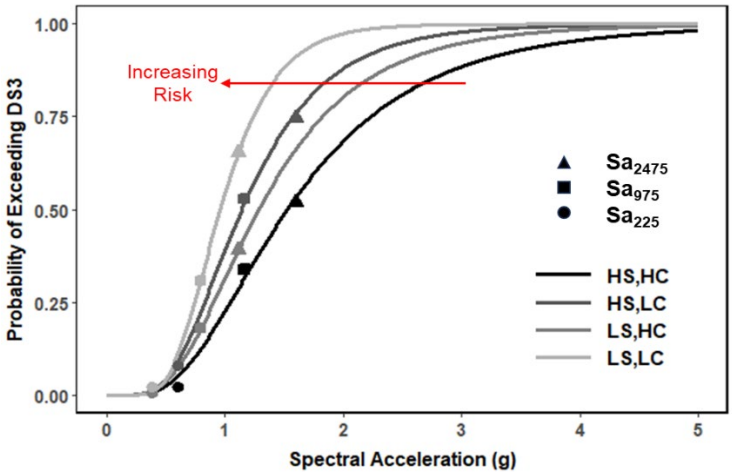

Figure 3-3 Sample Fragilities Illustrating the General Trend in Computed Risk for High/Low Seismicity (HS/LS) and High/Low Capacity (HC/LC) Bridge Columns

Risk has a direct application in CT-RBSD, as it allows quantification of the chances of a bridge experiencing a damage state in its lifetime, which is a tangible indicator of a bridge's performance for the stakeholders. Moreover, CT-RBSD allows the designer to directly include the target damage state in the analysis, granting them direct control over the design and its modification per the need.

4 Analysis Framework

4.1 Introduction

The primary objective of this study is to equip bridge designers with statistical parameter maps that can define a bridge's seismic demand at a given location for a specified hazard level. To develop these maps, a large number of locations needed to be analyzed within a comprehensive framework that accounts for both multiple locations and hazard levels. A previous study on CT-RBSD (Yoon et al., 2019) introduced a general framework using 10 locations, incorporating variable site conditions and an existing bridge design. While this study provided a robust methodology with practical examples for designing and analyzing bridge columns under the CT-RBSD procedure, it highlighted the need for further analysis to refine DI_L distributions across California. Building on this foundation, the current study expands the framework by incorporating a broader statistical analysis of DI_L variation across multiple locations in California, considering a larger pool of bridge columns. The following sections detail the assessment framework used for each location and the data sources utilized for map generation.

4.2 Primary Input Data

This study integrates the assessment framework with a set of preliminary input data that can define different hazard levels, column properties, and geographical variation comprehensively. This data provides details for a broad range of input parameters characterized as follows –

1. **Hazard Intensity**: Hazard levels of ground motions with an assumption that the hazard curve may be divided into low, high, and extreme ground motion hazard zones and are divided into three groups based on their intensities:
    - Low Intensity: average return period of 225 years (return periods between 1 year to 600 years).
    - High Intensity: average return period of 975 years (return periods between 600 years to 1725 years).
    - Extreme Intensity: average return period of 2475 years (return periods between 1725 years to 3000 years).
2. **Shear Wave Velocity, V_{S30}**: Two shear wave velocity values are taken as the representative values for the two sites, 259 m/s for site class D and 537 m/s for site class C.

    Moving forward, shear wave velocity will be represented using the term V_{S30}.
3. **Locations**: Locations were selected based on a 25-mile by 25-mile grid for the important regions of California. For the Bay Area and Southern California, a

finer grid of 5-mile by 5-mile was considered. The locations that were analyzed for the development of the maps are presented in Figure 4-1.

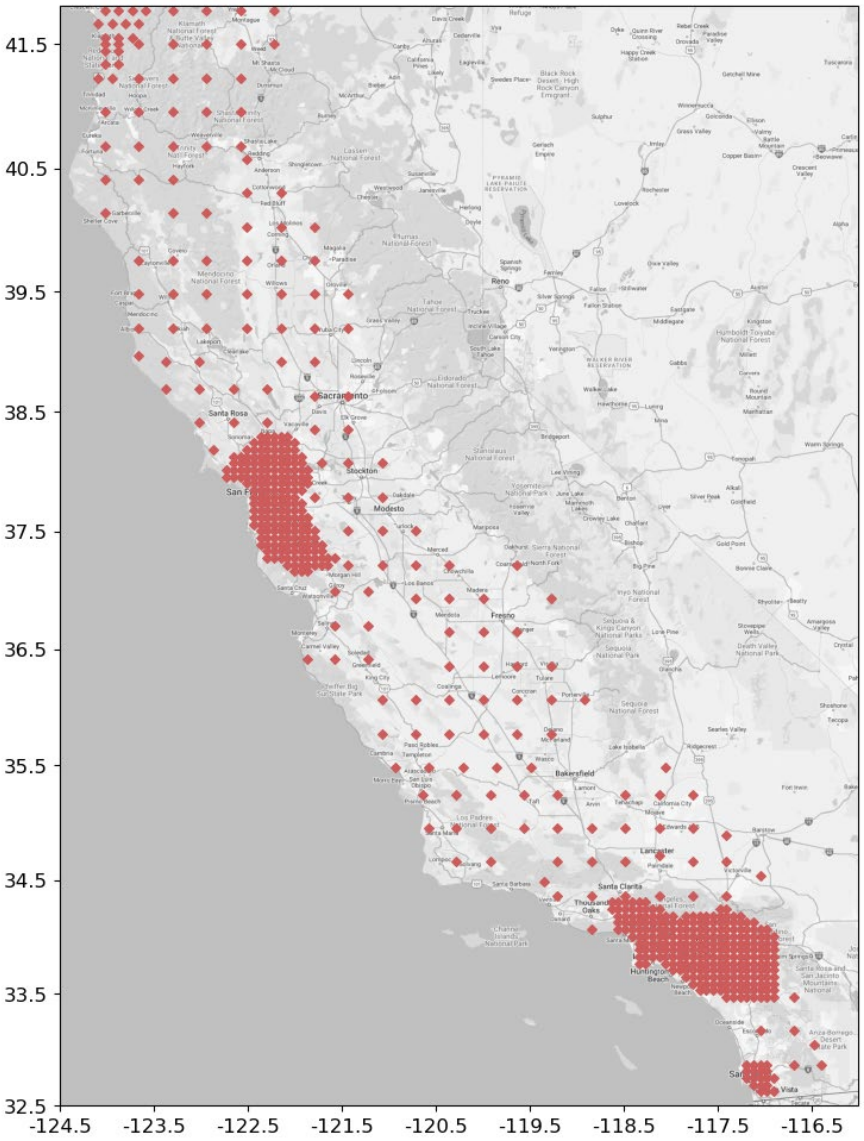

Figure 4-1 Layout of Locations Across California used In This Study

4. Columns: A matrix of 3,456 bridge columns with variable properties, as outlined in Table 4-1, was established for use at each location. This matrix comprehensively accounts for all possible column design parameters, with each design uniquely defined by a set of six geometrical parameters listed in the table. Each column undergoes reinforcement and shear checks in accordance with AASHTO-BDS and SDC 2.0. Once these checks are completed, a preliminary design evaluation is performed using the Equivalent Static Analysis (ESA) method, as outlined in SDC 2.0. According to SDC 2.0, an ordinary bridge column is expected to sustain major damage under a 975-year hazard, which corresponds to a Damage Index (DI) of 0.35 in CT-RBSD terms. In this

study, a design DI range of 0.3 to 0.4 is considered to obtain a comprehensive understanding of Caltrans ordinary bridge column demands. Based on this design DI range, a shortlist of column designs is developed for time history analysis.

Table 4-1 Column Properties Matrix

Column Height (ft)	20, 30, 40, 50	
Axial Force (% f'_cA_g)	5, 10, 15	
Reinforcement Ratio (%)	1, 1.75, 2.5	*f'_c is the expected concrete strength*
Column Diameter (ft)	5, 6, 7, 8	*A_g is the gross cross-sectional area of the column*
Hoop Size	#5, #6, #7, #8	
Hoop Spacing (in)	3, 4, 5, 6, 7, 8	

4.3 Statistical Analysis Framework

The assessment framework presented in this section delivers a seismic demand distribution for a given location and hazard level. The location parameters (latitude, longitude, and site class) along with the hazard level are the starting point for the assessment framework. The method can be replicated for other hazard levels and locations by changing the input parameters. The detailed assessment framework (Figure 4-2) consists of the following steps: -

1. Set the location and hazard level to be analyzed and determine the input parameters accordingly – Latitude, Longitude, Site Class (or V_{S30}), and Return period.
2. From the USGS website (Unified Hazard Tool - earthquake.usgs.gov/nshmp/) obtain the UHS (Uniform Hazard Spectrum) for the target location and hazard.
3. Perform preliminary design using the ESA method and determine the design DI (or DI_{ESA}) for each column in the matrix.
4. Select columns that satisfy the design criteria, i.e., DI_{ESA} between 0.3 and 0.4, and satisfy the AASHTO BDS and SDC2.0 requirements.
5. Determine the set of unique time periods from the selected columns and obtain the important earthquake events using the deaggregation tool of the USGS Unified Hazard Tool.
6. Simulate and scale ground motions for the identified seismic events. Ensure the secondary intensity measures (IMs) follow the appropriate ground motion models.

7. Perform time history analysis on the bridge columns in Step #4 using the ground motions generated in Step #6.
8. Post-process the raw data to compute demand DI (DI_L) statistical parameters.

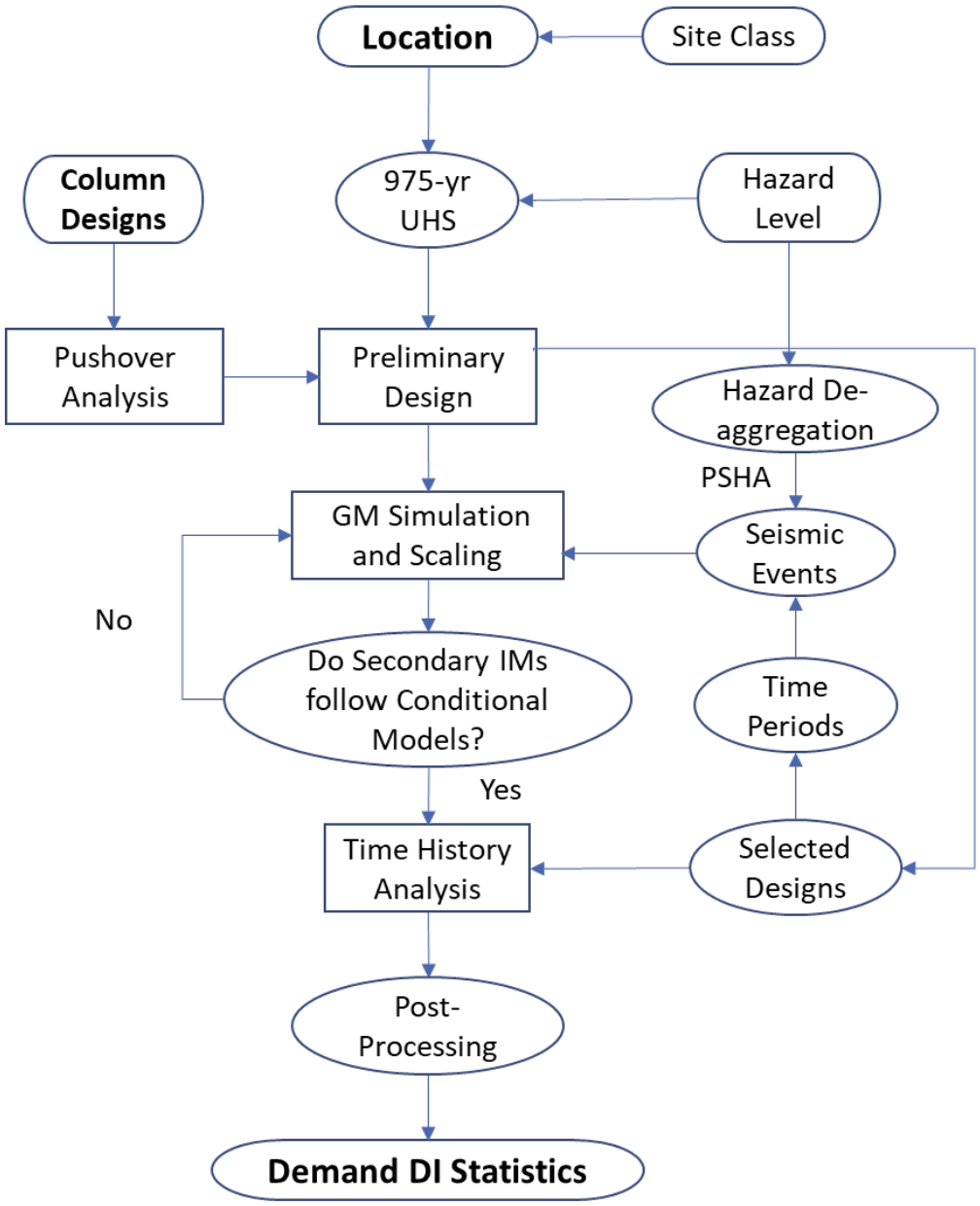

Figure 4-2 Analysis Framework

5 Structural Modeling

5.1 Introduction

The previous chapter provided detailed information on the data and framework that goes into the development of the maps of the demand coefficient of variation (δ_L) and nonlinear displacement adjustment factor. The crucial part of the process is developing analytical models for columns resembling the modern bridge columns used in California. Caltrans Seismic Design Criteria considers the bridge column to be the seismically critical member (SCM), which may develop flexural cracks under lateral loading. SDC assumes a bridge column behavior similar to a cantilever column with dead weight at the top. When lateral loads are applied to the column, the column rotates about a plastic hinge developed internally. Thus, the lateral displacement of the column's top is the summation of the displacement caused by the rotation around the plastic hinge and the elastic lateral displacement of the elastic part of the column (Figure 5-1).

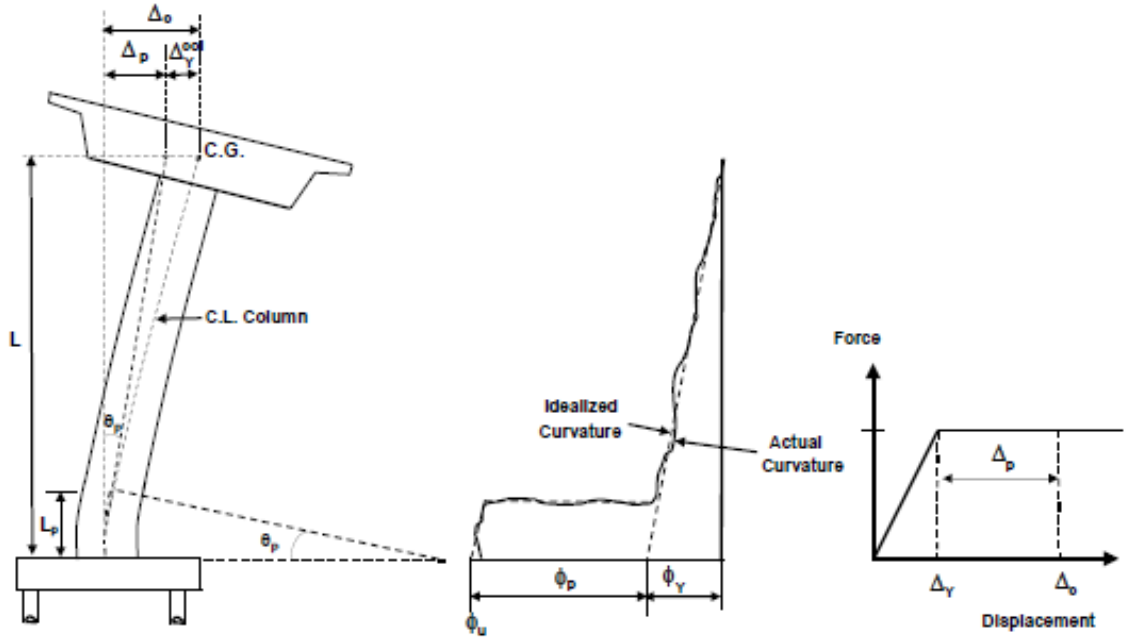

Figure 5-1 Column Behavior per SDC2.0 (Caltrans, 2019)

Based on the description of the column's behavior provided by SDC2.0, 3D finite element models are prepared for each column. These models are developed in the open-source finite element modeling software OpenSees (McKenna et al. 2010), widely used for structural engineering research purposes. This chapter provides detailed information on the development of these models along with the methods in which they are implemented.

5.2 Finite Element Modelling

OpenSees modeling starts once the shortlist of columns (i.e., geometrical properties and confinement steel properties) is complete. The OpenSees models are first used for pushover analysis to determine the important parameters - Yield Displacement (D_y or Δ_y), Ultimate/Capacity Displacement (D_u or Δ_u), Lateral Strength (F_y), Elastic Stiffness (K_e) and Natural Time-period (T_n); followed by NTHA conducted on the same model. The common modeling characteristics of each column are as follows –

- Dead load equivalent to the Axial Force parameter of Table 5-1 is applied at the top of the column, where f'_c is the expected unconfined concrete strength.
- Pushover analysis is conducted in a single direction (lateral direction as per section 4.3.2 of SDC), while NTHA is conducted with two horizontal components of ground motion time series.
- Material properties are defined as suggested in Table 5-1. CT-RBSD uses the ultimate hoop strain of 0.18 (rather than 0.09 according to SDC2.0. This value is based on the earlier study by Yoon et al. (2019), where section analysis results were tuned to arrive at the same ultimate displacement as observed in experimental tests while using ultimate hoop strain as the tuning parameter.

Table 5-1 Material Properties

Expected Unconfined Concrete Strength	5 ksi
Unconfined concrete compressive strain (spalling)	0.005
Ultimate unconfined compressive strain (at max compressive stress)	0.002
Expected Yield Strength of Steel	68 ksi
Expected Yield Strain of Steel	0.0023
Ultimate Tensile Strain of Confinement Steel	0.18
Ultimate Tensile Strain of Longitudinal Reinforcement Steel	0.12 for #10 and smaller, 0.09 for #11 and larger

- Columns are considered cantilever columns with their base fixed in all 6 DOFs.
- Columns are modeled with the BeamWithHinges element model in OpenSees, where the plastic hinge length, L_p, is defined as per Section 5.3.4 of SDC2.0:

$$L_p = 0.08L + 0.15 f_{ye} d_{bl} > 0.3 f_{ye} d_{bl} \quad (5.1)$$

Where f_{ye} is the expected yield strength of steel reinforcement (ksi), d_{bl} is the nominal bar diameter of longitudinal column reinforcement (in), and L is the Length of SCM from the point of maximum moment to the point of contra flexure (in).

- Concrete fibers and longitudinal steel reinforcement fibers for the columns are modeled as two separate fibers. Therefore, the number of fibers in angular directions for both concrete and longitudinal steel equals the number of longitudinal rebars being provided, and fibers in the radial direction are 20 for core concrete and 2 for cover concrete.
- For steel, ReinforcingSteel material in OpenSees is used, while Concrete01 is used for concrete modeling.
- As hoops cannot be modeled explicitly in OpenSees, the column core was modeled as confined concrete with a stress-strain curve defined by Mander's model (Mander et al., 1988), for the specific hoop arrangement. Cover concrete properties are described using Mander's model but with no confinement.

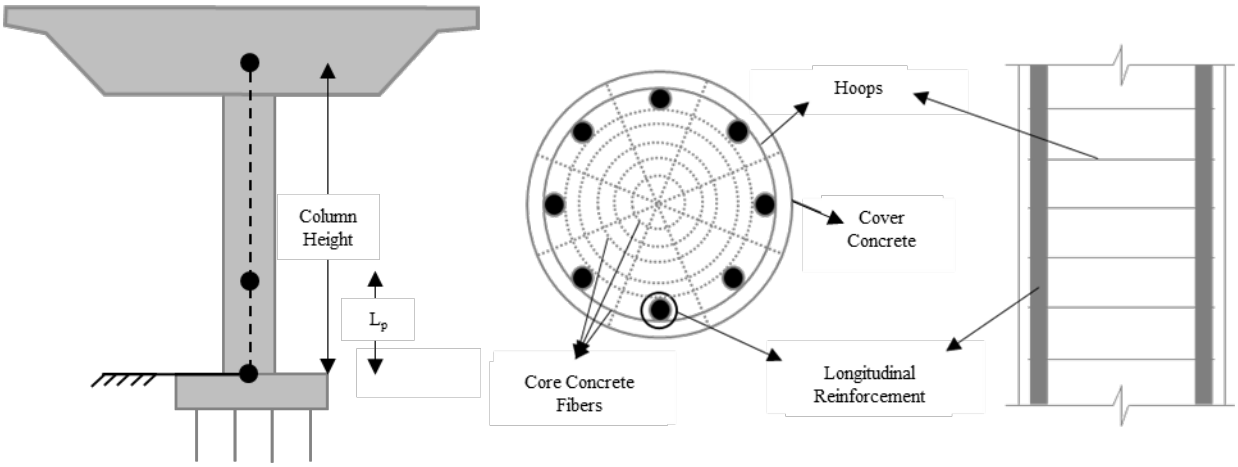

Figure 5-2 Schematic Illustration of The Bridge Model

5.3 Static Analysis

5.3.1 Inelastic Static Analysis (ISA)

Pushover analysis, also known as Inelastic Static Analysis (as per SDC 2.0), is performed for each possible column design using OpenSees to generate the column section's moment-curvature curve. The analysis provides key structural properties, including yield displacement, capacity displacement, lateral strength, elastic stiffness, and natural period, derived from the pushover curves. A displacement-controlled analysis is conducted by applying lateral displacement in the transverse direction, as recommended in Section 4.3.2 of SDC 2.0. The resulting moment-curvature relationship at the column base is idealized as a bilinear curve using the equivalent area technique to determine key parameters such as yield curvature (ϕ_Y), capacity (or ultimate) curvature (ϕ_U), cracked moment of inertia (I_{cr}), and plastic moment capacity (M_P).

The moment-curvature curve generated in OpenSees is then transformed into an idealized elastoplastic moment-curvature curve (Figure 5-3) by equating the areas under the original and

idealized curves. The idealization process begins by estimating the secant slope of the moment-curvature curve (E_cI_{cr}), which is defined as the line connecting the origin to the point where the extreme reinforcement reaches the yield strain. This relationship is expressed as $E_cI_{cr} = M_y/\phi_y$, where E_c represents the concrete's modulus of elasticity, M_y is the moment at which the extreme longitudinal steel reaches its yield strain, and ϕ_y is the corresponding curvature at yield. The ultimate curvature (ϕ_U) is identified as the point where either the core concrete reaches its ultimate strain or the extreme longitudinal reinforcement reaches its ultimate strain, whichever occurs first.

Once these parameters are established, the area under the moment-curvature curve (U) and the idealized bilinear model are equated to estimate the idealized yield curvature (ϕ_Y) and plastic moment capacity (M_P) (see Equation 5.3).

$$U = 0.5\phi_Y M_Y + (\phi_U - \phi_Y)M_Y \tag{5.3}$$

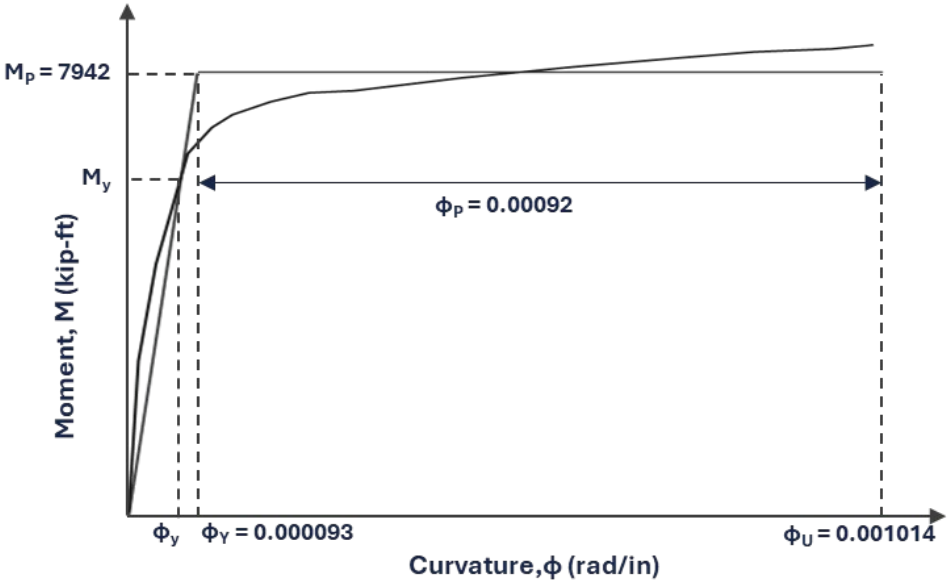

Figure 5-3 Moment-Curvature Curve and Idealized Bilinear Moment-Curvature Curve for Column Height = 30 ft, Diameter = 4 ft, Axial Load = 15% of f'_cA_g, Long. Rebar - 20 #11, Hoops: #8 @ 5 in

The moment and curvature parameters identified are then used to estimate the yield displacement (Δ_Y), plastic displacement (Δ_P), and capacity/ultimate displacement (Δ_C) (Equation 5.4 – 5.8). These equations assume the bridge column is a cantilever column with fixed-free connections and its displacement capacity is defined by the rotation capacity of the member, which in turn is based on the curvature capacity of the plastic hinge (Figure 5-1).

$$\Delta_C = \Delta_Y + \Delta_P \tag{5.4}$$

$$\Delta_Y = \frac{L^2}{3}\phi_Y \tag{5.5}$$

$$\Delta_P = \theta_P\left(L - \frac{L_P}{2}\right) \tag{5.6}$$

$$\theta_P = L_P \phi_P \tag{5.7}$$

$$\phi_P = \phi_U - \phi_Y \tag{5.8}$$

Where L is the distance from the point of maximum moment to the point of contra-flexure (typically taken as the length of the column), L_P is the equivalent plastic hinge length and θ_P is the plastic hinge rotation capacity.

The effective stiffness (K_e) is estimated as per the assumption of the cantilever column using Equation 5.9 and is eventually used to estimate the natural time period of the column (T_n). The shear capacity (V_P) is estimated for the cantilever column as per Equation 5.11.

$$K_e = \frac{3EI_{cr}}{L^3} \tag{5.9}$$

$$T_n = 2\pi \sqrt{\left(\frac{W_{top}}{gK}\right)} \tag{5.10}$$

$$V_P = \frac{M_P}{L} \tag{5.11}$$

Where W_{top} is the dead weight at the top of the column

5.3.2 Equivalent Static Analysis (ESA)

Once the idealized bilinear moment-curvature curves are generated for each column in the matrix, a preliminary design or shortlisting of columns is performed according to the Equivalent Static Analysis (ESA) procedure of SDC2.0. According to the design criteria, ESA is conducted for an earthquake hazard level with a 975-year average return period. The steps for the preliminary design according to ESA are –

1. Obtain the spectral acceleration UHS curve for the 975-year average return period hazard using the USGS Unified Hazard tool (explained in Chapter 6).
2. Using the generated UHS curve, the spectral acceleration value, $Sa(T_n)$ at the natural period (T_n) of the column is calculated.
3. The equivalent shear force (V_{eq}) at the top of the column is calculated by multiplying $Sa(T_n)/g$ by the dead weight applied at the top of the column.

$$V_{eq} = Sa(T_n) \cdot W \tag{5.12}$$

4. Using the elastic stiffness calculated in pushover analysis (K_e), the demand displacement (D_{ESA}) is computed using Equation (5.13)

$$D_{ESA} = V_{eq}/K_e \tag{5.13}$$

5. Calculate DI_{ESA} using the Equation:

$$DI_{ESA} = \frac{D_{ESA} - D_y}{D_u - D_y} \tag{5.14}$$

For the purposes of this study, the DI_{ESA} is the primary parameter that determines the selection of the column. The other parameter is the time period of the column, which should fall between 0.7 sec and 3 sec, representing the modern-day bridge column. If the DI_{ESA} falls between 0.3 and 0.4, and the time period falls between 0.7 sec and 3 sec, we selected the column to be further used for NTHA.

6 Ground Motion Hazard Modeling

6.1 Introduction

The study by Yoon et al. (2019) used Caltrans' Online ARS tool for generating acceleration response spectrum (ARS) for the three hazard levels considered (225 yr., 975 yr., 2475 yr. average return period); the same tool was used to obtain the corresponding events data. However, this method was modified for this study due to the closure of the ARS tool and the introduction of the USGS Unified Hazard tool for the same purpose. Caltrans' Online ARS tool, developed as per the SDC2.0, used SDC2.0 estimated Near-Fault and Basin factors as an added amplification to the hazard spectrum estimated via the USGS tool. However, the state-of-the-art USGS tools are based on the updated National Seismic Hazard Maps (2018) and have both these factors implicitly present in the hazard calculations (refer to Appendix B for further details). Therefore, this study does not follow the SDC2.0 recommendation for the amplification of spectral ordinates and uses the spectral acceleration values produced by the USGS tool with no amplification.

6.2 Hazard Curve and Deaggregation

The USGS Unified Hazard Tool requires the site and hazard-dependent input data to generate hazard curves and deaggregation results. The geographical parameters of the site are given as the latitude and longitude, along with the site class or shear wave velocity. The tool also requires a value for the return period of the earthquake hazard being considered and a spectral period for deaggregation. A rupture forecast edition is also needed for hazard calculations and deaggregation; for this study, the latest edition, i.e., "NSHM Conterminous U.S. 2018" was utilized. When all the inputs are set, the hazard curves for target average return periods and a Uniform Hazard Spectrum (i.e., UHS) are generated. The UHS is used to obtain spectral acceleration at the natural period of the column (i.e., $Sa(T_n)$).

The major faults and their respective dominating events are obtained using the deaggregation tool for each column's natural period. Deaggregation results are generated in terms of a list of faults with their respective dominating events, defined by the event Magnitude (M), rupture distance (R_{RUP}), azimuth angle (α), and contribution (c). These faults are also categorized based on the source sets during aggregation. A single fault may appear in multiple source sets with different event parameters. However, the sum of all the contributions from each source set sums to a total contribution of 100%. Therefore, events are ranked and considered based on their total contribution to the seismic hazard.

The USGS Unified Hazard Tool has a limited number of inbuilt spectral period values; they are 0 (PGA), 0.01, 0.02, 0.03, 0.05, 0.075, 0.1, 0.15, 0.2, 0.25, 0.3, 0.4, 0.5, 0.75, 1, 1.5, 2, 3, 4, 5, 7.5 and 10 seconds. However, column model periods fall into a continuum between 0.7 to 3 seconds. Therefore, an interpolation process is needed to combine the deaggregation results from the two

nearby periods from the USGS Unified Hazard Tool list to the target period for a column. For example, if the natural period of the column is 0.8 sec, deaggregation results from the periods 0.75 sec and 1 sec from the USGS Unified Hazard Tool are used for this interpolation. For simplicity of explanations, let's call the spectral periods near the natural periods T_{dn} and T_{up}, where T_{dn} is the smaller value. An example of such interpolation is provided in Figures 6-1 to 6-3.

The interpolation scheme assigns a unique identifier to dominating events. From the USGS Unified Hazard tool documentation and multiple trials, it was observed that the rupture distance (R_{RUP}) and azimuth (α) are the unique identifiers for those events. Two events having the same source set $\{R_{RUP}, \alpha\}$ are identified from the deaggregation results of T_{up} and T_{up}. Their contribution is then interpolated per the spectral ordinates $Sa(T_{dn})$ and $Sa(T_{up})$.

$$c(T_1) = c(T_{dn}) + \frac{\big(Sa(T_1) - Sa(T_{dn})\big)}{\Big(Sa\big(T_{up}\big) - Sa(T_{dn})\Big)}\Big(c\big(T_{up}\big) - c(T_{dn})\Big) \tag{6.1}$$

Events originating from the same point on the fault usually have the same magnitude but, in some cases, it can differ by a small amount. For the latter, magnitude values are interpolated similarly to those for contribution.

After obtaining the dominating events, and their respective contribution and fault names, the next step is to assign the number of ground motions generated for each event for a ground motion set representing a seismic hazard level. The latter is a function of the event's contribution to the set. Per the recommendations by Yoon et al. (2019), each ground motion set has 51 ground motions. In other words, for a unique combination of Location, V_{S30}, column time-period, and hazard level, a set of 51 ground motions is simulated (and scaled as discussed later). These 51 ground motions are distributed among all the dominating events as per their contribution. Finally, the number of ground motions of each event (gm_i) is calculated per their contribution in the complete set, rounded off to the closest integer as shown in Equation (6.2).

$$gm_i = \frac{c_i}{\sum c_i} \times 51 \tag{6.2}$$

Where c_i is the contribution by event i, and $\sum c_i$ is the sum of all contributions for that deaggregation set.

Source Set ↳ Source	Type	r	m	ε_0	lon	lat	az	%
UC33brAvg_FM32	System							26.71
Little Salmon (Onshore) [2]		2.65	7.13	-0.56	124.210°W	40.777°N	240.28	14.47
Table Bluff [0]		9.55	7.10	-0.23	124.255°W	40.697°N	211.83	2.92
Mad River - Trinidad fault zone (alt2) [1]		16.81	7.37	0.81	124.031°W	40.891°N	48.09	2.48
Little Salmon (Offshore) [0]		3.01	7.12	-0.43	124.215°W	40.780°N	249.61	1.00
UC33brAvg_FM31	System							25.80
Little Salmon (Onshore) [2]		2.65	7.12	-0.55	124.210°W	40.777°N	240.28	13.95
Table Bluff [0]		9.55	7.10	-0.24	124.255°W	40.697°N	211.83	2.82
Little Salmon (Offshore) [0]		3.01	7.12	-0.43	124.215°W	40.780°N	249.61	1.03

Figure 6-1 Seismic Hazard Deaggregation for Eureka - 259 m/s - 225 Hazard - 1 sec Spectral Period

Source Set ↳ Source	Type	r	m	ε_0	lon	lat	az	%
UC33brAvg_FM32	System							25.99
Little Salmon (Onshore) [2]		2.65	7.12	-0.54	124.210°W	40.777°N	240.28	14.15
Table Bluff [0]		9.55	7.09	-0.25	124.255°W	40.697°N	211.83	2.92
Mad River - Trinidad fault zone (alt2) [1]		16.81	7.36	0.84	124.031°W	40.891°N	48.09	2.31
UC33brAvg_FM31	System							25.11
Little Salmon (Onshore) [2]		2.65	7.12	-0.53	124.210°W	40.777°N	240.28	13.65
Table Bluff [0]		9.55	7.10	-0.25	124.255°W	40.697°N	211.83	2.82

Figure 6-2 Seismic Hazard Deaggregation for Eureka - 259 m/s - 225 Hazard - 0.75 sec Spectral Period

Fault Name	Magnitude (M)	RRUP (km)	Contribution (%)	Azimuth (Degrees)
Little Salmon Onshore	7.1	2.7	28.1	240.3
Table Bluff	7.1	9.6	5.6	211.8
Mad River Trinidad fault zone	7.4	16.8	2.5	48.1
Little Salmon Offshore	7.1	3.0	1.6	249.6

Figure 6-3 Seismic Hazard Deaggregation for Eureka - 259 m/s - 225 Hazard - 0.8 sec Spectral Period

6.3 Fault Parameters

Hazard deaggregation suggests the characteristic event scenarios in terms of fault names, event magnitude (M), rupture distance (R_{RUP}) and azimuth angle (α). Other important fault event parameters are obtained as suggested by Kaklamanos et al. (2011). The following list of event parameters is considered in simulating ground motions using Dabghi (2014).:

- **Moment Magnitude, M**: This is the event magnitude directly provided by hazard deaggregation results.

- **Rupture Distance, R_{RUP}**: The shortest distance from the site to the rupturing fault, also known as Rupture distance (R_{RUP}), is the distance provided by the deaggregation results from USGS.

- **Shear-Wave Velocity, V_{S30}**: The time-averaged shear-wave velocity over a subsurface depth of 30 meters. V_{S30} is an input parameter set at the start of the analysis by the user.

- **Source-to-Site Azimuth (α)**: As mentioned by Kaklamanos et al. (2011), source-to-site azimuth for a given site is the angle between the positive fault strike direction and the line connecting the site to the closest point on the surface projection of the top edge of the rupture (with clockwise angle assumed positive). They defined azimuth as a positive angle (between 0° and 180°) for sites on the hanging wall side and a negative angle (between -180° and 0°) for sites on the foot-wall side. Hazard deaggregation from USGS results only in positive azimuths ranging from 0° to 360°. This azimuth is modified as sgn(α)·(180° - α) as suggested by Kaklamanos et al. (2011), considering the distance calculations are symmetric for sites reflected across a line perpendicular to the site, passing through the center of the fault.

- **Hanging-wall flag, F_{HW}**: The hanging wall flag defines whether the site is on the hanging wall side of the fault (F_{HW} = 1) or the footwall side of the fault (F_{HW} = 0). This can be determined by the azimuth angle (α) obtained from deaggregation results and simplifying it, as mentioned earlier.

$$F_{HW} = \begin{cases} 0 & for\ 0° \leq \alpha \leq 180° \\ 1 & for\ -180° \leq \alpha \leq 0° \end{cases} \tag{6.3}$$

  These values follow the average values observed in the NGA West2 flatfile. An average azimuth of 50° and -50° was observed for sites on the hanging-wall (F_{HW} = 1) and footwall (F_{HW} = 0), respectively.

- **Rake Angle, λ**: Rake angle helps define the faulting style and can be determined from the USGS fault database. The fault database provides a numerical value for the rake angle. An inference needs to be made regarding the fault styling from that angle, based on the recommendation by Abrahamson et al. (2008):

$$30° \leq \lambda \leq 150° \rightarrow Reverse\ Faulting \tag{6.4}$$

$$-120° \leq \lambda \leq -60° \rightarrow Normal\ Faulting \tag{6.5}$$

$$-180° \leq \lambda < -120°, -60° < \lambda < 30°, \\ 150° < \lambda \leq 180° \rightarrow Strike-slip\ Faulting \tag{6.6}$$

  For the ground motion simulation model by Dabaghi (2014), a fault factor F is derived depending on the faulting style –

$$F = \begin{cases} 0 & for\ Strike-slip\ Faults \\ 1 & for\ Normal\ and\ Reverse\ Faults \end{cases} \tag{6.7}$$

- **Fault Dip Angle, δ**: Fault dip angle is directly taken from the USGS fault database (Will et al, 2008) mentioned against the fault name under study.

- **Depth-To-Top of Rupture, Z_{TOR}**: Similar to fault dip angle, the Z_{TOR} value is directly derived from the USGS fault database as the numerical.

- **Down-Dip Rupture Width, W**: The empirical relationships provided by Well and Coppersmith (1994) are deemed reasonable to determine the down-dip rupture width for the fault under consideration. Depending on the fault styling and the earthquake event moment magnitude (M), W is calculated as:

$$W = \begin{cases} 10^{-0.76+0.27M} & for\ strike-slip\ events \\ 10^{-1.61+0.41M} & for\ reverse\ events \\ 10^{-1.14+0.35M} & for\ normal\ events \end{cases} \quad (6.8)$$

- **Site Coordinate, Rx**: R_X is the horizontal distance to the top edge of rupture measured perpendicular to the site's strike and depends on the fault-site geometry. Kaklamanos et al. (2011) suggested equations to derive R_{RUP} for a given fault geometry, including the site coordinate R_X. However, the R_{RUP} value is provided upfront and is used to back-calculate R_X for a given geometry.

  For vertical faults (δ = 90°),

$$R_{RUP} = \sqrt{R_{JB}^2 + Z_{TOR}^2} \quad (6.9)$$

$$R_X = R_{JB} Sin\alpha \quad (6.10)$$

  For nonvertical faults (δ ≠ 90°),

$$R_{RUP} = \sqrt{\left(R'_{RUP}\right)^2 + R_Y^2} \quad (6.11)$$

Where

$$R'_{RUP} = \begin{cases} \sqrt{R_X^2 + Z_{TOR}^2} & for\ R_X < Z_{TOR}tan\delta \\ R_X sin\delta + Z_{TOR}cos\delta & for\ Z_{TOR}tan\delta \le R_X \le Z_{TOR}tan\delta + Wsec\delta \\ \sqrt{(R_X - Wcos\delta)^2 + (Z_{TOR} + Wsin\delta)^2} & for\ R_X > Z_{TOR}tan\delta + Wsec\delta \end{cases} \quad (6.12)$$

$$R_Y = |R_X cot\alpha| \quad (6.13)$$

  For cases where none of the equations result in an R_X value, we can assume that the site is directly above the fault and R_X is given by Equation (6.14).

$$R_X = \frac{1}{2} Wcos\delta \quad (6.14)$$

- **Length or Width of fault rupture between the epicenter and the site, $s_{or}d$**: For ground motion simulation using the Dabaghi (2014) model, one should provide the length or width of the fault rupture between the epicenter and the site, $s_{or}d$. As suggested by Dabaghi (2014), this can be derived using Equation (6.15)

$$s_{or}d = R_{RUP}|cot\theta_{or}\varphi| \tag{6.15}$$

  Where $\theta_{or}\varphi$ is the directivity angle used to define the site direction concerning the fault. In the case of vertical faults (δ = 90°), the directivity angle is equal to the azimuth angle (α) obtained from hazard deaggregation. For nonvertical faults (δ ≠ 90°), this angle is 45°, as recommended by Yoon et al. (2019).

- **Depth to VS = 1.0 km/s, $Z_{1.0}$**: Kaklamanos et al. (2011) suggested using recommendations of the GMM model developer for the calculation of $Z_{1.0}$. Since the ASK14 model (Abrahamson et al, 2013) is the GMM used for this study, the recommendations by Abrahamson and Silva (2008) for the estimation of the median $Z_{1.0}$ (m) are implemented according to Equation (6.16).

$$Z_{1.0} = \begin{cases} \exp(6.745) & for\ V_{S30} < 180\,\frac{m}{s} \\ \exp\left[6.745 - 1.35\,ln\left(\frac{V_{S30}}{180}\right)\right] & for\ 180 \le V_{S30} \le 500\,\frac{m}{s} \\ \exp\left[5.394 - 4.48\,ln\left(\frac{V_{S30}}{500}\right)\right] & for\ V_{S30} \ge 500\,\frac{m}{s} \end{cases} \tag{6.16}$$

6.4 Ground Motion Simulation and Scaling

The fault (or event) parameters are then passed onto the MATLAB code based on the Dabaghi (2014) model for ground motion simulation with two horizontal components. Although the previous section discussed multiple fault (or event) parameters, not all event parameters are needed for ground motion simulation. Out of the parameters mentioned, only Magnitude (M), Rupture Distance (R_{RUP}), Fault type (F), Depth to Top-of-Rupture (Z_{TOR}), Shear Wave Velocity (V_{S30}), Length or Width or fault rupture between epicenter and site ($s_{or}d$) and Directivity Angle (θ) are needed. The MATLAB code generates two acceleration time series for the two horizontal components and a scalar value dt, which is the time duration between waveform time steps.

Acceleration response spectrums are then generated using their acceleration time histories for horizontal components. Constant damping of 5% is assumed for response spectrum generation. These response spectra are then combined by taking the geometric mean of the spectral acceleration values for various periods. In other words, for a period T_i, the combined spectral acceleration is –

$$Sa(T_i) = \sqrt{Sa_1(T_i) \cdot Sa_2(T_i)} \tag{6.17}$$

Where $Sa(T_i)$ is the spectral acceleration value from the response spectrum of the first horizontal component at the period T_i, and $Sa_2(T_i)$ is the spectral acceleration value from the response spectrum of the second horizontal component at the period T_i. The acceleration response spectrum thus generated is then used to scale ground motions.

This research initially considered two scaling methods: Linear Scaling – Single Point (dubbed as Point Scaling) and Linear Scaling – Natural Period Range of $T_1 \pm 1$ sec (dubbed as Range Scaling). For point scaling, the spectral acceleration of the ground motion at the natural period of the column (T_1) is matched to the target response spectrum (acceleration UHS from USGS) for the target hazard. For range scaling, the scale factor is selected for which sum of squared errors between the target hazard spectrum and ground motion response spectrum ($e_i = \sum(S_{a,target} - S_{a,ground\ motion})^2$) is minimum. For the development of the maps, range scaling was used.

Validation of the ground motion simulation and scaling method used herein is needed before using the ground motions for NTHA. The validation is conducted by assessing the similarities/differences between secondary intensity measures (*SecIM*) of the simulated and scaled motions with SecIM models available in academic literature. To this end, a separate study was conducted to perform the validation; the process and results are presented in the next chapters of this report.

7 Model Validation

7.1 Validation of The Structural Model

The bridge column model, developed in OpenSees (details in Chapter 5), must be validated against existing research before further application. The model's behavior is expected to replicate that observed in physical tests, ensuring that key capacity parameters—such as yield, capacity, and stiffness—align with those calculated by Caltrans designers using in-house tools like xSECTION. This validation ensures that the demand parameters estimated in this study accurately reflect real-world bridge behavior while maintaining consistency with Caltrans design methods.

Lehman and Moehle (2000) investigated the performance of well-confined concrete bridge columns, which are equivalent to modern Caltrans bridge columns, under lateral loading. Their experiments involved multiple columns with varying longitudinal reinforcement ratios and aspect ratios, as detailed in Table 7-1. The same material properties—including concrete strength (4.5 ksi), reinforcing steel yield strength (67 ksi), and reinforcing steel ultimate strength (91.4 ksi)—were used to develop the OpenSees model for each column, as described in Chapter 5.

The lateral loading was applied following a monotonically increasing cyclic pattern, as illustrated in Figure 7-1. The experimental and simulated responses are compared in Figure 7-2, where it can be observed that the OpenSees model accurately captures the behavior of all four columns, closely matching the experimental results. This validation confirms the reliability of the OpenSees model for response analysis in this study.

Additionally, the capacity parameters obtained from the OpenSees model were compared with values derived from xSECTION models, as shown in Table 7-2. The comparison indicates that the OpenSees results are consistent with xSECTION calculations, further reinforcing the model's validity for estimating bridge column demand and capacity.

Table 7-1 Column Details from Lehman and Moehle (2000)

Col. Des.	Column Height (ft)	Column Diameter (ft)	Aspect Ratio	Axial Load (kips)	No. of Long. Rebars	Diameter of Long. Rebars (in)	Long. Reinf. Ratio (%)	Trans. Hoop Diameter (in)	Trans. Hoop Spacing (in)
415	8	2	4	147	22	0.625	1.5	0.25	1.25
430	8	2	4	147	44	0.625	3	0.25	1.25
815	16	2	8	147	22	0.625	1.5	0.25	1.25
1015	20	2	10	147	22	0.625	1.5	0.25	1.25

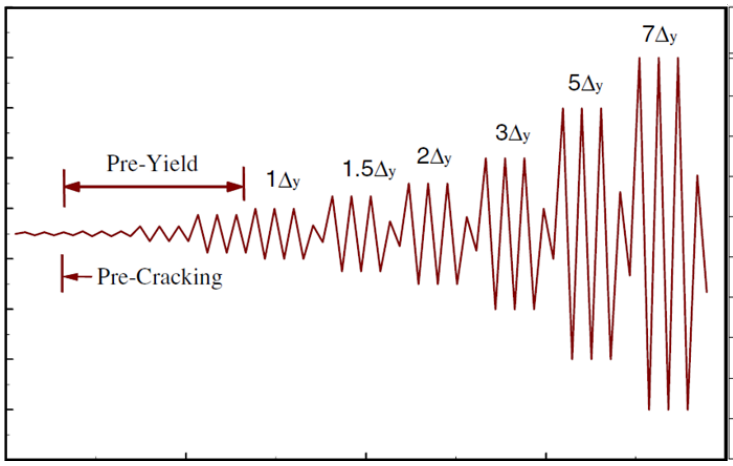

Displacement Level	L/D = 4	L/D = 8	L/D = 10
	0.06"	0.15"	0.2"
	0.15"	0.6"	0.8"
	0.3"		
First-Yield	0.75"	1.75"	2.5"
Δ_y	1"	3.5"	5"
$1.5\Delta_y$	1.5"	5.25"	7.5"
$2\Delta_y$	2"	7"	10"
$3\Delta_y$	3"	10.5"	15"
$5\Delta_y$	5"	17.5"	25"
$7\Delta_y$	7"		

Figure 7-1 Loading Protocol per Lehman and Moehle (2000)

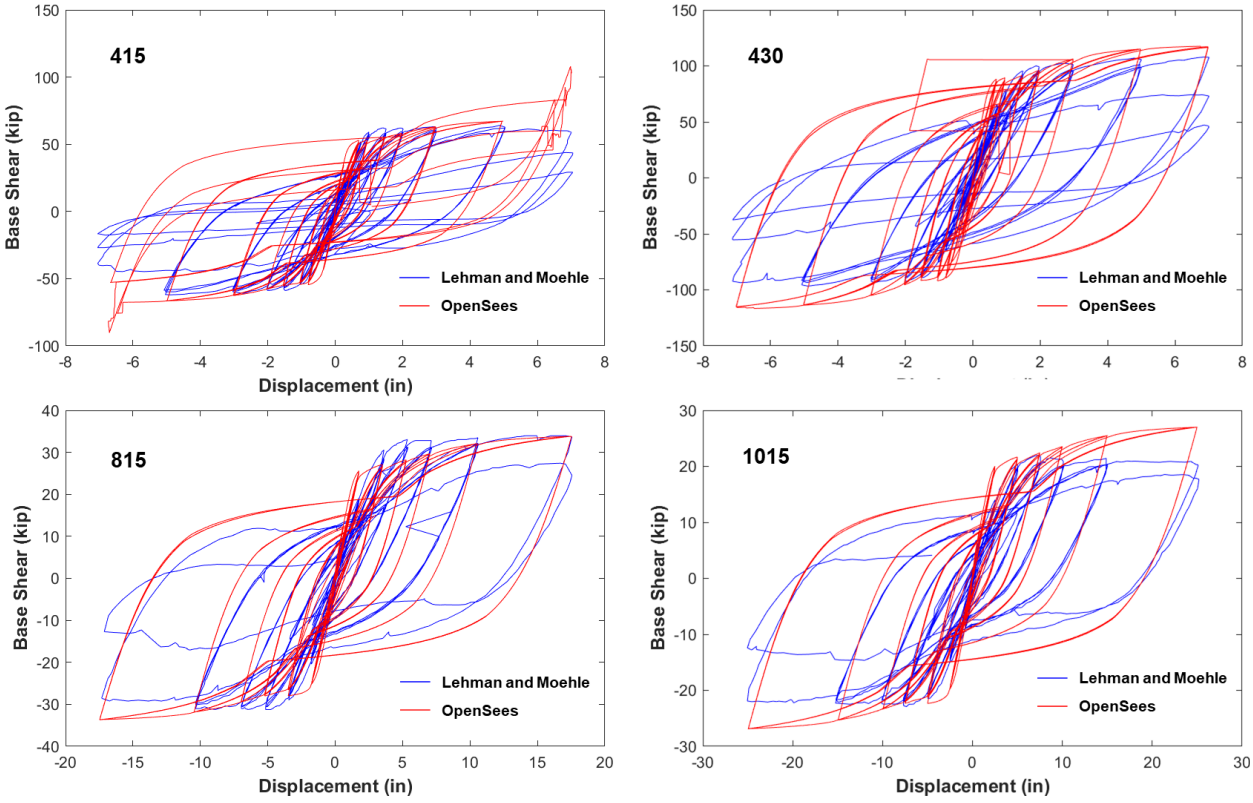

Figure 7-2 Cyclic Pushovers Comparison of OpenSees model to Lehman and Moehle (2000)

Table 7-2 Comparison of Capacity Parameters between OpenSees model and Lehman and Moehle (2000)

Col. Des.	Analysis Tool	Moment Capacity (kip-ft)	Capacity Curvature (rad/in)	Yield Curvature (rad/in)	Cracked Moment of Inertia (ft^4)
415	xSECTION	476.50	0.004151	0.000227	0.31
	OpenSees	491.00	0.004290	0.000236	0.32
430	xSECTION	785.60	0.003497	0.000244	0.47
	OpenSees	805.52	0.003473	0.000253	0.48
815	xSECTION	476.50	0.004151	0.000227	0.31
	OpenSees	491.00	0.004290	0.000236	0.32
1015	xSECTION	476.50	0.004151	0.000227	0.31
	OpenSees	491.00	0.004290	0.000236	0.32

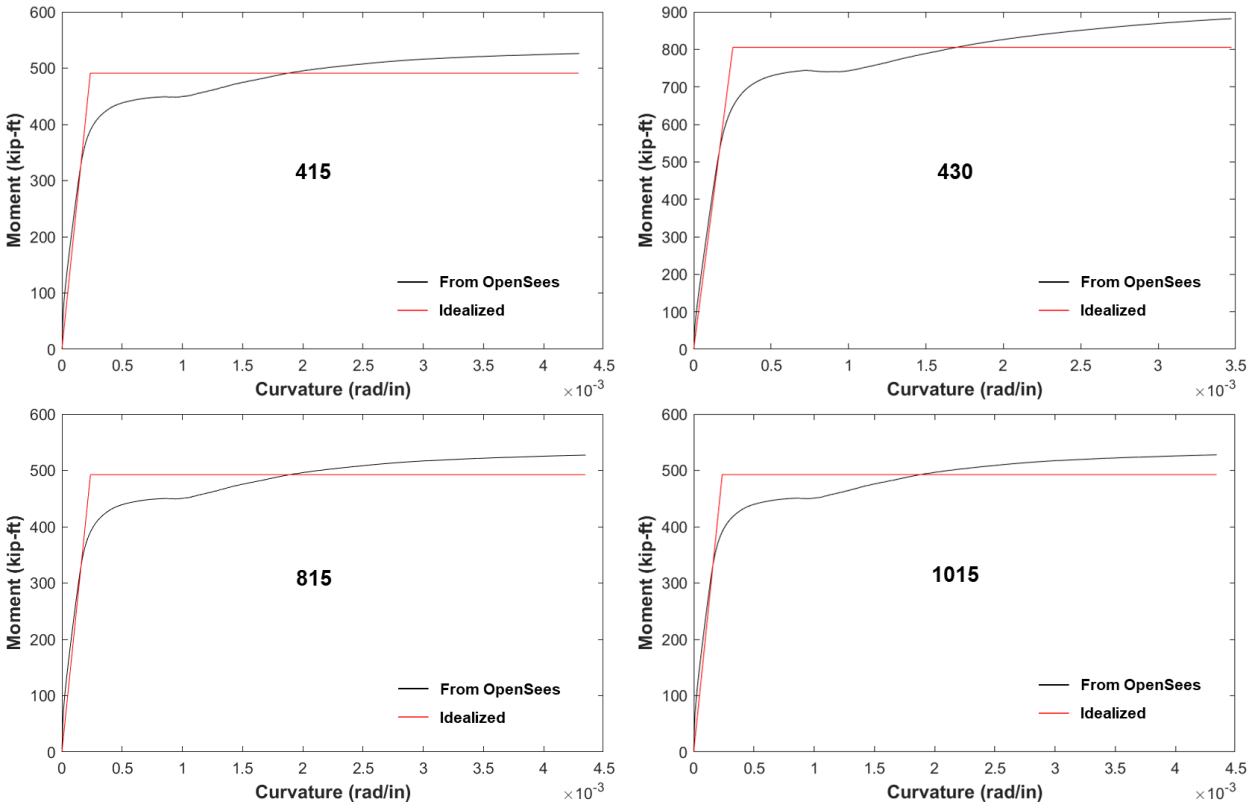

Figure 7-3 Moment-Curvature Curves for Test Columns

7.2 Validation of The Ground Motion Simulation Model

The simulated and scaled ground motions are expected to provide the intended intensity for the event, but their intensities must first be verified. The goal is to determine whether the ground motion simulation and scaling model produces a "realistic" ground motion time series. Here, the term "realistic" means that the generated ground motion series follows the trends observed in ground motion intensity measures (IMs) from past earthquakes.

The general approach for validation involves probabilistically assessing whether the secondary intensity measures (SecIMs) of the simulated and scaled ground motions align with peer-reviewed SecIM models. These models, developed by researchers, provide functional forms for the mean and standard deviation of SecIMs, conditioned on event parameters and a primary IM. Derived from historical earthquake data, these models offer an expected SecIM distribution for a given earthquake event.

This study evaluates six SecIMs: Peak Ground Acceleration (PGA), Peak Ground Velocity (PGV), Arias Intensity (AI), Cumulative Absolute Velocity (CAV), Significant Duration for 5-75% of Arias Intensity (D5-75), and Significant Duration for 5-95% of Arias Intensity (D5-95). The validation process is divided into three major steps:

1. *Assessing the Significance of SecIMs in Column Response*
   The first step determines which SecIMs influence bridge column response to seismic excitation. A linear regression model is used to describe column response as a function of SecIMs, and p-values are computed to assess significance. Any SecIM with a p-value greater than 0.05 (for a 5% significance level) is considered statistically insignificant in describing column response.

2. *Comparing SecIM Distributions with Peer-Reviewed Models*
   The second step evaluates whether the SecIM distribution from the simulated and scaled ground motion set (for a given event parameter set) aligns with peer-reviewed models. This is done by analyzing three key distribution features: mean, variance, and normality (at a 5% significance level).

   - The mean of SecIMs for the simulated and scaled ground motions is tested against the peer-reviewed model's estimated mean using a one-sample t-test.
   - The variance is checked using the Chi-squared variance test.
   - The Shapiro-Wilk Test is applied to assess whether ln(SecIM) from the simulated and scaled ground motions follows a lognormal distribution, as assumed in peer-reviewed models.

   In all three cases, the null hypothesis (H_0) states that the mean/variance matches that of the peer-reviewed model or that the distribution is normal. The null hypothesis is accepted if the test returns a p-value greater than 0.05.

3. *Validating Individual Ground Motion SecIMs Against Peer-Reviewed Distributions*

   The third and final step verifies whether SecIM values from individual ground motions fall within the peer-reviewed model's estimated distribution at a 5% significance level. This is assessed using a z-test, with the null hypothesis stating that the given SecIM value belongs to the expected distribution. The null hypothesis is accepted if the test returns a p-value greater than 0.05.

7.2.1 PEER-Reviewed Models for Secondary IM Conditioned on Event Parameters and a Primary IM

Several peer-reviewed models were used for the validation exercise. They are Abrahamson and Bhasin (2020) for PGV, Abrahamson et al. (2016) for Arias intensity, Macedo et al. (2021) for CAV, Silva et al. (1997) for significant durations, and ASK14 (Abrahamson et al, 2013) for PGA. These peer-revised models for SecIMs are conditional ground-motion models (CGMM) derived from the NGA-West2 (Bozorgnia et al, 2014) database. These peer-reviewed models estimate the mean and standard deviation value for a SecIM using a functional form shown in Equations (7.1) and (7.2).

$$\mu_{lnSecIM} = f\left(M, R, \theta, V_{S30}, Sa_{mean}(T)\right) \tag{7.1}$$

$$\sigma_{lnSecIM} = f\left(\sigma_{lnSa(T)}\right) \tag{7.2}$$

M, R, θ, and V_{S30} signify the event parameters, and $Sa(T)$ is the spectral acceleration on which SecIM is conditioned. (Please note that Equations 7.1 and 7.2 are just schematic equations and are not in the exact forms).

Estimates of the mean and variance of SecIM from peer-reviewed models are conditioned on the mean and variance of a spectral acceleration ($Sa(T)$), respectively. This condition requires having the best possible estimates of mean and variance for $Sa(T)$ for the event scenario. A surrogate for the best possible values can be estimated using one of the available NGA-West2 GMMs such as ASK14 (Abrahamson et al., 2013) for a given earthquake event scenario. However, these estimates cannot be labeled as best estimates for the event scenario, as ground motions are scaled based on the structures' natural period (T_n). As the SecIMs for the simulated and scaled ground motions are conditioned on $Sa(T_n)$, the estimates of the mean and variance of SecIM should be conditioned on $Sa(T_n)$, as shown in Equations (7.3) and (7.4).

$$\mu_{lnSecIM|Sa(T_n)} = f(M, R, \theta, \delta, V_{S30}, Sa_{med}(T)|Sa(T_n)) \tag{7.3}$$

$$\sigma_{lnSecIM|Sa(T_n)} = f\left(\sigma_{lnSa(T)|Sa(T_n)}\right) \tag{7.4}$$

The conditioning ($Sa(T)|Sa(T_n)$) can be achieved by utilizing the Conditional Mean Spectrum (CMS) introduced by Lin et al. (2013), where the conditioned mean and variance ($Sa(T)|Sa(T_n)$) is estimated based on ε calculated for $Sa(T_n)$. ε is the number of standard deviations by which a given ln (Sa) value differs from the predicted mean ln (Sa) value for a given magnitude and

distance. This ε is then modified to ε for other spectral periods using the correlation coefficient methodology for spectral accelerations by Baker and Jayaram (2008). The step-by-step guide for the estimation of conditioned spectral acceleration is as follows:

1. Estimate spectral acceleration value at the structure's natural period ($Sa(T_n)$) from the target UHS curve. Obtain the associated dominant event parameters (M, R, θ).

2. Calculate mean ($\mu_{lnSa(T)}(M, R, \theta, T_n)$) and standard deviation ($\sigma_{lnSa}(M, R, \theta, T_n)$) value for $lnSa(T_n)$) using one of the GMMs (ASK14 is used herein).

3. Calculate epsilon parameter ε for the spectral acceleration value at T_n using Equation (7.5)

$$\varepsilon(T_n) = \frac{lnSa(T_n) - \mu_{lnSa}(M, R, \theta, T_n)}{\sigma_{lnSa}(M, R, \theta, T_n)} \tag{7.5}$$

   Where $Sa(T_n)$ is the spectral acceleration value at the natural period of the column obtained from the UHS curve, $\mu_{lnSa}(M, R, \theta, T_1)$ and $\sigma_{lnSa}(M, R, \theta, T_1)$ are the mean and standard deviation values for $Sa(T_n)$ estimated using ASK14.

4. Calculate correlation coefficient $\rho(T, T_n)$ from Baker and Jayaram's (Baker and Jayaram, 2008) work.

5. Estimate the conditioned mean and standard deviation values for $Sa(T)$ as shown in Equations (7.6) and (7.7).

$$\mu_{lnSa(T)|lnSa(T_n)} = \mu_{lnSa(T)}(M, R, \theta, T) + \rho(T, T_n)\sigma_{lnSa}(M, \theta, T)\varepsilon(T_n) \tag{7.6}$$

$$\sigma_{lnSa(T)|lnSa(T_n)} = \sigma_{lnSa}(M, R, \theta, T)\sqrt{1 - \rho^2(T, T_n)} \tag{7.7}$$

6. Calculate mean ($\mu_{lnSecIM|Sa(T_n)}$) and standard deviation ($\sigma_{lnSecIM|Sa(T_n)}$) for SecIM using the PEER-reviewed models.

$$\mu_{lnSecIM|Sa(T_n)} = f(M, R, \theta, \delta, V_{S30}, Sa_{med}(T)|Sa(T_n)) \tag{7.8}$$

$$\sigma_{lnSecIM|Sa(T_n)} = f\left(\sigma_{lnSa(T)|Sa(T_n)}\right) \tag{7.9}$$

7. CMS is used to arrive at the best estimate of the mean and variance of SecIM distributions.

7.2.2 Data for GMM Validation

The validation exercise was conducted for two sets of ground motion – one set was simulated and scaled as per the methodology provided in Chapter 6; the second set was selected and scaled from the NGA-West2 database. NGA-West2 ground motions were included to have a reference point and also to see how simulated ground motions fare against the recorded ground motions. These

ground motions were selected for the given earthquake event scenario and scaled like how it is conducted for simulated ground motions. The calculation of mean and standard deviation for SecIM as per the peer-reviewed models and conditioned on $Sa(T_n)$ ($\mu_{lnSecIM|Sa(T_n)}$ and $\sigma_{lnSecIM|Sa(T_n)}$) as per the methodology suggested in the previous section. The validation exercise was conducted with the following limitations:

- Four locations were considered:
    - Eureka (Latitude = 40.790, Longitude = -124.179)
    - Oakland (Latitude = 37.800, Longitude = -122.280)
    - LA Downtown (Latitude = 34.050, Longitude = -118.259)
    - San Diego (Latitude = 32.724, Longitude = -117.158)
- Only one case of V_{S30} (259 m/sec) was considered.
- Only point scaling was considered. Point scaling forces a match between the spectral acceleration at the natural period ($Sa(T_n)$) to the target UHS and brings the most variation to the ground motion than range scaling. Moreover, CMS works best with point scaling.
- Three hazard levels are considered: 225-year, 975-year, and 2475-year average return period.
- Only two sets of columns were used for analysis for each location – with the natural period of 1 sec and 2 sec. The column details can be seen in Table 7-3. For this purpose, DI is computed directly from the force-deformation curve of the column, rather than relying on column section moment-curvature analysis, which would otherwise result in larger DI values. This approach ensures a more accurate representation of column performance under seismic loading.
- To simplify the verification process, it was decided to go for only the top three event scenarios (E1, E2, E3) obtained from hazard deaggregation by the USGS tool. The number of representative ground motions for each event was calculated using Equation (6.2), where the total number of ground motions for the given hazard was kept constant at 51.

Table 7-3 Column Properties for SecIM Sensitivity Check

Natural Time Period Model	Location	Column Height (ft)	Axial Load (% $f'_c A_g$)	Longitudinal Reinforcement (%)	Column Diamater (in)	Hoop Size (#)	Hoop Spacing (in)	Natural Time Period, T_n (sec)	DI_{ESA} 975 yr Hazard	D_{Dmd} for 975 yr Hazard	D_{Cpt} for 975 yr Hazard
1 Sec	Eureka	30	0.1	2.5	60	#6	5	1.08	0.32	3.83	4.95
	Oakland	30	0.15	1.75	84	#8	4	1.03	0.32	3.81	4.99
	LADT	30	0.1	1	96	#8	3	0.92	0.34	3.53	4.25
	SD	20	0.15	1	60	#7	6	1.06	0.30	2.76	3.47
2 Sec	Eureka	50	0.1	2.5	72	#5	5	1.92	0.32	3.31	4.39
	Oakland	40	0.15	1.75	72	#7	5	1.86	0.38	3.85	4.31
	LADT	50	0.1	1	96	#7	3	1.92	0.35	3.10	3.59
	SD	30	0.15	1	60	#6	5	1.86	0.30	2.53	3.14

For a given location, hazard level, and column's natural period, hazard deaggregation from the USGS hazard tool is conducted to obtain the top three event scenarios. Hence, the total number of event scenarios is 72 (4 locations (*LID*) × 3 hazards (*RP*) × 2 natural periods (T_n) × 3 event scenarios (*E*)). Two sets of ground motions are gathered for each event scenario – simulated ground motions from the Dabaghi (2014) model and selected ground motions from NGA-WEST2; both sets are scaled as per point scaling. The target UHS curve is obtained from the USGS hazard tool for the given hazard level. Once the ground motions are simulated/selected and scaled to the target level, their SecIM values are computed. Simultaneously, the mean and standard deviation are estimated for each SecIM using the peer-reviewed models (clubbed with CMS). Once all the ground motions and the corresponding SecIMs are generated, one can estimate the distribution statistics and compare them with the $\mu_{lnSecIM|\mathrm{LID}|Sa(T_1)|\mathrm{RP}|\mathrm{E}}$ and $\sigma_{lnSecIM|\mathrm{LID}|Sa(T_1)|\mathrm{RP}|\mathrm{E}}$ estimated using the peer-reviewed models.

7.2.3 Results and Conclusion

7.2.3.1 Sensitivity of Column Response to SecIM

After preparing the ground motions as mentioned in the previous section and calculating the SecIMs, we perform nonlinear time history analysis (NTHA) using those ground motions. First, the column response for each ground motion is recorded in the two horizontal directions and clubbed together using the vector combination. The maximum displacement (d_{max} *or* Δ_{max}) is then taken as the maximum absolute value for the combined vector displacement.

$$d_{max} \text{ or } \Delta_{max} = \max\left(\left|\sqrt{d_x^2 + d_y^2}\right|\right) \tag{7.10}$$

Where d_x is the displacement in the x-direction for a time step and d_y is the corresponding displacement in the y-direction for that time step.

The column drift ratio or drift (cdr) and the damage index (di) for the ground motion are calculated using Equations (7.11) and (7.12), respectively.

$$cdr = {\Delta_{max}}/{\Delta_y} \tag{7.11}$$

$$di = \frac{\Delta_{max} - \Delta_y}{\Delta_u - \Delta_y} \tag{7.12}$$

Where Δ_y and Δ_u are the column's yield displacement and ultimate displacement, respectively.

Usually, linear regression fitting for column response vs. a ground motion intensity measure is performed on a logarithmic scale. However, since di can have a value of less than 0, regression in a logarithmic scale is impossible for di. Therefore, two types of regression are checked – $ln\ (cdr)$ vs. $ln\ (SecIM)$ and di vs. $SecIM$. As mentioned earlier, the results are evaluated in *p*-values for a 5% significance level, i.e., if the *p*-value is more than 0.05, then the coefficient for the SecIM term in the regression model can be assumed to be 0.

For each location (*LID*), hazard level (*RP*), and natural period (T_n), a vector of column responses, denoted as *CDR* and *DI* for drifts and damage indices, respectively, and the secondary IMs (*SecIM*) (Equations 7.13 and 7.14) are developed. These vectors are then used for linear regression. Note that linear regression is conducted for a target hazard. Since 51 ground motions represent each hazard level, the vector lengths for *CDR*, *DI,* and *SIM* are 51.

$$\begin{gathered} ln(CDR) = [\ln(cdr_1)\ \ln(cdr_2)\ \cdots\ \ln(cdr_n)]^T \\ vs \\ ln(SecIM) = \left[[\ln(SecIM_1)\ \ln(SecIM_2)\ \cdots\ \ln(SecIM_n)\right]^T \end{gathered} \tag{7.13}$$

$$\begin{gathered} \mathrm{DI} = [\ di_1\ di_2 \cdots\ di_n]^T \\ vs \\ SecIM = [SecIM_1\ SecIM_2\ \cdots SecIM_n]^T \end{gathered} \tag{7.14}$$

The inference from estimated *p*-values of linear regression for the SecIM terms is shown in Figure 7-5 to Figure 7-8. *p*-values greater than 0.05 signify column responses' insensitivity to that SecIM. From the figures, it can be seen that column responses are consistently sensitive to PGV. In addition, there are hints of sensitivity to CAV, AI, and the two durations ($D_{5\text{-}75}$ and $D_{5\text{-}95}$), but only consistent sensitivity can be seen to PGV. Moreover, this was seen for both NGA-West2 ground motions and the simulated and scaled ground motions used in this study. From this, a conclusion was made that the column models have responses sensitive to the secondary IM of PGV.

7.2.3.2 Comparison Between the Distribution of SecIM and Peer-Reviewed Models

The next step is to evaluate the similarity between the SecIM distributions and their respective peer-reviewed models. For each of the 72 earthquake events, the mean and standard deviation of each SecIM are computed from the simulated and scaled ground motions (or the selected NGA-West2 ground motions). These values are then compared against the corresponding mean and

standard deviation estimated from the peer-reviewed models ($\mu_{lnSecIM|Sa(T_1)}$ and $\sigma_{lnSecIM|Sa(T_1)}$) from the peer-reviewed models.

To assess these differences, a One-Sample *t*-test is used for comparing means, while a Chi-squared variance test is applied to compare variances. Since the Chi-squared test compares variances rather than standard deviations, the estimated standard deviations are first squared before conducting the test. Additionally, the Shapiro-Wilk test is used to examine whether the *ln*(SecIM) distribution from ground motions follows a normal distribution, as expected for a lognormal SecIM distribution. All three tests return a binary result (0 or 1) at a 5% significance level. A result of 0 indicates acceptance of the null hypothesis (H_0 is true), while a result of 1 signifies rejection of the null hypothesis (H_0 is false).

- For the mean and variance tests, the null hypothesis states that the mean and variance of SecIMs from the ground motion set and the peer-reviewed models are equal.
- For the normality test, the null hypothesis states that the ln(SecIM) distribution follows a normal distribution.

Figures 7-9 and 7-10 illustrate the results of these hypothesis tests for NGA-West2 ground motions and simulated/scaled ground motions, respectively. The results show that for variance and normality tests, the null hypothesis holds true in most cases for both NGA-West2 and simulated ground motions. However, for the mean tests, the null hypothesis is mostly false, indicating a significant difference between the mean SecIM values from ground motions and those predicted by peer-reviewed models.

7.2.3.3 Comparison of SecIM with equivalent peer-reviewed models

The SecIM distributions for the simulated and scaled ground motions (as well as the NGA-West2 ground motions) do not fully align with the distributions from peer-reviewed models. To address this discrepancy, it was decided to ensure that the SecIM values of the ground motions in each set adequately cover the expected range from peer-reviewed models. Specifically, no more than 5% of the ground motions should have SecIM values outside the 5% significance level of the peer-reviewed models for each earthquake event scenario. The proportion of ground motions with SecIM values within this range is reported at the hazard level in Tables 7-4 and 7-5. Values highlighted in green indicate cases where more than 50% of ground motions satisfy this criterion, signifying that the majority of ground motions align with the 5% significance level of peer-reviewed models.

The NGA-West2 ground motions appear to perform better than the simulated and scaled ground motions in terms of individual SecIM values. For simulated and scaled ground motions, the proportion of PGA, CAV, and AI values within the 5% significance level of peer-reviewed models is relatively low. However, this discrepancy can be practically disregarded, as the column models exhibit low sensitivity to these SecIMs.

In the case of PGV, which was found to carry meaningful information regarding column response, most of the simulated and scaled ground motions have PGV values within the expected range.

While the overall PGV distributions do not exactly match those from peer-reviewed models, the average PGV values for most cases fall within the 5% significance level of the mean PGV value suggested by peer-reviewed models.

These findings indicate that simulated and scaled ground motions from the Dabaghi (2014) model can be used under the following two conditions: a) The average PGV of the simulated and scaled set for a given earthquake event scenario should fall within the 25%-75% confidence interval of the peer-reviewed model for PGV, and b) PGV values for individual ground motions should fall within the 5%-95% confidence interval of the peer-reviewed model for PGV.

7.2.3.4 Validation of SecIM for The Simulated and Scaled Ground Motion Set with Equivalent Peer-Reviewed Models

The within-event residuals were analyzed to assess the validity of the simulated and scaled ground motions based on this study's model. Since PGV was identified as the most important secondary intensity measure (SecIM) for this study, the analysis was conducted exclusively for PGV. The Abrahamson and Bhasin (2020) conditional model for PGV has a functional form as –

$$\begin{aligned} ln(PGV) = a_1 + f_1(M)\, ln[PSA(T_{PGV})] + a_4(M-6) \\ + a_5(8.5-M)^2 + a_6\, ln\left[R_{RUP} + 5e^{0.4(M-6)}\right] \\ + [a_7 + a_8(M-5)]\, ln\left(\frac{V_{S30}}{425}\right) + \delta B + \delta W \end{aligned} \tag{7.15}$$

$$\sigma^2_{lnPGV} = f_1^2(M)\sigma^2_{lnPSA(T_{PGV})} + \sigma^2_{lnPGV|PSA(T_{PGV})} \tag{7.16}$$

in which M is the moment magnitude, R_{RUP} is the rupture distance in kilometers, the PSA is the 5% damped spectral acceleration in g, V_{S30} is the time-averaged shear-wave velocity over the top 30 m in m/sec, and δB and δW are the between-event and within-event residuals, respectively. $\sigma_{lnPGV|PSA(T_{PGV})}$ is 0.33.

The PGV conditional model indicates that PGV values are conditioned on the spectral acceleration (PSA) at T_{PGV}, $PSA(T_{PGV})$, which is magnitude-dependent. Consequently, the distribution of PGV for a given ground motion set is inherently conditioned on the distribution of $PSA(T_{PGV})$. To evaluate the within-event residuals, the $PSA(T_{PGV})$distribution parameters were derived from the observed values in the ground motion set (Figure 7-4). The residuals were found to be centered around zero and exhibited no dependency on $PSA(T_{PGV})$.

In conclusion, the ground motion model used in this study is consistent with the PGV conditional model, validating its applicability for this analysis.

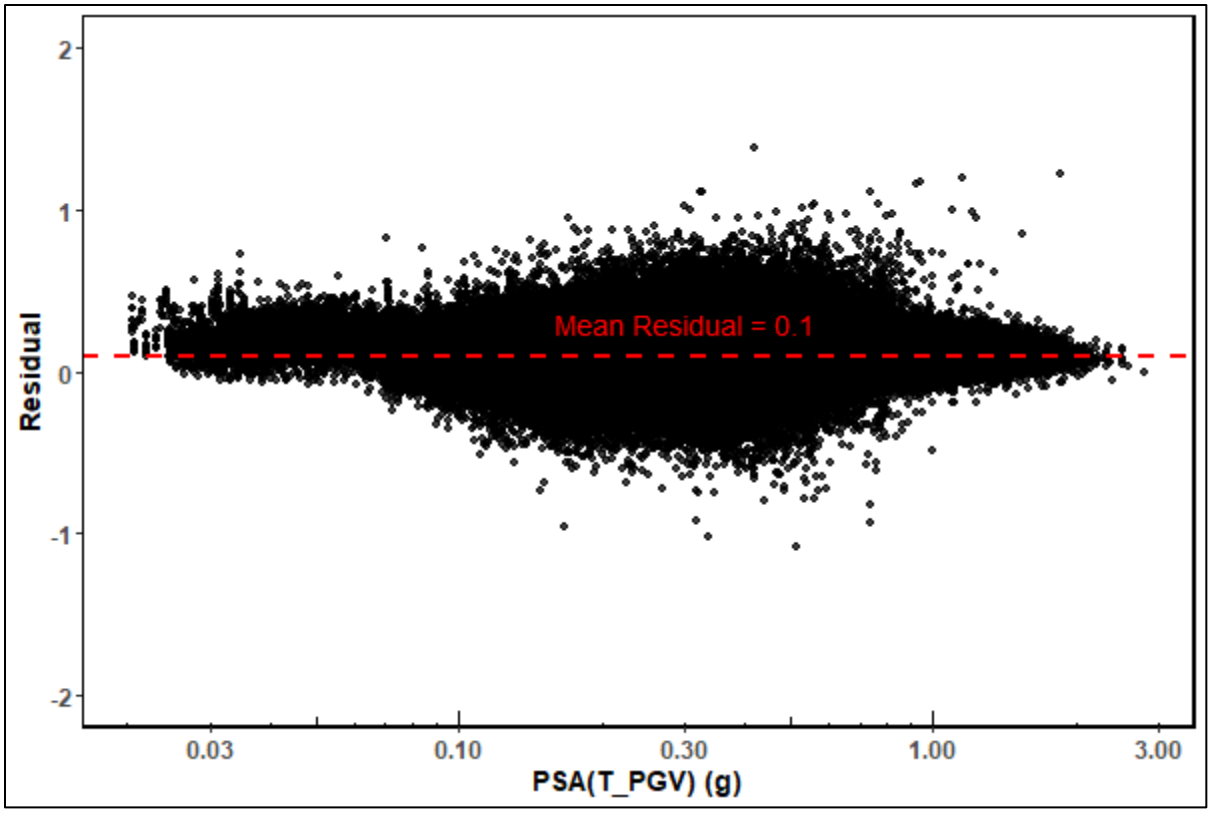

Figure 7-4 PSA(T_{PGV}) Dependency of Within-Event Residuals

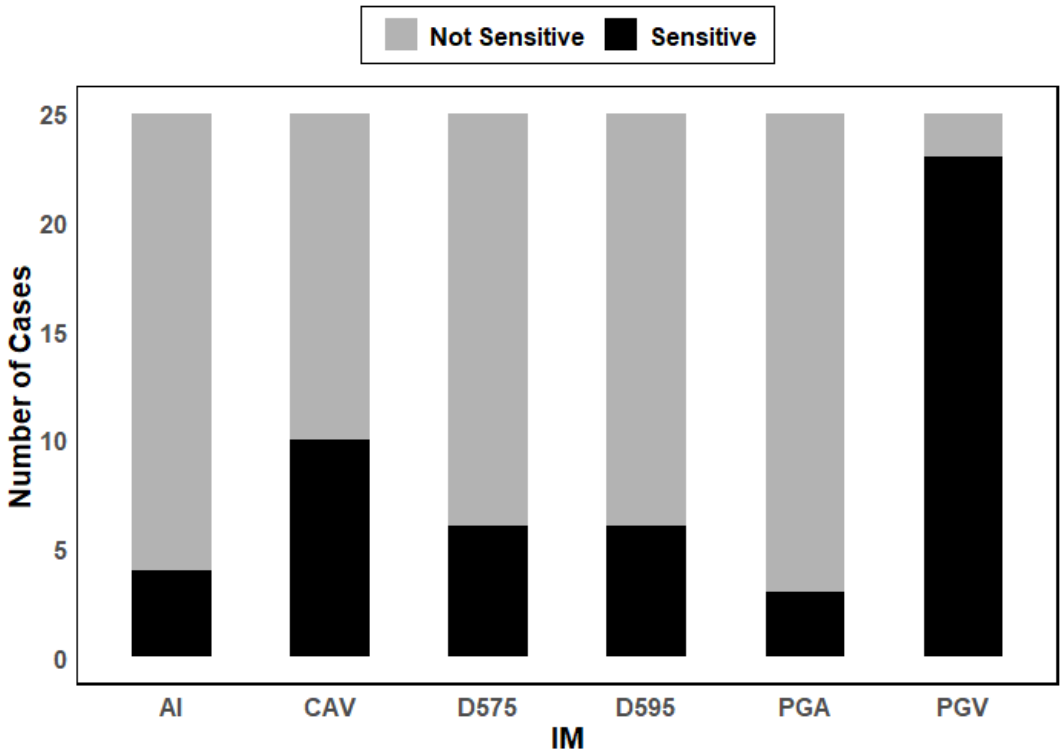

Figure 7-5 Sensitivity of *DI* to *SecIM* for NGA-WEST2 Ground Motions

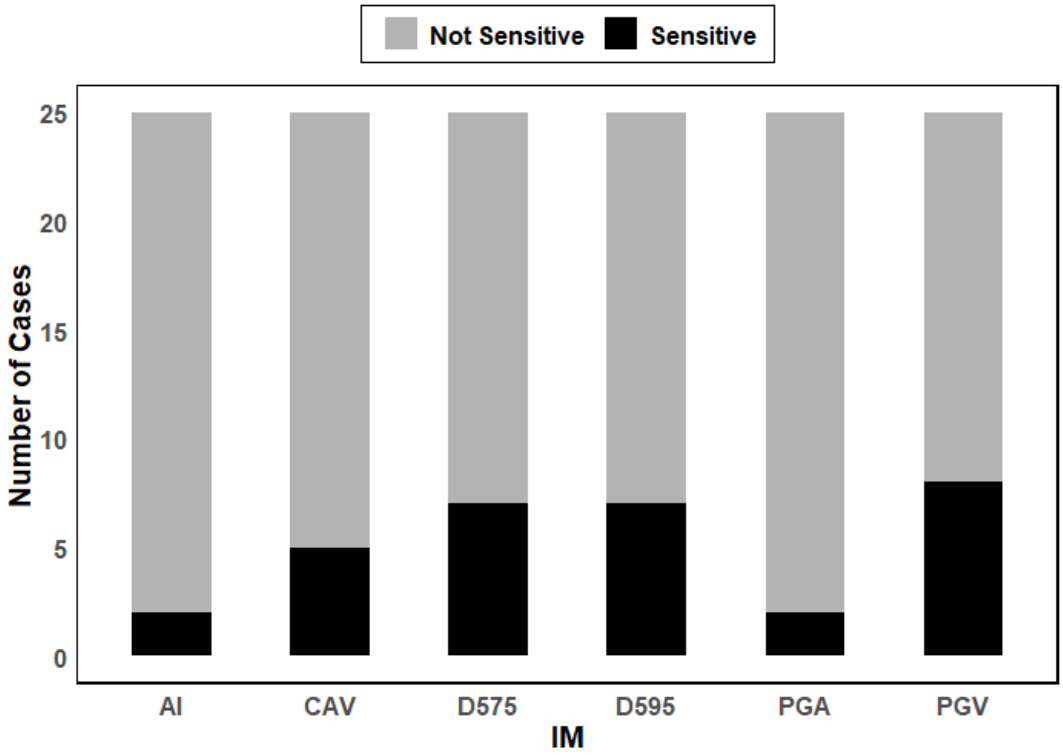

Figure 7-6 Sensitivity of *DI* to *SecIM* for Simulated Ground Motions

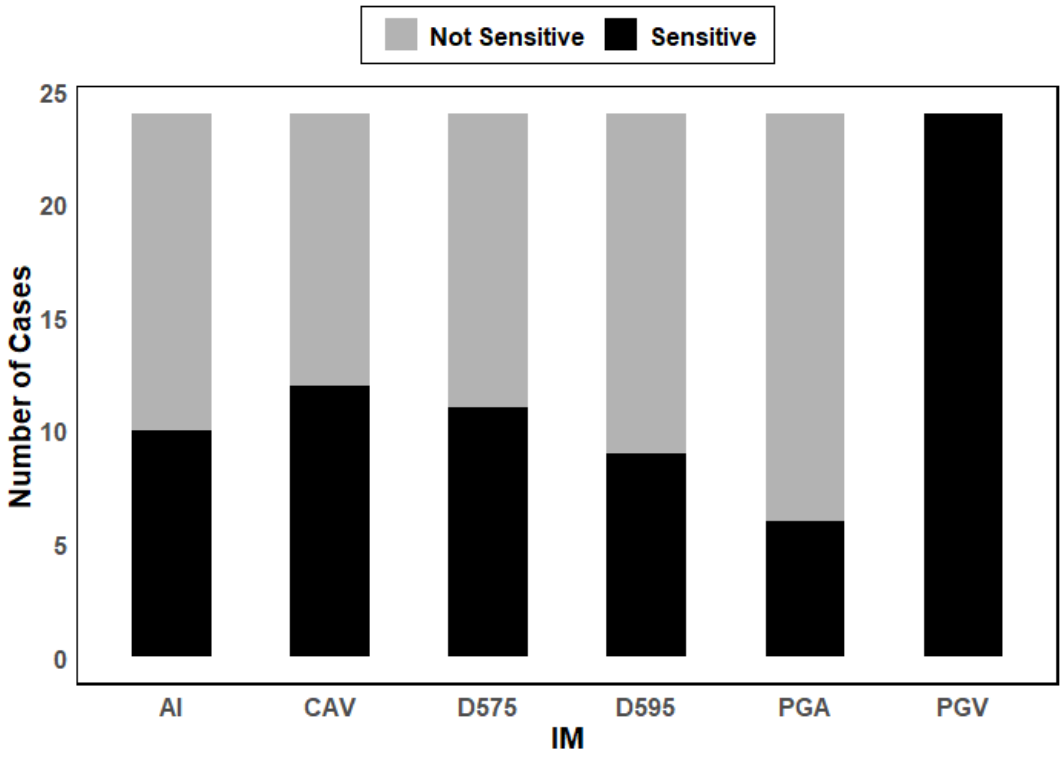

Figure 7-7 Sensitivity of *ln*(*CDR*) to *ln*(*SecIM*) for NGA-WEST2 Ground Motions

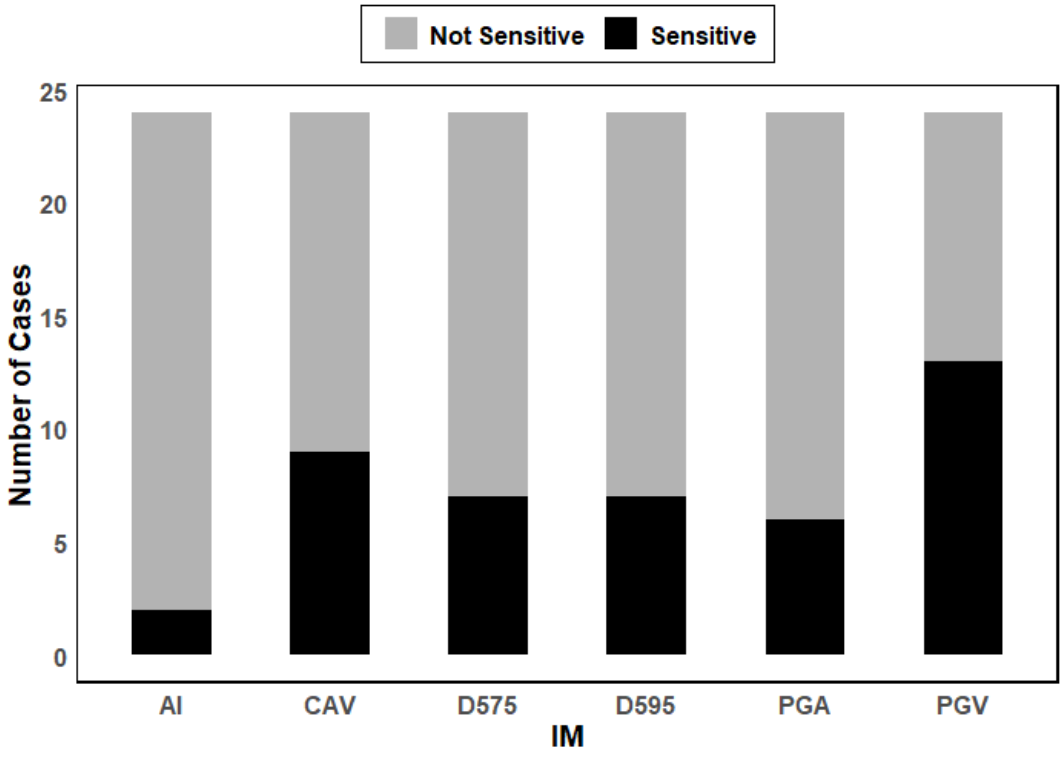

Figure 7-8 Sensitivity of *ln*(*CDR*) to *ln*(*SecIM*) for Simulated Ground Motions

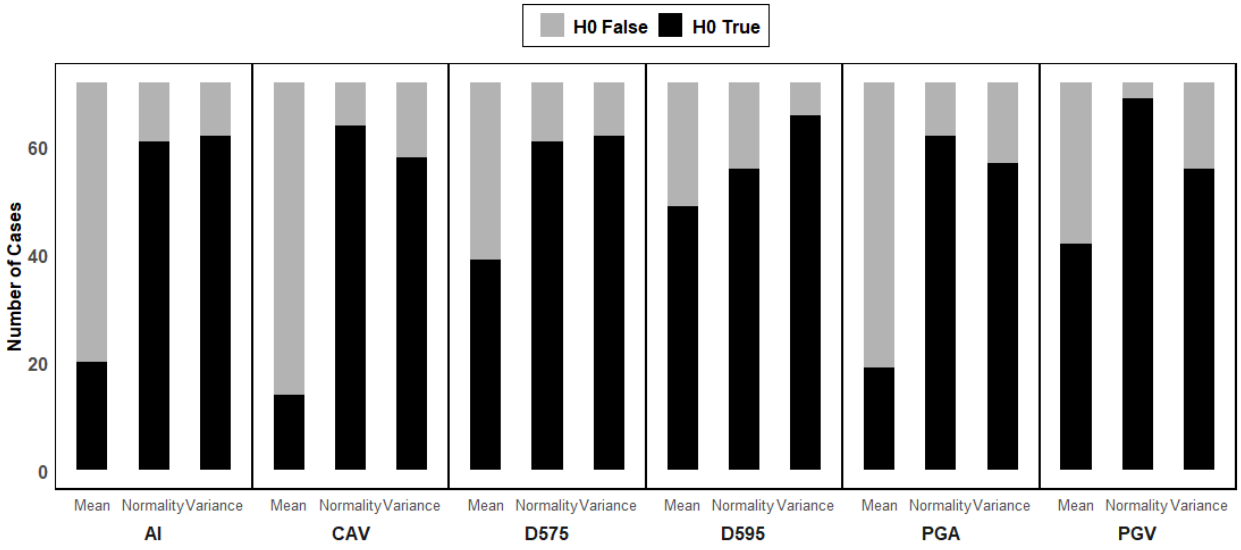

Figure 7-9 Mean, Normality and Variance Tests for NGA-WEST2 Ground Motions

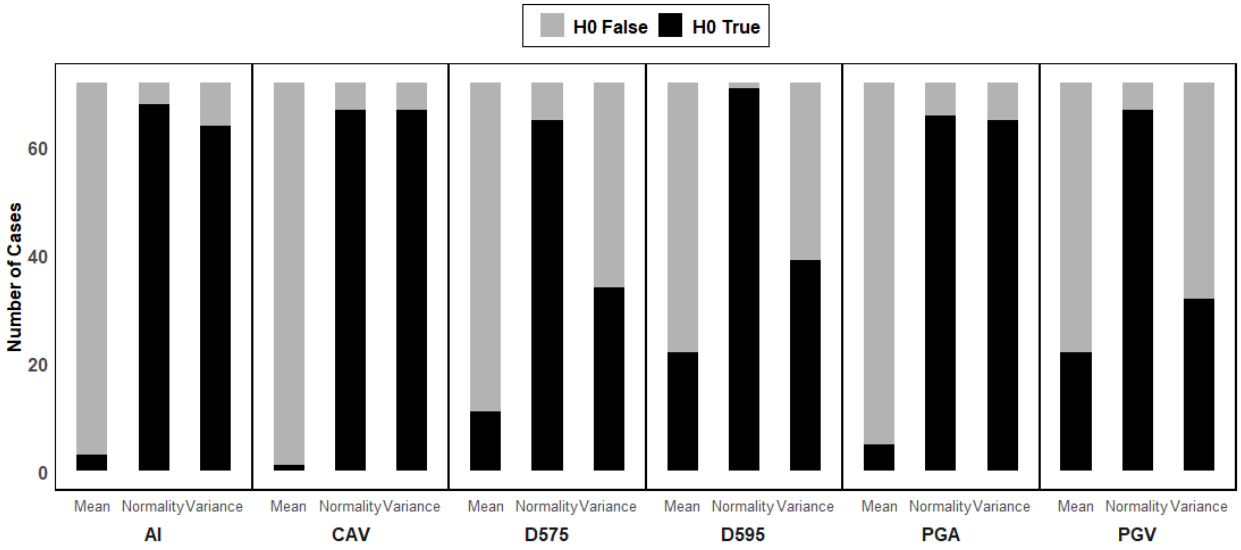

Figure 7-10 Mean, Normality and Variance Tests for Simulated Ground Motions

Table 7-4 *SecIM*s within PEER-Reviewed Models for NGA-WEST2 Ground Motions

		T_n = 1 sec						T_n = 2 sec					
		PGA	CAV	AI	PGV	D575	D595	PGA	CAV	AI	PGV	D575	D595
Eureka	225-year	88.2	49.0	82.4	98.0	68.6	70.6	82.4	72.5	82.4	94.1	76.5	88.2
	975-year	52.9	31.4	41.2	90.2	66.7	66.7	66.7	27.5	47.1	78.4	60.8	64.7
	2475-year	47.1	17.6	15.7	78.4	64.7	64.7	43.1	15.7	17.6	54.9	60.8	62.7
Oakland	225-year	78.4	45.1	74.5	100.0	68.6	82.4	82.4	51.0	76.5	90.2	70.6	82.4
	975-year	64.7	33.3	43.1	90.2	74.5	76.5	60.8	27.5	45.1	82.4	70.6	78.4
	2475-year	51.0	27.5	35.3	88.2	78.4	78.4	39.2	21.6	25.5	70.6	74.5	78.4
LA Downtown	225-year	90.2	66.7	92.2	100.0	74.5	70.6	90.2	58.8	90.2	100.0	70.6	62.7
	975-year	80.4	70.6	76.5	100.0	88.2	88.2	23.5	60.8	47.1	100.0	58.8	35.3
	2475-year	45.1	52.9	62.7	94.1	88.2	90.2	52.9	60.8	58.8	82.4	88.2	88.2
San Diego	225-year	56.9	82.4	94.1	82.4	45.1	43.1	62.7	82.4	78.4	98.0	49.0	43.1
	975-year	90.2	90.2	100.0	90.2	90.2	84.3	92.2	84.3	90.2	96.1	82.4	84.3
	2475-year	49.0	74.5	78.4	100.0	86.3	84.3	82.4	80.4	86.3	96.1	86.3	86.3

Table 7-5 *SecIM*s within PEER-Reviewed Models for Simulated Ground Motions

		T_n = 1 sec						T_n = 2 sec					
		PGA	CAV	AI	PGV	D575	D595	PGA	CAV	AI	PGV	D575	D595
Eureka	225-year	54.9	15.7	35.3	94.1	56.9	52.9	66.7	17.6	49.0	80.4	54.9	52.9
	975-year	29.4	0.0	3.9	82.4	52.9	52.9	35.3	2.0	2.0	23.5	47.1	43.1
	2475-year	17.6	0.0	0.0	70.6	47.1	43.1	21.6	0.0	0.0	13.7	49.0	49.0
Oakland	225-year	27.5	3.9	15.7	100.0	70.6	74.5	31.4	2.0	15.7	68.6	66.7	66.7
	975-year	37.3	5.9	11.8	92.2	41.2	39.2	27.5	0.0	13.7	66.7	56.9	58.8
	2475-year	9.8	0.0	0.0	78.4	51.0	51.0	2.0	0.0	0.0	29.4	60.8	62.7
LA Downtown	225-year	41.2	15.7	29.4	98.0	70.6	70.6	62.7	29.4	45.1	90.2	60.8	58.8
	975-year	21.6	21.6	23.5	100.0	98.0	96.1	0.0	7.8	2.0	82.4	74.5	54.9
	2475-year	17.6	9.8	17.6	98.0	96.1	90.2	13.7	11.8	11.8	52.9	100.0	96.1
San Diego	225-year	21.6	58.8	41.2	100.0	72.5	51.0	23.5	68.6	39.2	100.0	74.5	62.7
	975-year	35.3	39.2	51.0	100.0	96.1	96.1	72.5	72.5	74.5	98.0	96.1	90.2
	2475-year	9.8	9.8	11.8	100.0	100.0	96.1	45.1	39.2	41.2	96.1	98.0	98.0

8 Results and Discussion

The Nonlinear Time History Analysis (NTHA) of bridge column models produces two horizontal displacement components—longitudinal ($d_{x,i}$) and transverse ($d_{y,i}$)—at the column's top node for each time step i. The primary displacement demand of interest in this study is the maximum transverse displacement over the entire ground motion duration, considering all possible ground motion orientations. However, since the bridge column model used in this study is uniform in all directions, it is not necessary to rotate the ground motion to determine the orientation with the highest displacement demand. Instead, a hypothetical direction can be assumed, where the displacement is represented by the vector sum of the longitudinal and transverse components. This approach is equivalent to identifying the ground motion orientation that results in the maximum transverse displacement (further details are provided in Appendix B).

At each time step, the longitudinal and transverse displacement components are combined in vector form, and the maximum displacement (d_{max} or Δ_{max}) is defined as the largest absolute value of the resultant vector displacements across all time steps. Using this estimated d_{max}, the damage index (DI) for the given column and ground motion is then computed, as defined in Equation (8.2).

$$d_{max}\ or\ \Delta_{max} = \max\left(\left|\sqrt{d_{x,i}^2 + d_{y,i}^2}\right|\right) \tag{8.1}$$

$$DI = \frac{\Delta_{max} - \Delta_y}{\Delta_u - \Delta_y} \tag{8.2}$$

The CT-RBSD approach assumes that the DI follows a lognormal distribution as a random variable. This assumption was qualitatively examined using raw DI values obtained for high and extreme ground motion hazard levels across a selected set of locations (see Figure 8-1). The figure further illustrates that, depending on the value of Δ_{max}, DI can occasionally take values below 0 or above 1, particularly in low ground motion hazard scenarios.

Since DI is assumed to be lognormally distributed, values less than 0 are not compatible with this assumption. To address this issue, a logical correction was applied. A DI value below 0 indicates that the column has not yet reached its yield point, and can therefore be reasonably set to DI = 0. Conversely, a DI value exceeding 1 suggests that the column has surpassed its ultimate capacity, effectively indicating failure, and can thus be set to DI = 1.

Additionally, OpenSees, the structural analysis software used in this study, sometimes produces excessively large displacement values during column failure, leading to highly skewed distributions. To mitigate this issue, a post-processing method termed "Full Clubbing" was implemented. Various post-processing techniques were evaluated based on their impact on probability of exceedance, which is the primary focus of CT-RBSD. Full Clubbing was selected

as the most logically sound approach, as endorsed by the review team. For a detailed discussion of this methodology and its evaluation, readers are referred to Appendix A.

To understand the maps better, there are some key points to remember –

- These maps are categorized based on the two important parameters:
    - The V_{S30} used for analysis – 259 m/s and 537 m/s.
    - The hazard levels – 225-yr, 975-yr, and 2475-yr return period.
- The DI_L demand parameters are estimated per the Full-Clubbing post-processing method, including the adjustment factor. If the displacement demand from NTHA is more than the capacity displacement, it is considered equal to the capacity displacement. This helps disregard any numerical skewness while maintaining the fact that the ground motion caused collapse.
- For locations with low seismicity (like locations across Central Valley) to the extent that none of the column designs passed the 0.3 DI design limit per the CT-RBSD design criteria, a representative column, along with all its hoop arrangements, was selected to be analyzed for these locations (Table 8-1).

Table 8-1 Column Designs for The "Special" locations

Column Height (ft)	Axial Load (% f'_cA_g)	Column Diameter (ft)	Longitudinal Reinforcement (%)	Hoop Size (#)	Hoop Spacing (in)	Natural Time Period (sec)
20	0.15	5	1.75	5, 6, 7, 8	4, 5, 6, 7, 8	0.8

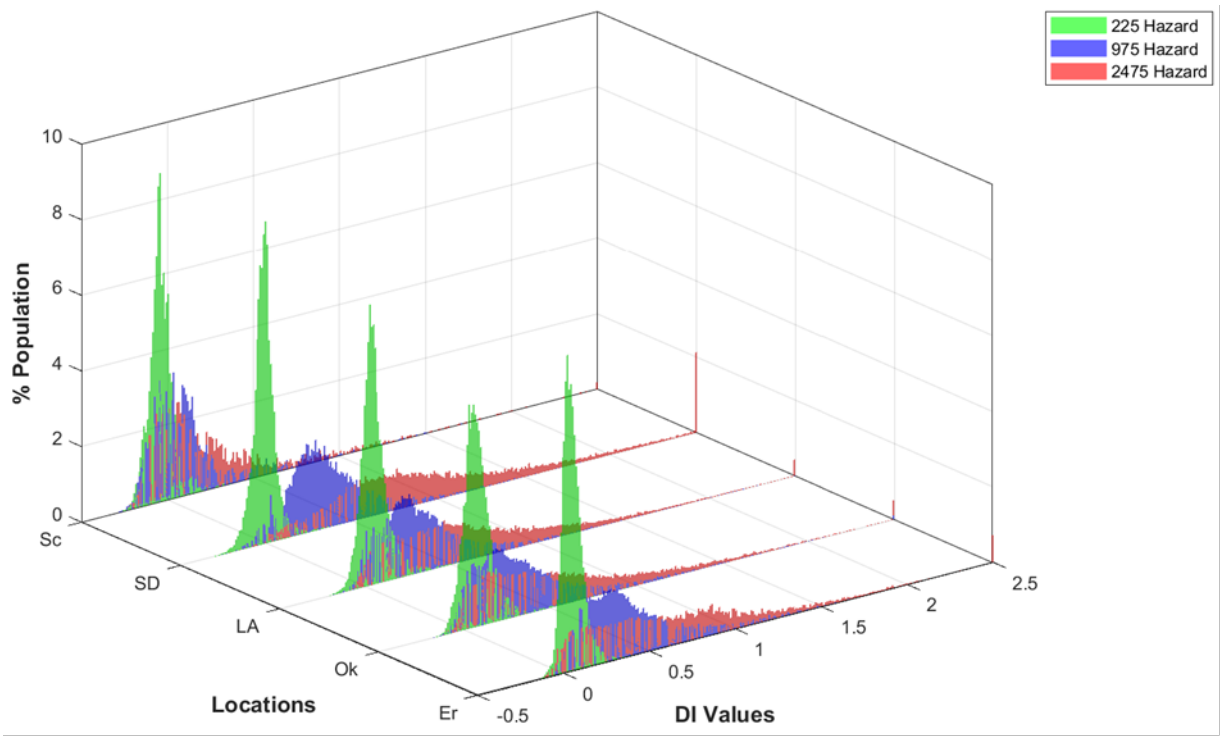

'Er' = Eureka (Latitude = 40.790, Longitude = -124.179); 'Ok' = Oakland (Latitude = 37.800, Longitude = -122.280); 'LA' = Los Angeles (Latitude = 34.050, Longitude = -118.259); 'SD' = San Diego (Latitude = 32.724, Longitude = -117.158); 'Sc' = Sacramento (Latitude = 38.577, Longitude = -121.494)

Figure 8-1 DI_L Distribution for DI_{ESA} between 0.3 and 0.4, and V_{S30} = 259 m/s

8.1 DI_L Parameters

The maps of δ_L (DI_L coefficient of variation) and φ_L (nonlinear adjustment factor for demand displacement) for a 25x25-mile grid of California are presented from Figure 8-2 to Figure 8-7 and Figure 8-20 to Figure 8-25, respectively. For high-importance regions of the Bay Area and Southern California, the grid was refined to 5x5-mile and contour maps were developed using the widely used spatial interpolation method, universal kriging. These contours are presented in Figure 8-8 to Figure 8-19 and Figure 8-26 to 8-37.

8.1.1 δ_L Estimates

The DI_L maps presented here provide a good insight into the variation of DI_L parameters not just over locations of California, but also for the changes in site class (or V_{S30}) and hazard level. To give bridge designers an extensive set of parameters needed to study bridge designs as per CT-RBSD, two separate sets of maps were generated by considering all the locations uniformly as either site class D or C. Since site class D corresponds to higher seismicity, μ_L and σ_L were seen to be higher for V_{S30} of 259 m/s, regardless of the hazard level or the design group considered. Similarly, δ_L was seen to be lower for 259 m/s than the 537 m/s V_{S30} case. An expected trend was observed in the case of hazard level as well. μ_L and σ_L increase with the increase in hazard level,

regardless of the category considered. The increase in σ_L was observed to be less than the increment observed in μ_L, and this translated to a decrease in δ_L with the increase in hazard level. Further research and analysis are needed to understand any other trend seen in the maps.

8.1.2 φ_L Estimates

At the inception of CT-RBSD, the mean demand DI parameter (μ_L) used in the reliability integral was left open for estimation as felt suitable by the designer. It was left to the bridge designer to opt for a method (like SDC2.0's ESA method) or take an alternative route of using a set of ground motions to estimate a μ_L for the bridge in question. The ESA estimated DI assumes linear elastic behavior by the column and does not factor in the nonlinear behavior during an earthquake event, while the other method of μ_L estimation by conducting NTHA of the column for a set of ground motions is an extremely time- and effort-extensive process. To sum up, there needs to be a method by which the designer can best estimate the μ_L value for the column at that specific location, using the data generated in the CT-RBSD study.

A suggested method to estimate $\mu_L$would be to calculate the elastic displacement for the column, i.e., D_{ESA}, and amplify it using a pre-defined adjustment factor that includes the effect of the column's nonlinearity and the location's seismicity. This approach is relatively simple to implement and will provide the designer with complete autonomy in their approach to estimate μ_L. From the data generated in this study, the observed adjustment (φ) for a ground motion response can be estimated as in Equation (8.3). For a given hazard and location, the average of all possible column designs' median adjustment factors (φ_L) is taken as the representative value. The designer can read this value from the maps and use it per Equation (8.4) to get the mean demand (μ_L).

$$\varphi = \frac{D_D}{D_{ESA}} \tag{8.3}$$

$$\mu_L = \frac{\varphi_L \times \Delta_{ESA} - \Delta_y}{\Delta_u - \Delta_y} \tag{8.4}$$

Where D_D is the observed displacement and D_{ESA} is the displacement estimated as per the ESA method. The adjustment is performed at the displacement level and not on the DI level to ensure no numerical issue arises during the estimation of φ. As often observed, the DI_L as well as the DI_{ESA} value for a 225-year hazard level can be low, which may cause numerical errors in the estimation of φ.

The maps for φ_L are provided in Figure 8-20 to Figure 8-37, in a manner similar to δ_L maps. Although δ_L maps showed a trend with respect to hazard level and site class, the φ_L maps did not result in any such trend. However, an acute trend of φ_L values more than 1 were observed at multiple locations irrespective of the hazard level and the site class. This signifies that moving away from the equal displacement rule assumption would make sense since the nonlinear displacement on average is more than the elastic displacement. Since the elastic demand is usually lower than the nonlinear demand, using elastic demand will underestimate the probability of

exceeding a damage state. In general, a bridge designer may prefer a slight overestimation rather than an underestimation of any performance demand parameter. Hence, using nonlinear displacement would be more beneficial to closely replicate the performance of a bridge. Using the φ_L parameter provided in this report will help simplify this issue to a great extent. An example of how to use the adjustment factor and COV parameter for the design and assessment of a bridge is provided in the upcoming section.

8.1.3 Application of The Proposed Maps

To demonstrate the use of the demand statistical parameter maps provided in this report, the risk of exceeding DS5 in 75 years (bridge's lifespan) for a set of columns was evaluated using the maps. The column details and the corresponding site details are provided in Table 8-2. The columns are selected such that they satisfy the design criteria of SDC2.0. In other words, the columns were assumed to be first designed per the SDC2.0 criteria and were evaluated for their performance using the CT-RBSD approach. The approach would need the designer to estimate the pushover curve for the column using two different methods – the CT-RBSD method where the ultimate hoop strain is 0.18; and the SDC2.0 method where the ultimate hoop strain is 0.09. The SDC pushover will be used to design the column per SDC2.0 criteria, whereas the CT-RBSD pushover will go into its assessment as per CT-RBSD.

To calculate the risk of exceeding DS5 in 75 years, a fragility curve for DS5 was integrated over the hazard curve as suggested in Chapter 3. The fragility curve was estimated by fitting a cumulative lognormal distribution with exceedance probabilities as the representative cumulative densities, and their respective hazard spectrum spectral accelerations as the quantiles. To estimate risk per the maps, the hazard-specific probabilities of exceedance were calculated with δ_L directly coming from the maps, while μ_L estimated per the previous section (Table 8-4). The ESA displacement demand for the three hazard levels was calculated for each of these columns per the methodology provided in Chapter 5. The φ_L and the δ_L values were read from the maps for the site class (V_{S30}), hazard level, and DI design group corresponding to the column. The μ_L for each hazard level was then calculated using Equation 8.4. The map estimated risks were compared to the risk estimated per the NTHA results to prove the effectiveness of the said procedure. As seen in Table 8-6, the risk values estimated per the maps are close to the risk values estimated from the NTHA results.

Table 8-2 Example Application of Proposed Maps for Risk Assessment

S.No.	Site Class (VS30 in m/s)	Latitude	Longitude	Col. Dia. (ft)	Col. Ht. (ft)	Axial Load (%f'c Ag)	Dead Weight on Top (kips)	No. of Long. Reinf. Rebars	Dia. of Long. Reinf. Rebars (in)	Long. Reinf. Ratio (%)
1	D (259)	37.563	-122.149	5	50	0.05	778	50	1.128	1.75
2	D (259)	37.733	-121.934	6	40	0.05	1100	52	1	1
3	C (537)	33.769	-117.478	6	30	0.1	2098	52	1	1
4	D (259)	38.130	-122.293	6	40	0.05	1100	52	1	1
5	C (537)	34.067	-118.053	6	30	0.15	3116	65	1.41	2.5
6	D (259)	33.769	-117.478	5	50	0.05	778	56	1.27	2.5
7	C (537)	34.008	-117.262	7	40	0.05	1497	56	1.128	1
8	C (537)	37.563	-122.149	7	30	0.1	2855	56	1.128	1
9	D (259)	34.008	-117.262	5	40	0.05	764	50	1.128	1.75
10	D (259)	34.067	-118.053	7	50	0.05	1525	56	1.128	1
11	D (259)	33.169	-116.687	7	50	0.1	2911	77	1.27	1.75
12	C (537)	37.733	-121.934	5	40	0.1	1471	56	1.27	2.5

Table 8-3 Example Application of Proposed Maps for Risk Assessment Continued...

S.No.	Hoop Size (#)	Hoop Spacing (in)	Trans. Reinf. Vol. Ratio	Ultimate /Capacity Disp. (in)	Yield Disp. (in)	Col.'s Natural Period (sec)	DI Design for 975-yr	Sa from 225-yr UHS (g)	Sa from 975-yr UHS (g)	Sa from 2475-yr UHS (g)
1	5	5	0.0044	51.22	11.30	2.30	0.40	0.27	0.52	0.72
2	8	4	0.0116	48.46	5.96	1.60	0.36	0.44	0.85	1.19
3	8	5	0.0092	26.58	3.30	1.30	0.36	0.31	0.70	1.02
4	8	5	0.0092	48.89	5.93	1.60	0.31	0.40	0.78	1.09
5	7	7	0.0051	14.95	3.54	1.30	0.34	0.21	0.46	0.69
6	6	5	0.0063	58.99	12.17	2.10	0.39	0.33	0.72	1.03
7	5	5	0.0031	22.87	4.74	1.40	0.30	0.22	0.55	0.86
8	7	6	0.0050	15.54	2.71	1.10	0.33	0.31	0.57	0.78
9	8	8	0.0070	46.00	7.59	1.70	0.40	0.35	0.84	1.30
10	8	8	0.0049	45.72	7.69	1.90	0.30	0.25	0.54	0.80
11	7	6	0.0050	35.89	8.09	2.20	0.31	0.16	0.36	0.59
12	7	8	0.0054	33.17	7.61	2.00	0.30	0.20	0.39	0.56

Table 8-4 Example Application of Proposed Maps for Risk Assessment Continued...

S.No.	φ_L from Maps, 225-yr	φ_L from Maps, 975-yr	φ_L from Maps, 2475-yr	Disp. Demand per ESA, 225-yr	Disp. Demand per ESA, 975-yr	Disp. Demand per ESA, 2475-yr	μ_L per Maps, 225-yr	μ_L per Maps, 975-yr	μ_L per Maps, 2475-yr
1	0.91	1.19	1.28	14.02	27.13	37.57	0.04	0.53	0.92
2	0.96	1.23	1.31	10.95	21.23	29.63	0.11	0.48	0.77
3	1.03	1.04	1.12	5.20	11.73	16.92	0.09	0.38	0.67
4	0.94	1.20	1.38	9.90	19.39	27.20	0.08	0.40	0.74
5	1.03	1.12	1.20	3.35	7.45	11.09	0.00	0.42	0.86
6	0.91	1.05	1.09	13.80	30.41	43.90	0.01	0.42	0.76
7	1.06	0.99	1.09	4.22	10.19	15.92	0.00	0.30	0.69
8	1.06	0.91	1.15	3.71	6.94	9.48	0.10	0.28	0.64
9	0.88	1.01	1.02	9.52	22.78	35.32	0.02	0.40	0.74
10	0.94	1.21	1.28	8.73	19.13	28.27	0.01	0.41	0.75
11	0.89	0.94	0.99	7.20	16.69	26.93	0.00	0.27	0.67
12	1.01	0.99	1.15	7.65	15.31	21.74	0.00	0.29	0.68

Table 8-5 Example Application of Proposed Maps for Risk Assessment Continued...

S.No.	δ_L from Maps, 225-yr	δ_L from Maps, 975-yr	δ_L from Maps 2475-yr	P(DS5) per Maps, 225-yr	P(DS5) per Maps, 975-yr	P(DS5) per Maps, 2475-yr	μ_L per NTHA, 225-yr	μ_L per NTHA, 975-yr	μ_L per NTHA, 2475-yr
1	1.30	0.56	0.30	0.02%	14.52%	59.35%	0.10	0.58	0.89
2	1.16	0.54	0.30	0.43%	10.18%	38.43%	0.10	0.49	0.85
3	1.50	0.58	0.36	0.52%	5.13%	25.10%	0.06	0.43	0.62
4	1.21	0.57	0.30	0.18%	6.12%	32.48%	0.09	0.46	0.75
5	1.72	0.63	0.30	0.00%	8.26%	50.56%	0.03	0.42	0.76
6	1.30	0.56	0.36	0.00%	6.98%	36.77%	0.05	0.43	0.71
7	1.63	0.69	0.33	0.00%	2.88%	26.97%	0.01	0.31	0.66
8	1.53	0.80	0.31	0.65%	3.28%	18.78%	0.03	0.21	0.54
9	1.41	0.57	0.37	0.00%	5.86%	34.17%	0.05	0.47	0.78
10	1.40	0.56	0.28	0.00%	6.06%	34.76%	0.03	0.43	0.85
11	1.91	0.60	0.34	0.00%	1.43%	23.72%	0.00	0.27	0.67
12	1.40	0.65	0.34	0.00%	2.48%	25.50%	0.03	0.26	0.71

Table 8-6 Example Application of Proposed Maps for Risk Assessment Continued...

S.No.	δ_L per NTHA, 225-yr	δ_L per NTHA, 975-yr	δ_L per NTHA, 2475-yr	P(DS5) per NTHA, 225-yr	P(DS5) per NTHA, 975-yr	P(DS5) per NTHA, 2475-yr	Risk of Exceeding DS5 in 75 yrs per Maps	Risk of Exceeding DS5 in 75 yrs per NTHA
1	0.96	0.39	0.22	0.16%	15.16%	59.87%	4.03%	4.03%
2	0.96	0.48	0.26	0.17%	9.64%	50.73%	3.19%	3.61%
3	1.14	0.54	0.51	0.07%	7.00%	21.46%	1.85%	1.66%
4	0.82	0.56	0.34	0.05%	9.04%	34.77%	2.63%	2.93%
5	1.88	0.45	0.32	0.05%	4.77%	36.68%	2.68%	2.27%
6	1.29	0.42	0.29	0.07%	4.64%	29.09%	2.69%	2.29%
7	2.76	0.45	0.25	0.00%	0.81%	18.63%	1.65%	1.49%
8	1.72	1.11	0.52	0.06%	2.59%	14.51%	1.56%	1.13%
9	1.23	0.57	0.30	0.03%	10.54%	38.89%	2.27%	2.94%
10	1.78	0.60	0.28	0.06%	7.96%	50.72%	2.54%	3.16%
11	4.37	0.41	0.30	0.00%	0.20%	23.37%	1.96%	2.15%
12	1.92	1.03	0.26	0.08%	4.12%	27.21%	2.29%	2.46%

8.1.4 Future Studies

The maps presented in this study are the result of a detailed methodology that rigorously accounts for both column design uncertainty and ground motion uncertainty in the design process. This work is intended to serve as a steppingstone for future studies aimed at helping designers quantify bridge demand within a probabilistic framework.

For future research on CT-RBSD, the following considerations are recommended:

1. Expanding the geographical coverage of the maps by incorporating additional grid points across California. Currently, a 5×5 mile grid has been comprehensively analyzed for the Bay Area and Southern California. Extending this grid-based approach to include other regions, particularly coastal California, is advised.

2. Identifying regions with extreme values of δ_L or φ_L. Some areas, such as Northern California, exhibit high δ_L values and low φ_L values, warranting further investigation.

3. Incorporating full bridge models instead of column models for analysis. This would provide a more realistic estimate of the actual demand experienced by bridges. The next phase of the CT-RBSD study will focus on this refinement.

4. Developing prediction equations for demand parameters based on the data generated in this study. These equations could estimate demand parameters (e.g., DI, demand ductility, drift)

as a function of event parameters (e.g., IMs, M, R, θ), facilitating broader applications of the findings.

5. Establishing performance targets for bridge design. While performance-based design considers risk as a performance metric, the appropriate risk threshold for design decisions remains undefined and should be determined by asset owners. The bridge designs explored in this study can serve as a reference for defining "good" performance targets based on risk values associated with selected design configurations.

6. Improving the capacity fragility curves.

7. Development of δ_L or φ_L maps for column designs with design DI outside the range of 0.3-0.4 considered in this study. For example, recovery bridges are expected to have better performance than ordinary bridges, resulting in design DI lower than 0.3, and can be targeted for next generation demand maps.

By addressing these points, future research can further enhance the practical applications of CT-RBSD, providing more robust decision-making tools for bridge engineers and asset managers.

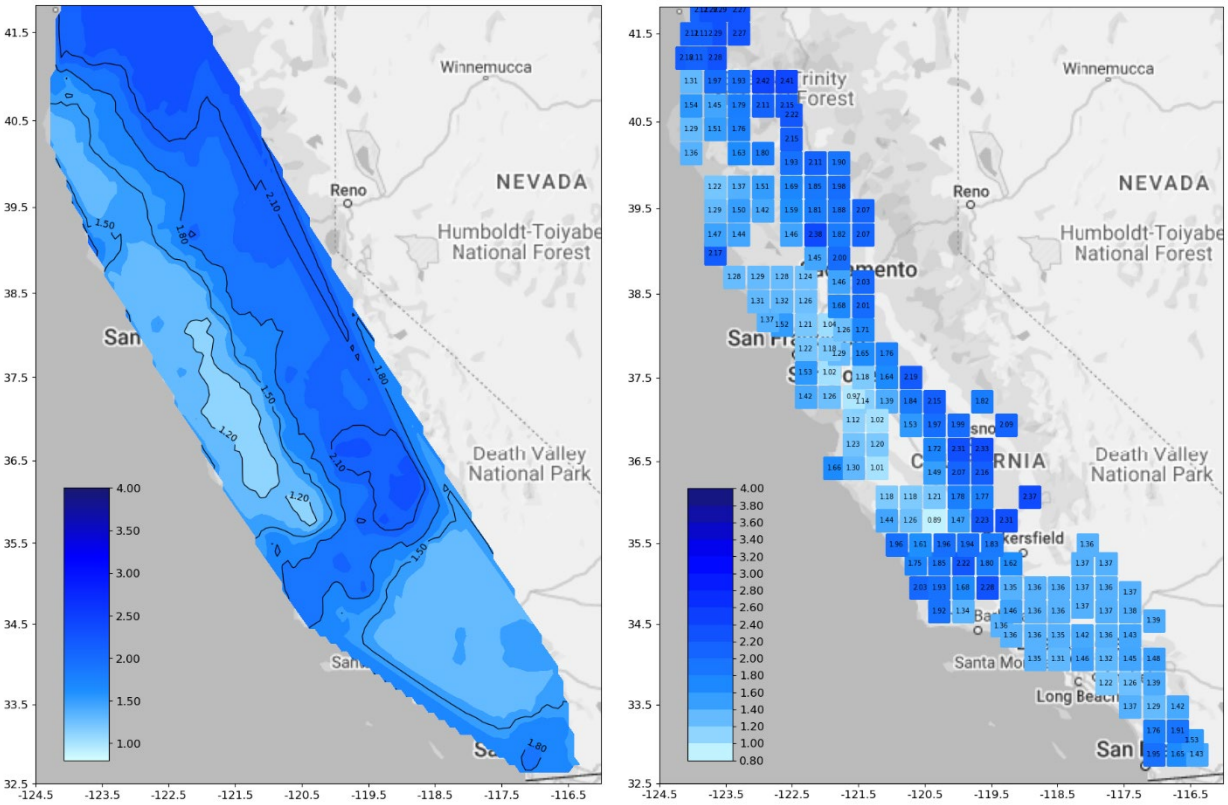

Figure 8-2 δ_L for 225-yr, Site Class D

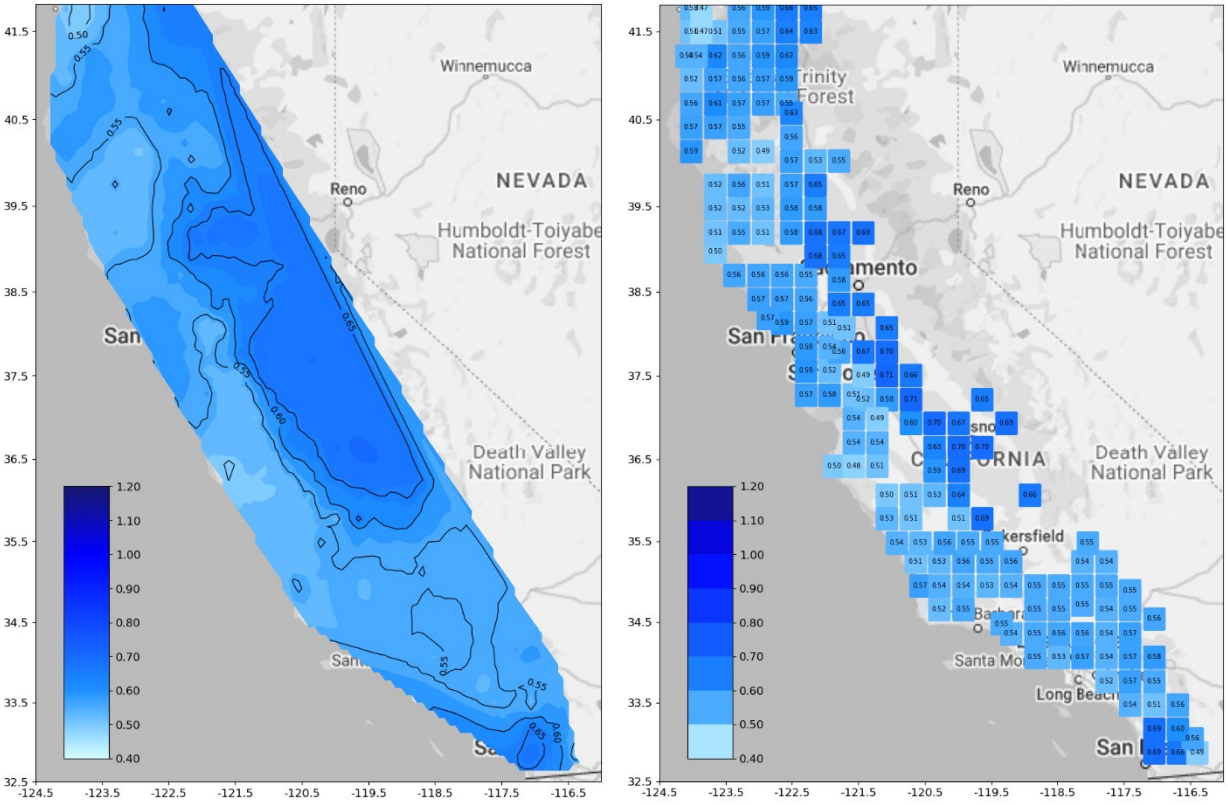

Figure 8-3 δ_L for 975-yr, Site Class D

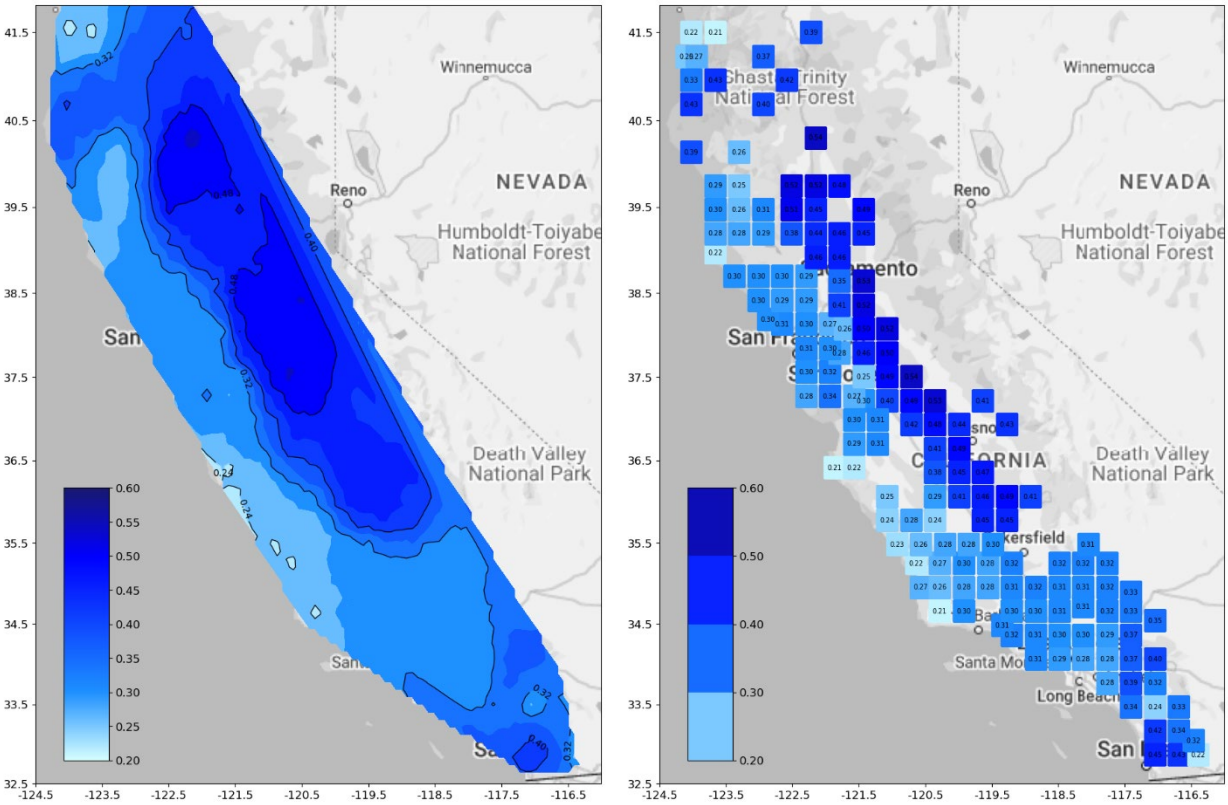

Figure 8-4 δ_L for 2475-yr, Site Class D

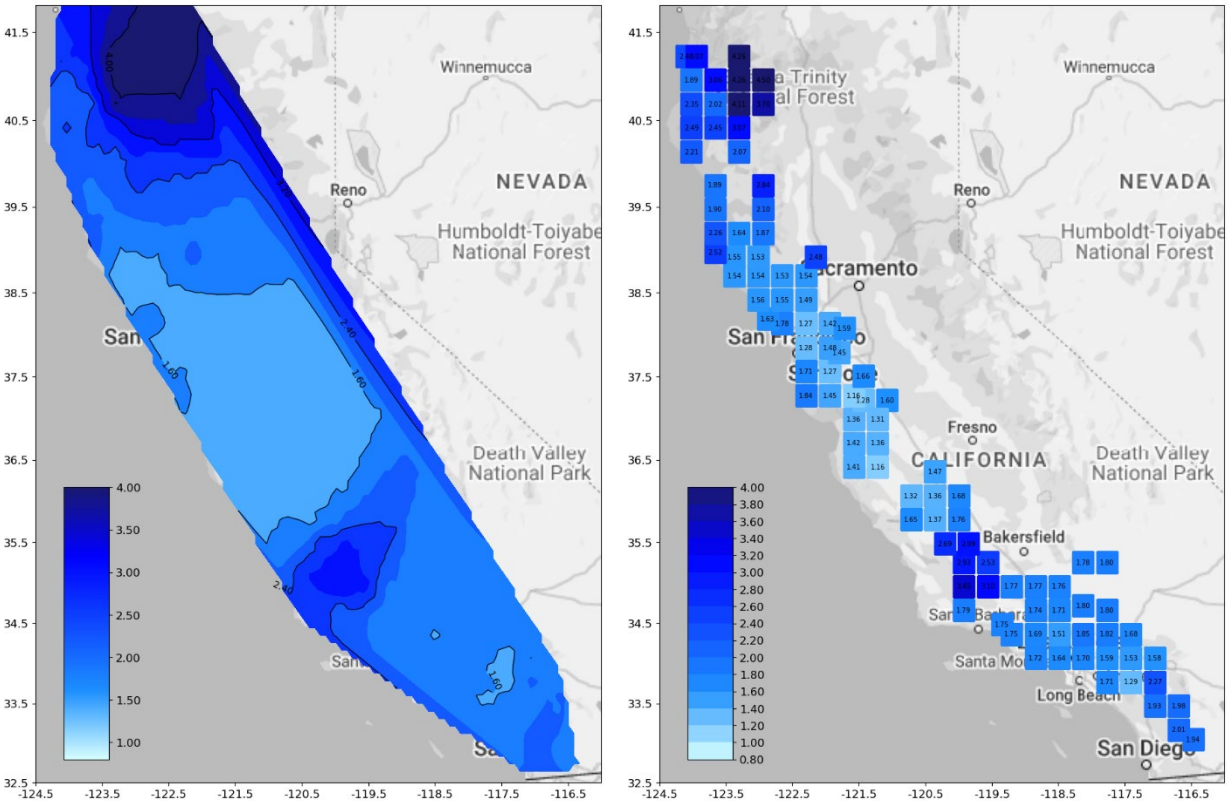

Figure 8-5 δ_L for 225-yr, Site Class C

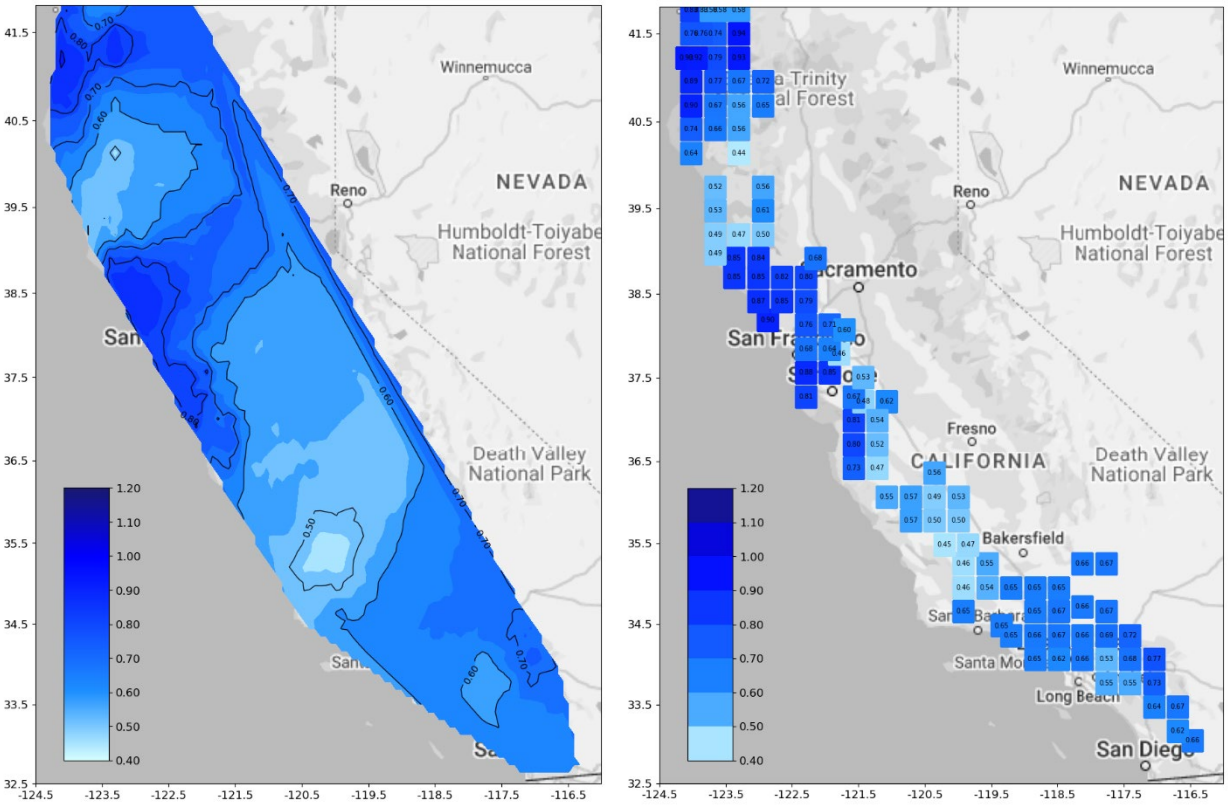

Figure 8-6 δ_L for 975-yr, Site Class C

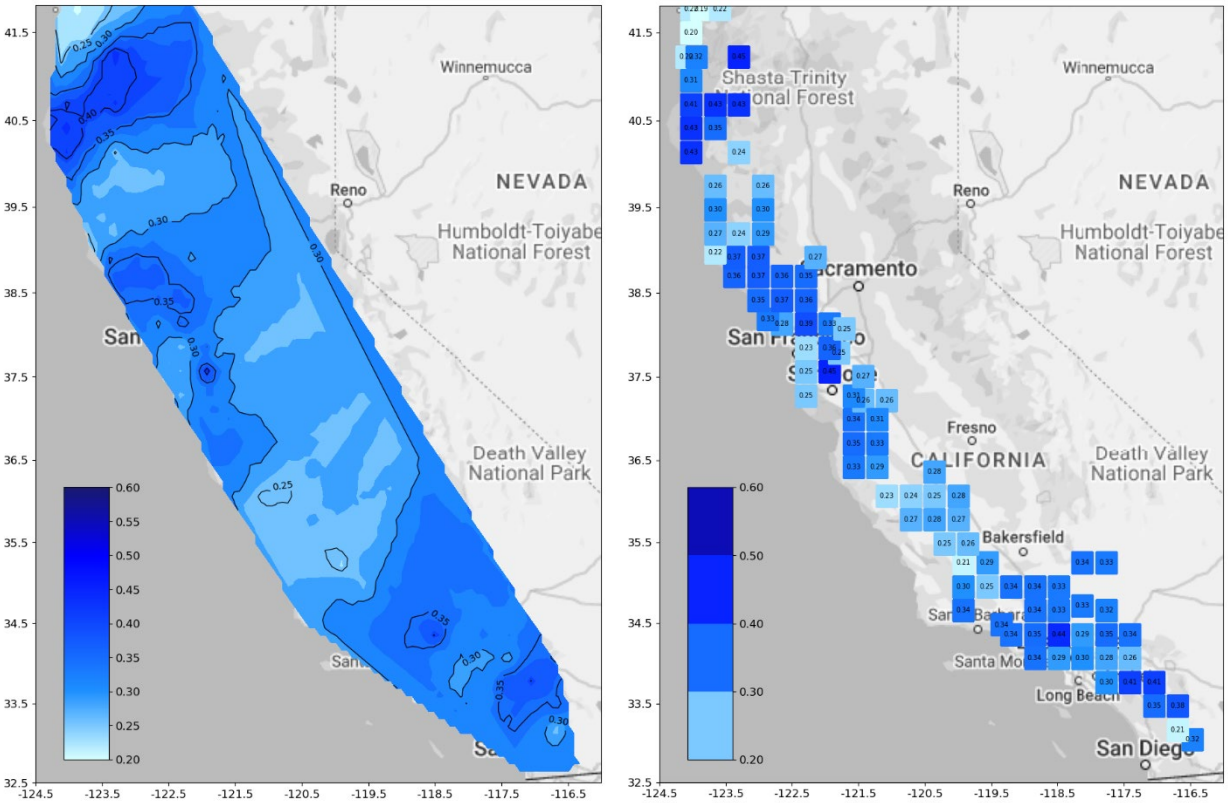

Figure 8-7 δ_L for 2475-yr, Site Class C

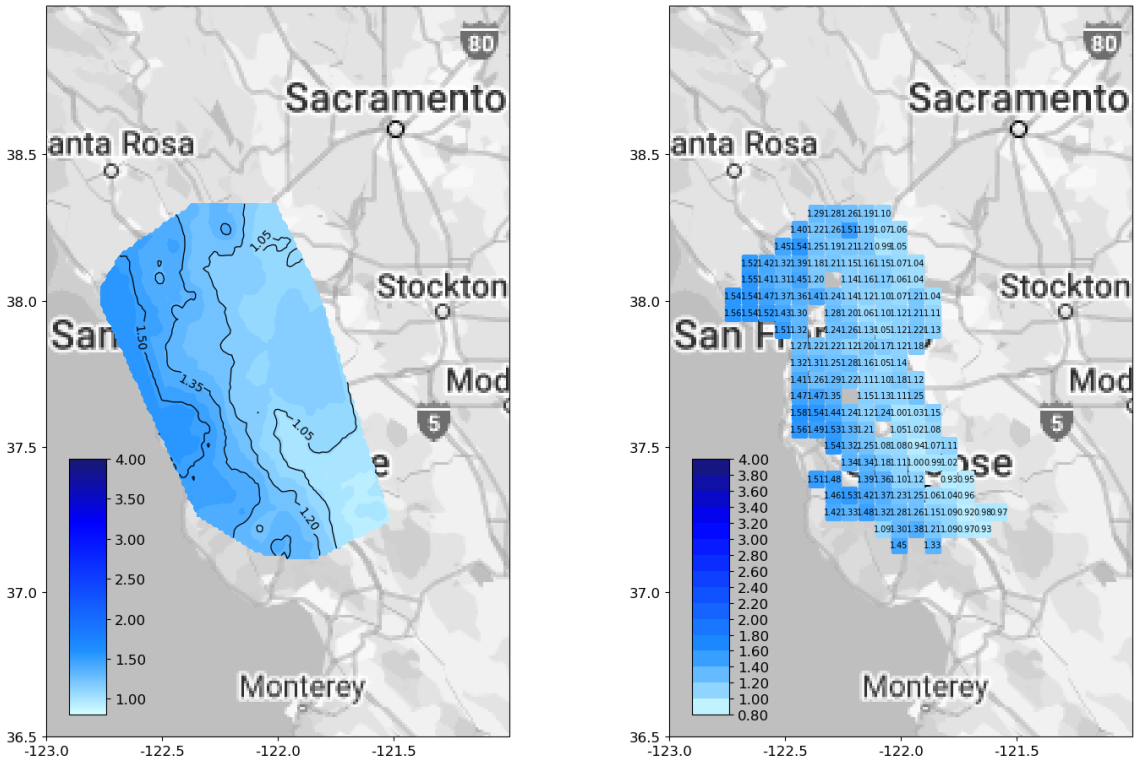

Figure 8-8 δ_L for Bay Area, 225-yr, Site Class D

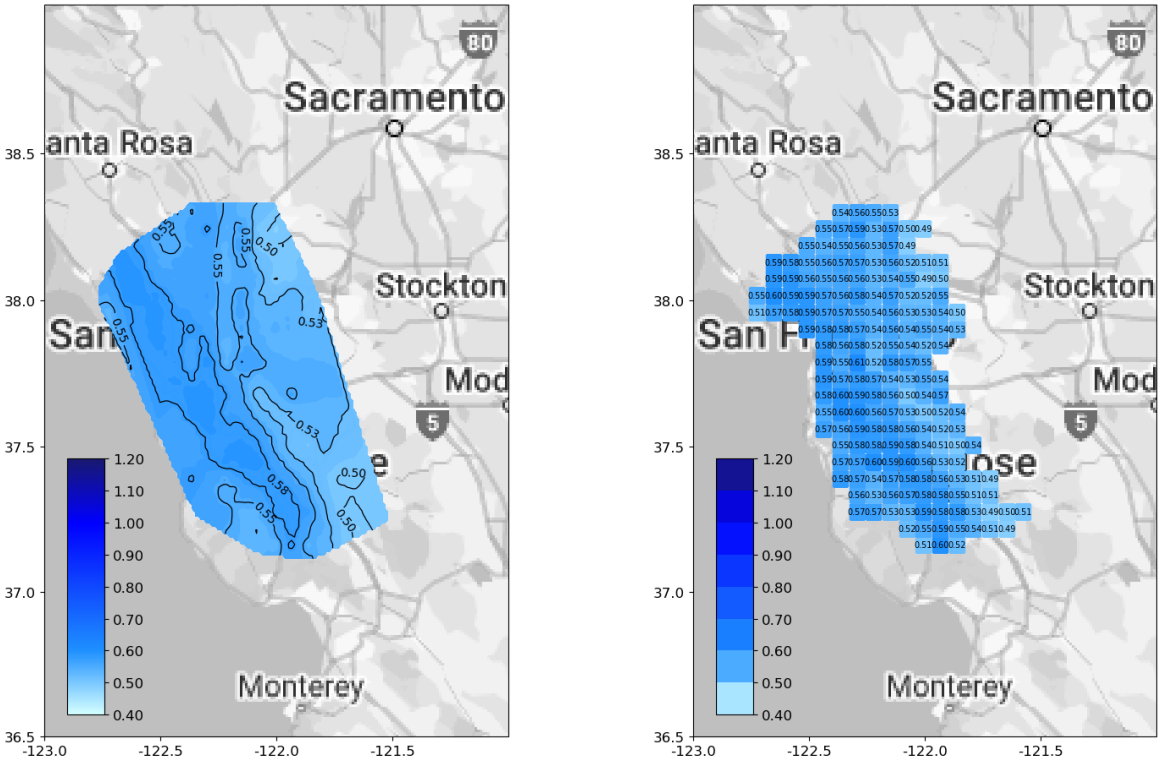

Figure 8-9 δ_L for Bay Area, 975-yr, Site Class D

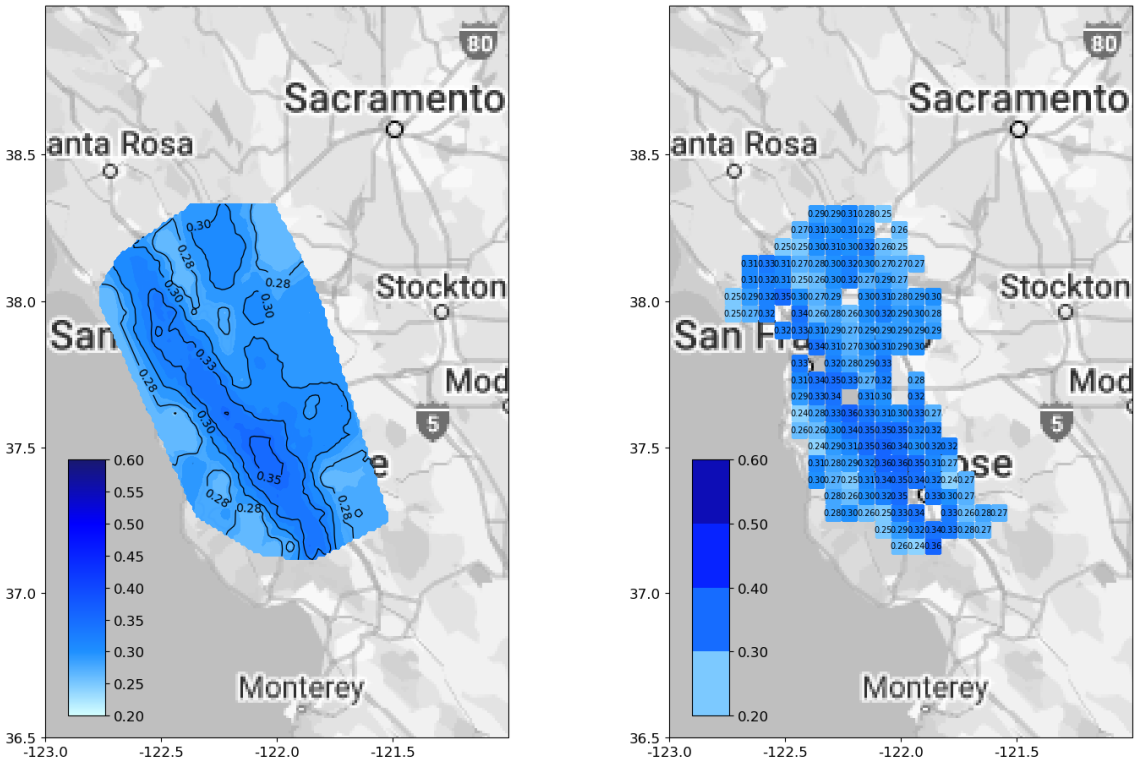

Figure 8-10 δ_L for Bay Area, 2475-yr, Site Class D

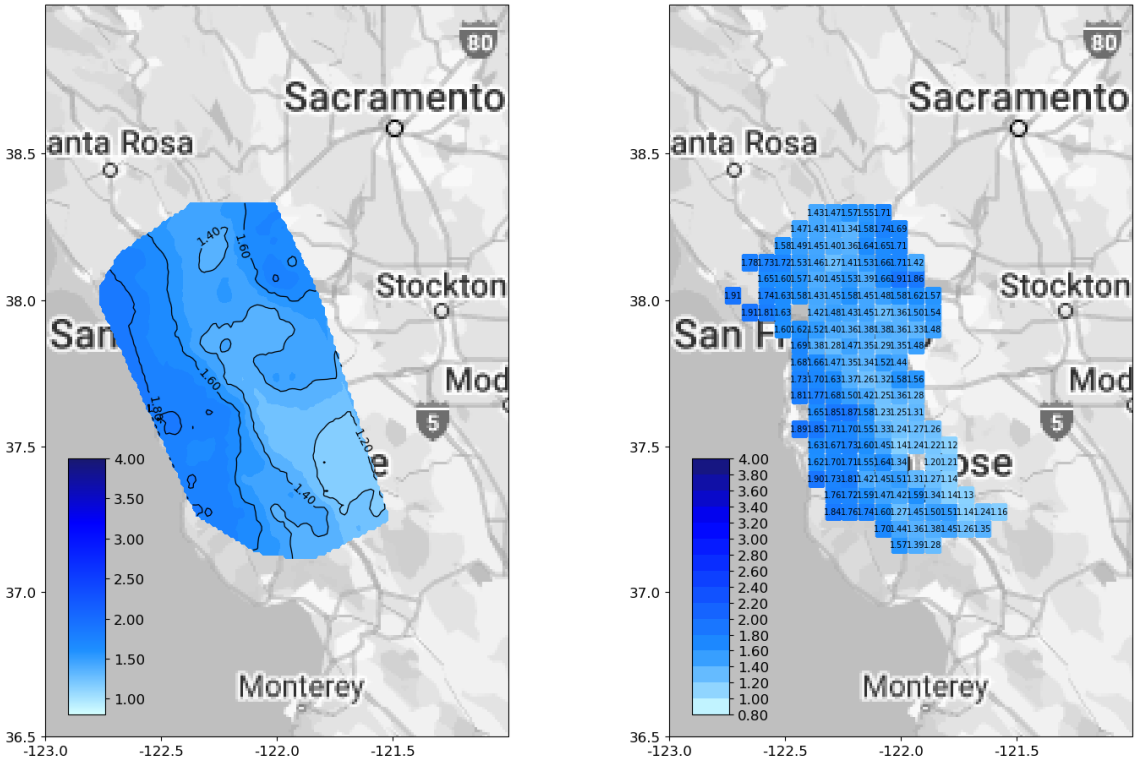

Figure 8-11 δ_L for Bay Area, 225-yr, Site Class C

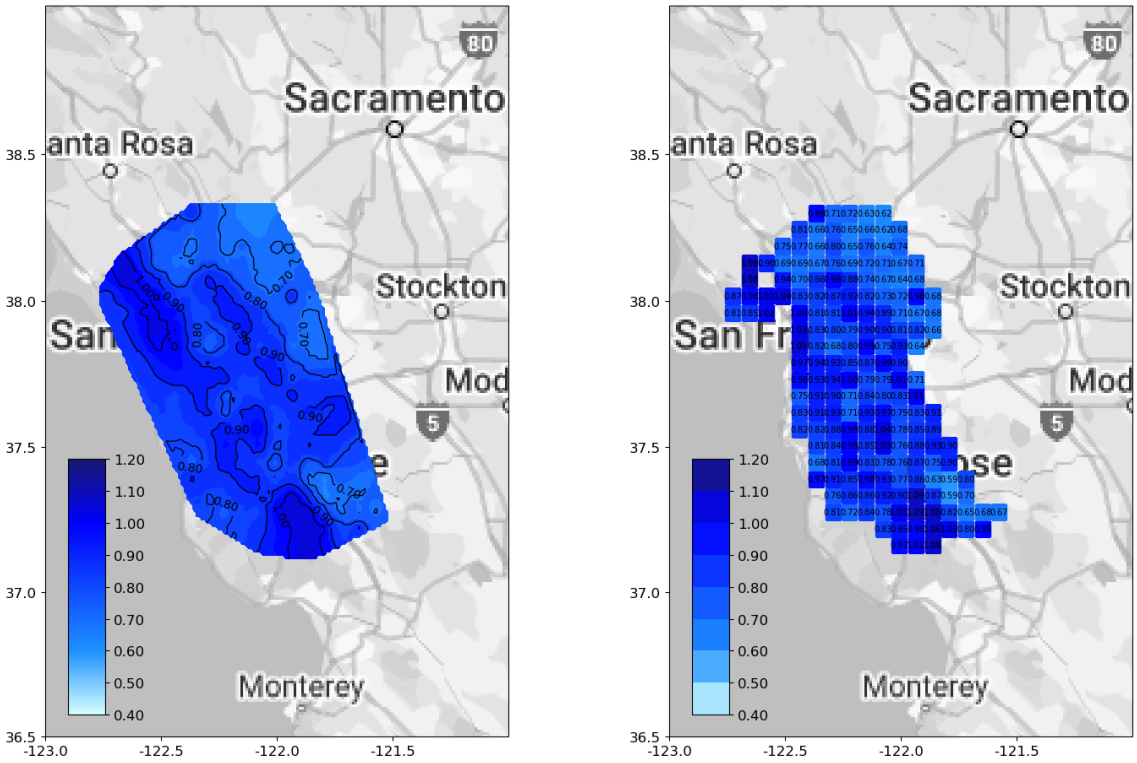

Figure 8-12 δ_L for Bay Area, 975-yr, Site Class C

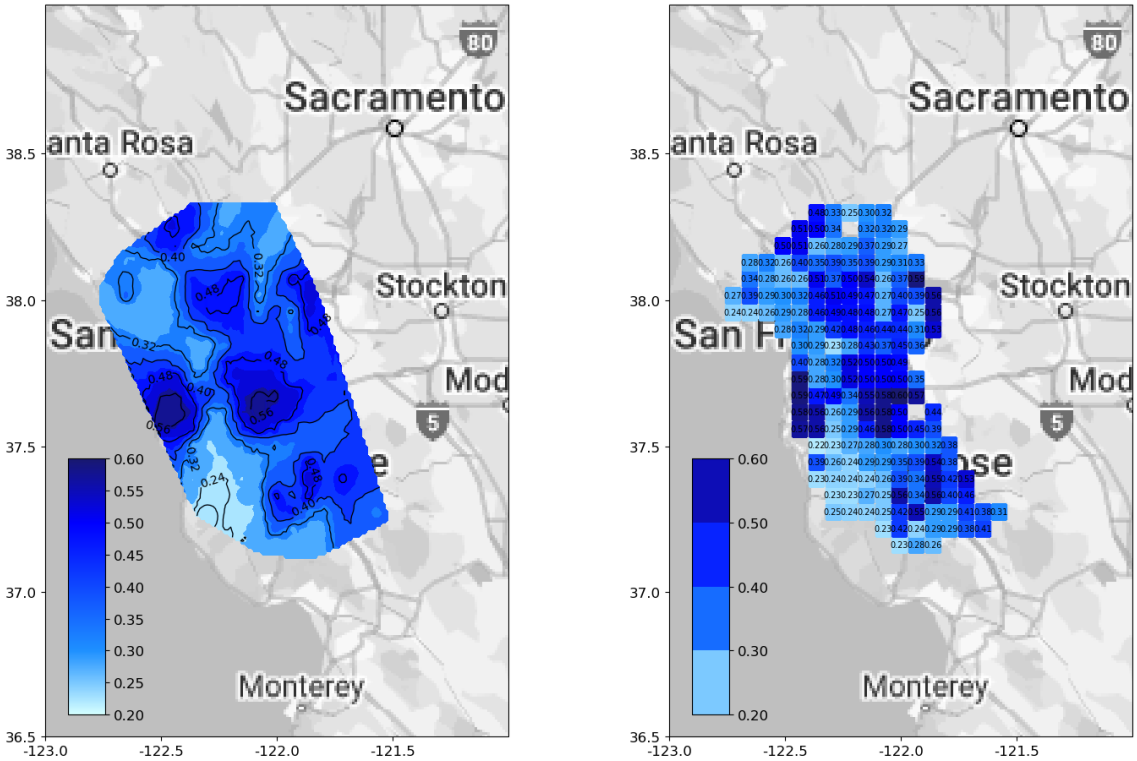

Figure 8-13 δ_L for Bay Area, 2475-yr, Site Class C

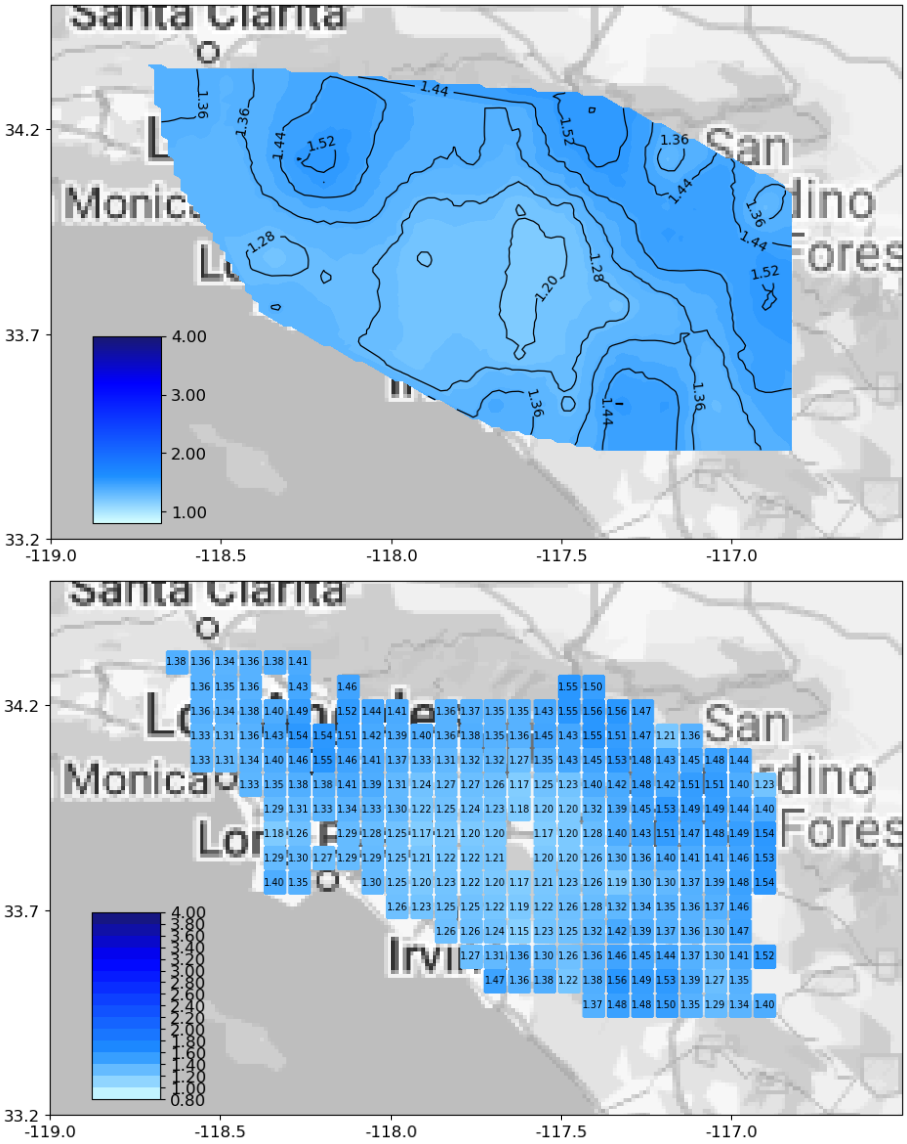

Figure 8-14 δ_L for LA Area, 225-yr, Site Class D

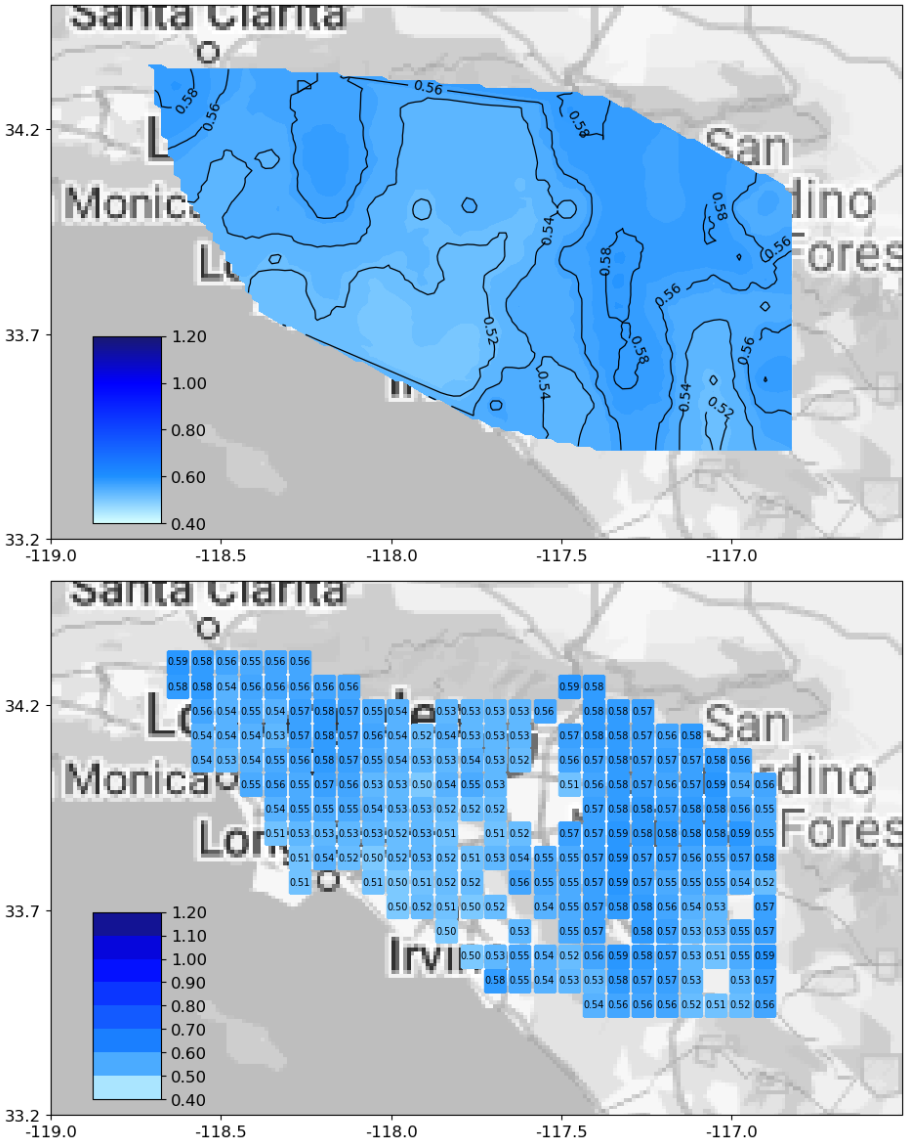

Figure 8-15 δ_L for LA Area, 975-yr, Site Class D

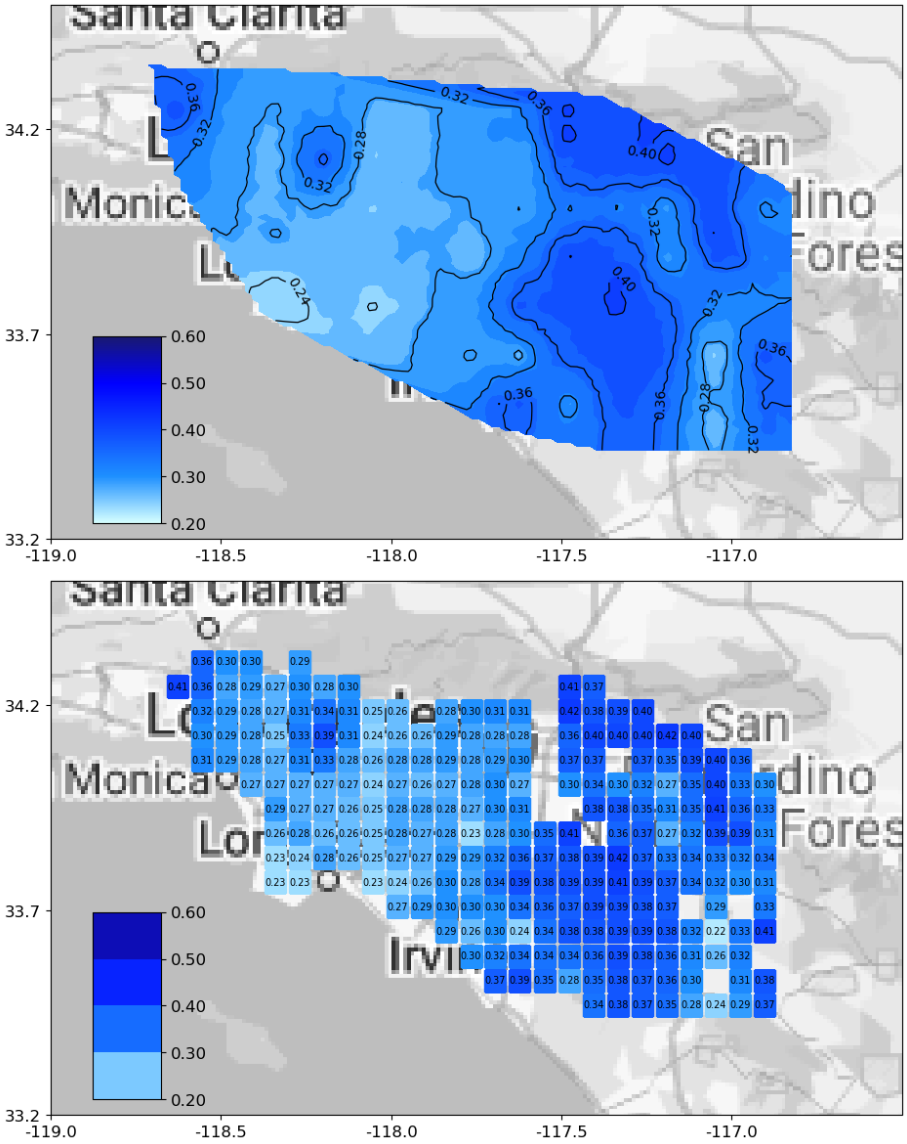

Figure 8-16 δ_L for LA Area, 2475-yr, Site Class D

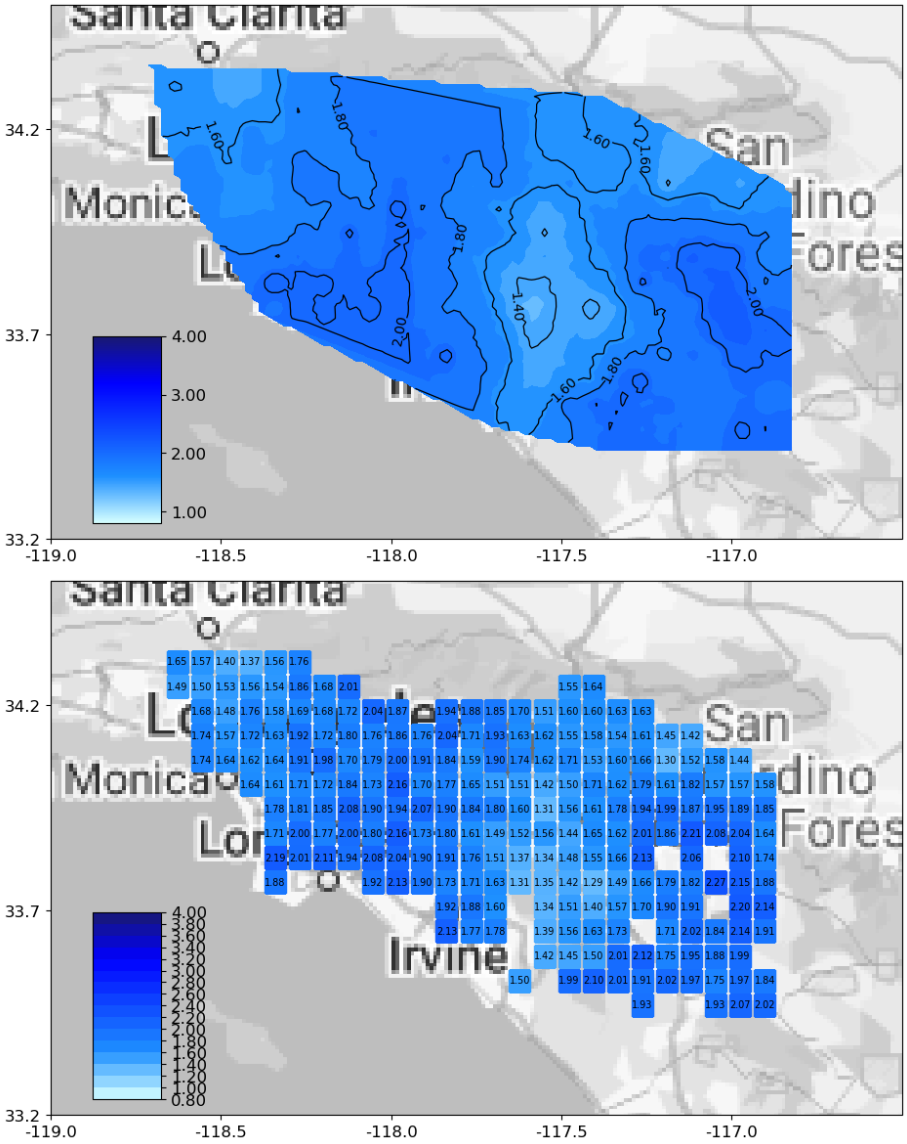

Figure 8-17 δ_L for LA Area, 225-yr, Site Class C

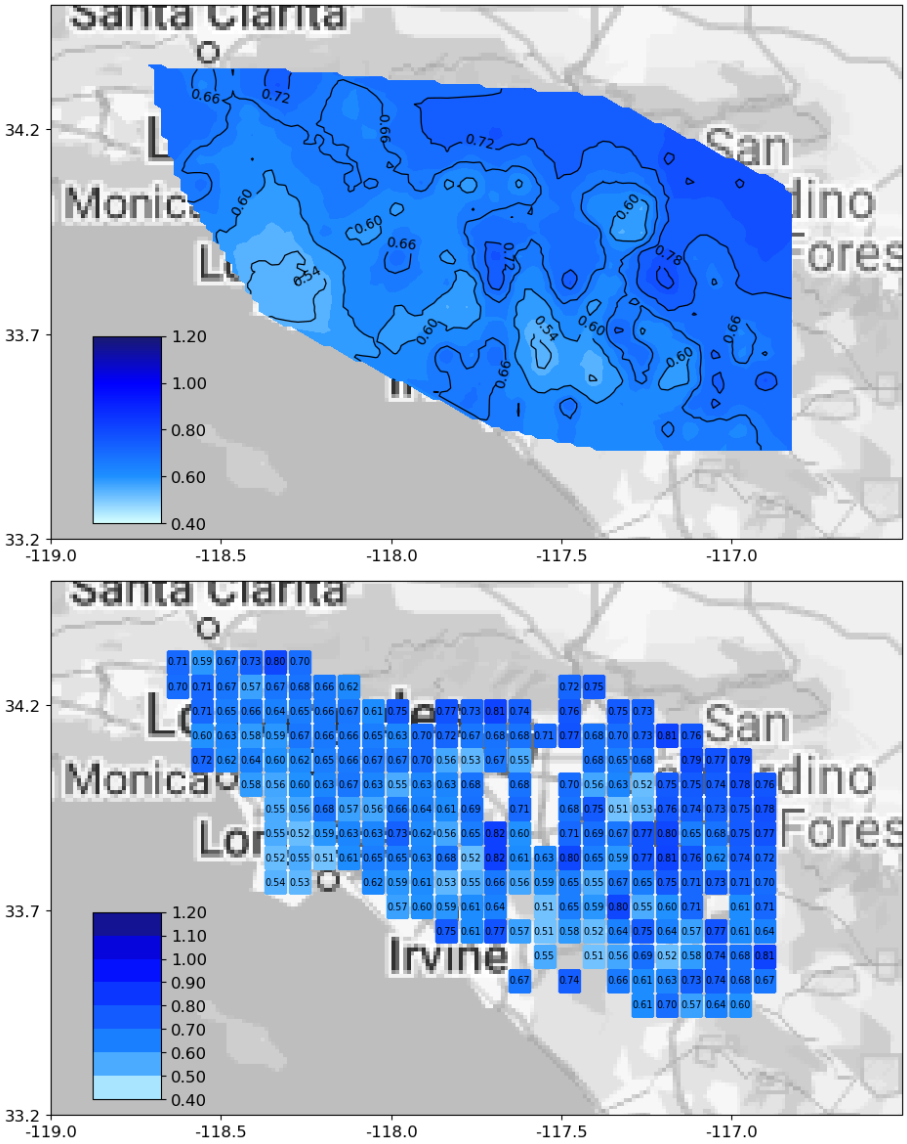

Figure 8-18 δ_L for LA Area, 975-yr, Site Class C

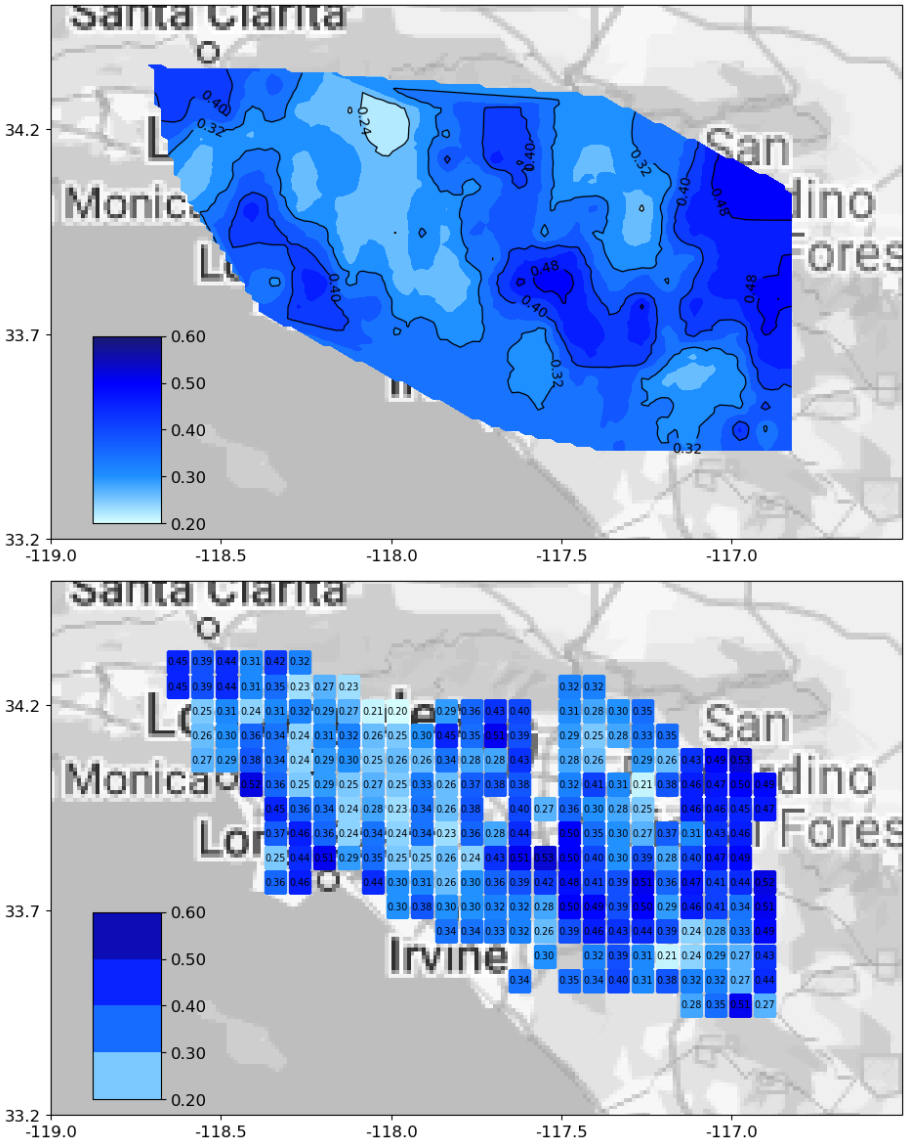

Figure 8-19 δ_L for LA Area, 2475-yr, Site Class C

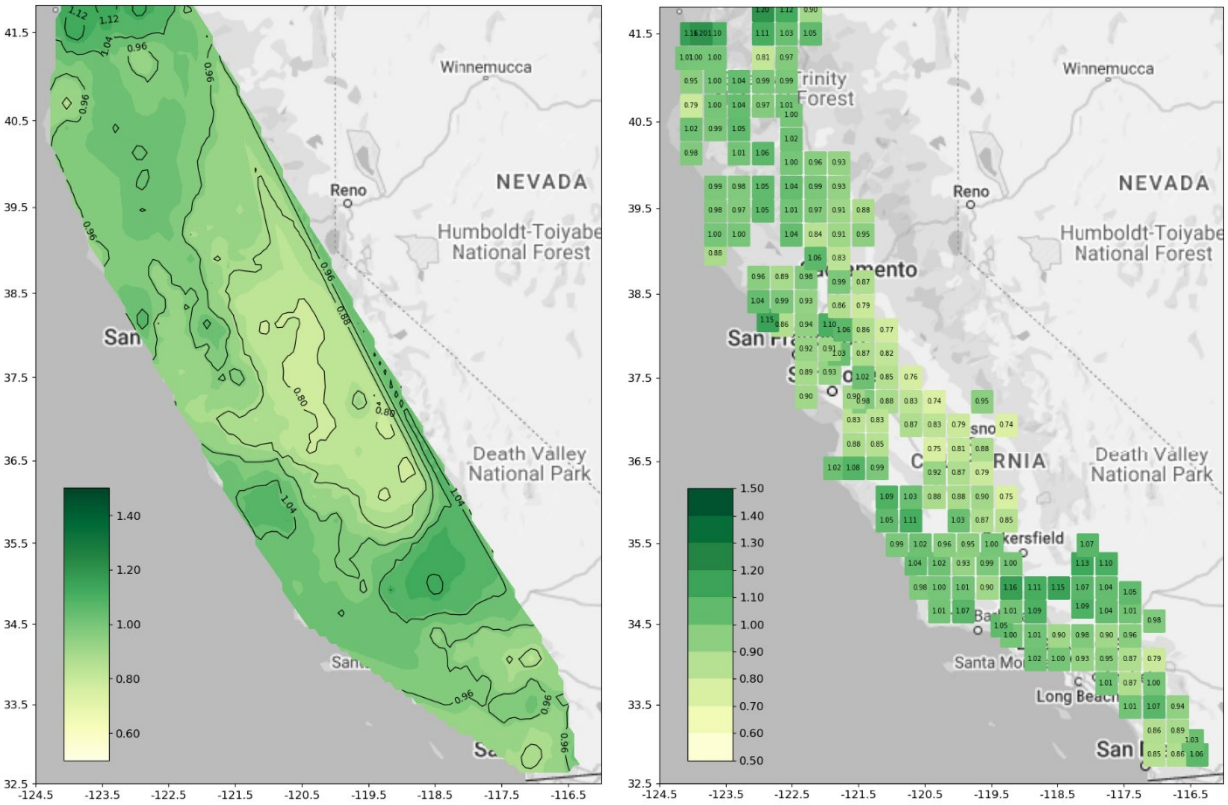

Figure 8-20 φ_L for 225-yr, Site Class D

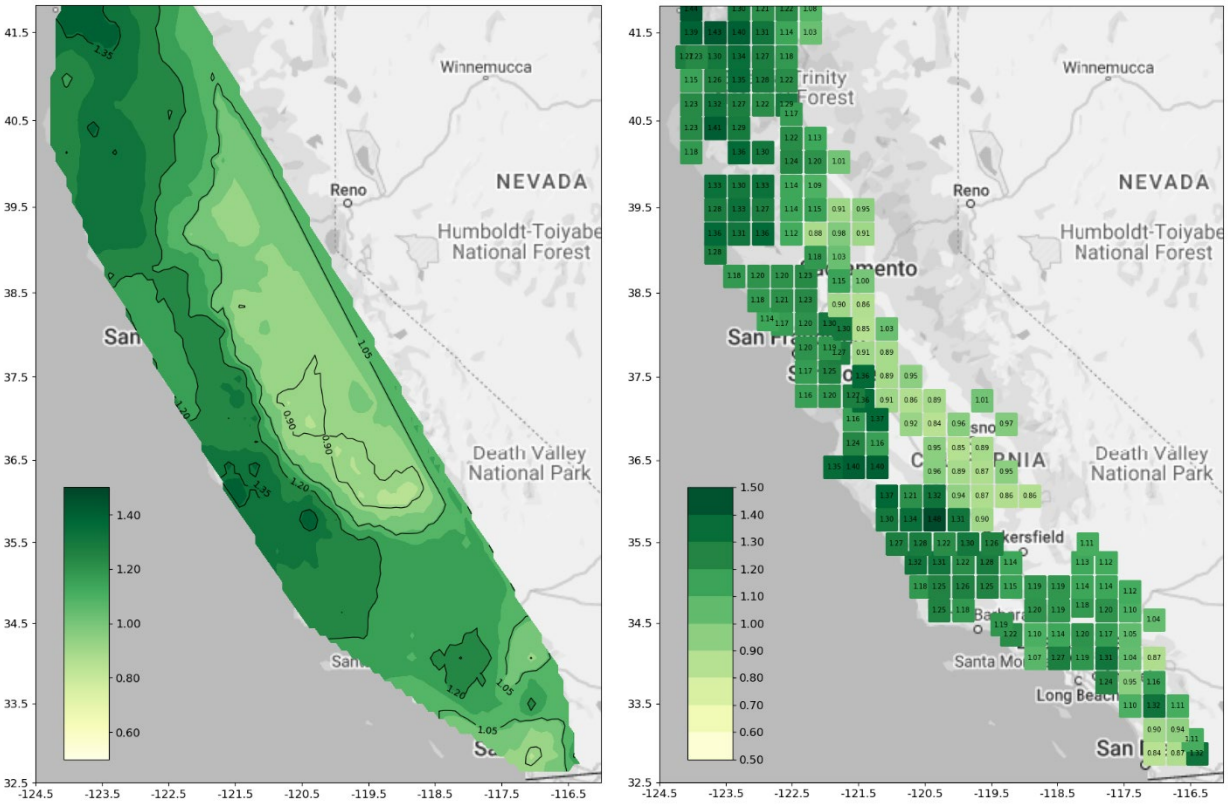

Figure 8-21 φ_L for 975-yr, Site Class D

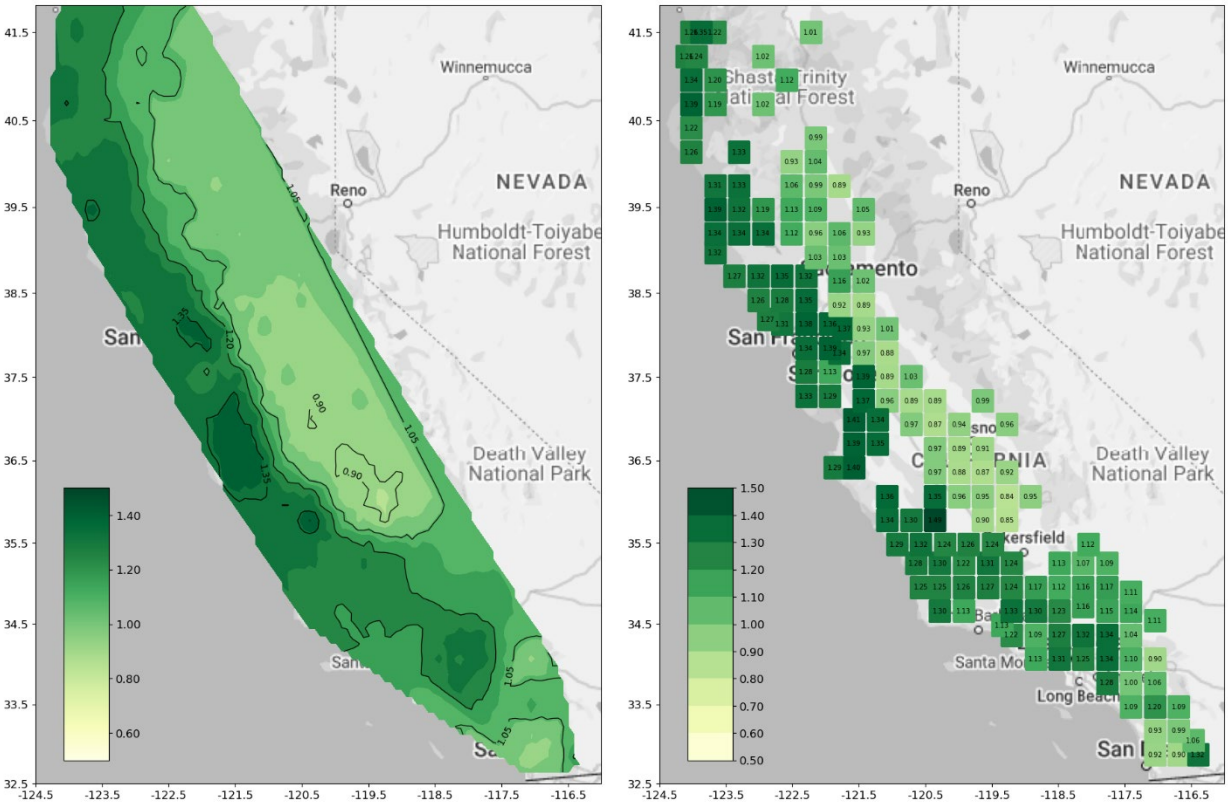

Figure 8-22 φ_L for 2475-yr, Site Class D

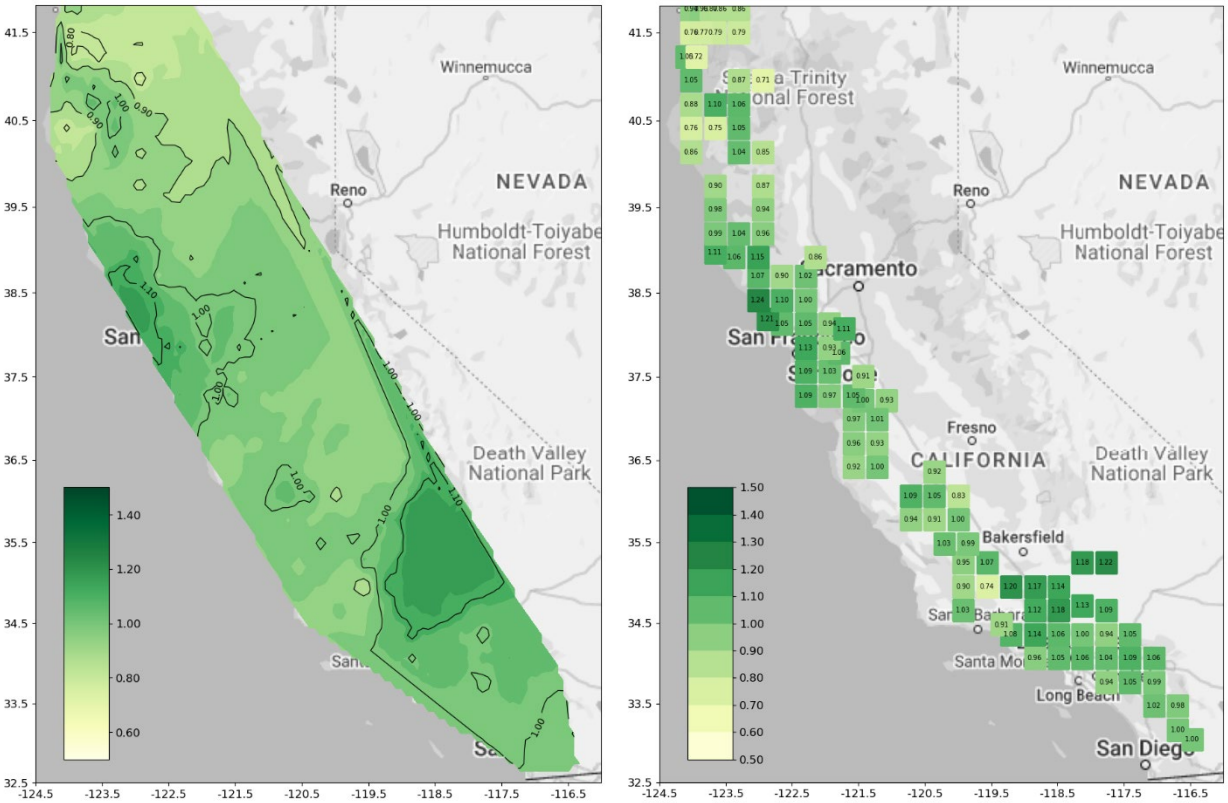

Figure 8-23 φ_L for 225-yr, Site Class C

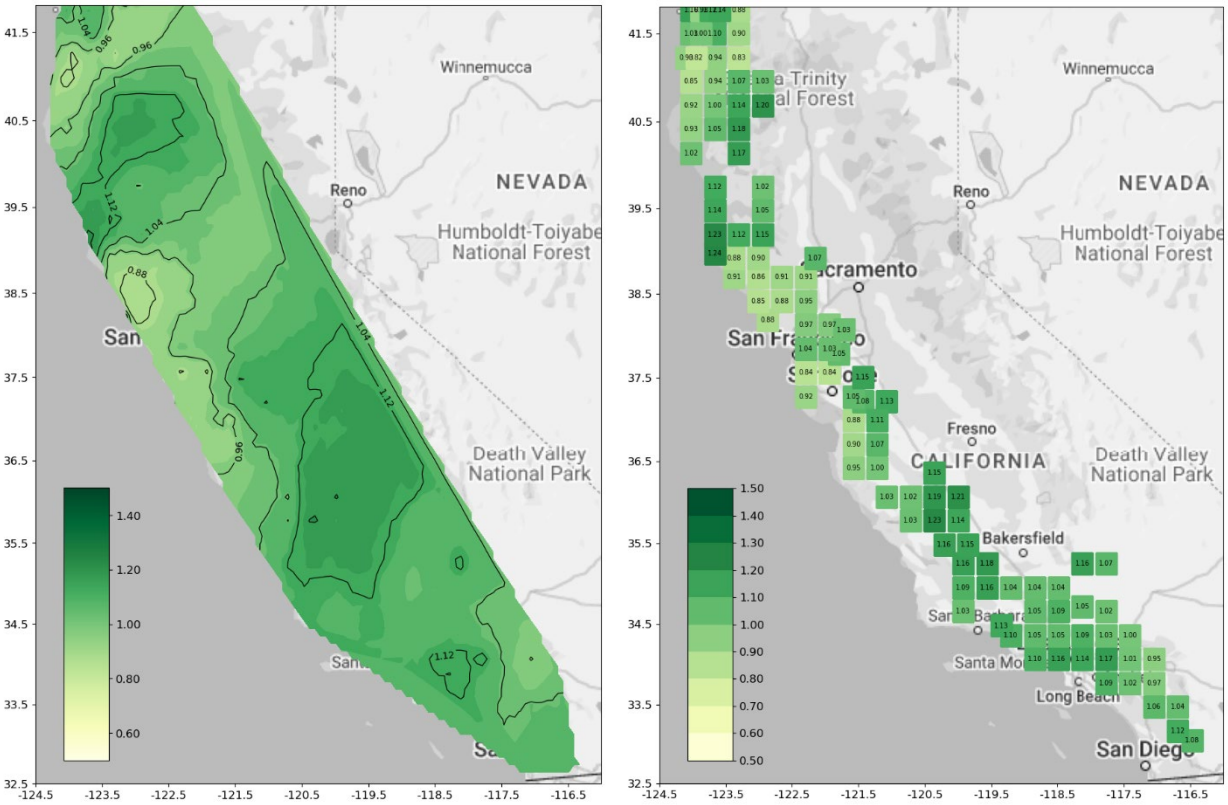

Figure 8-24 φ_L for 975-yr, Site Class C

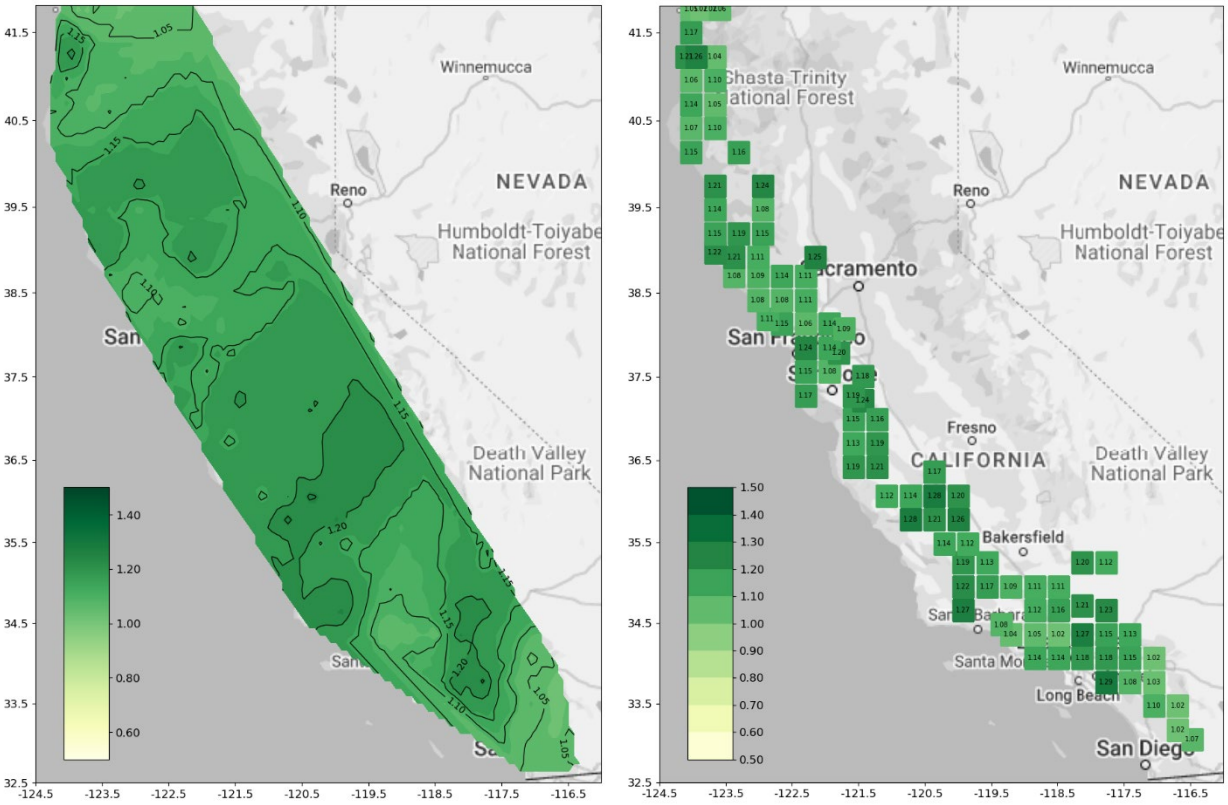

Figure 8-25 φ_L for 2475-yr, Site Class C

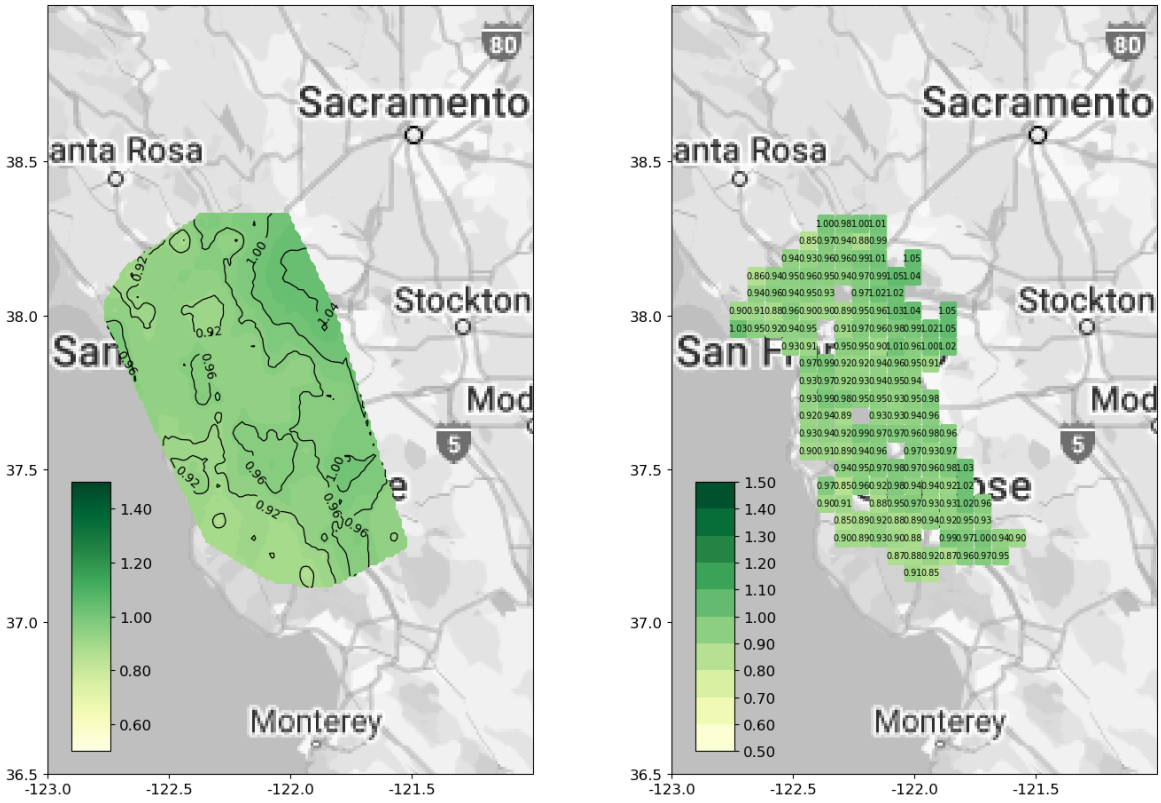

Figure 8-26 φ_L for Bay Area, 225-yr, Site Class D

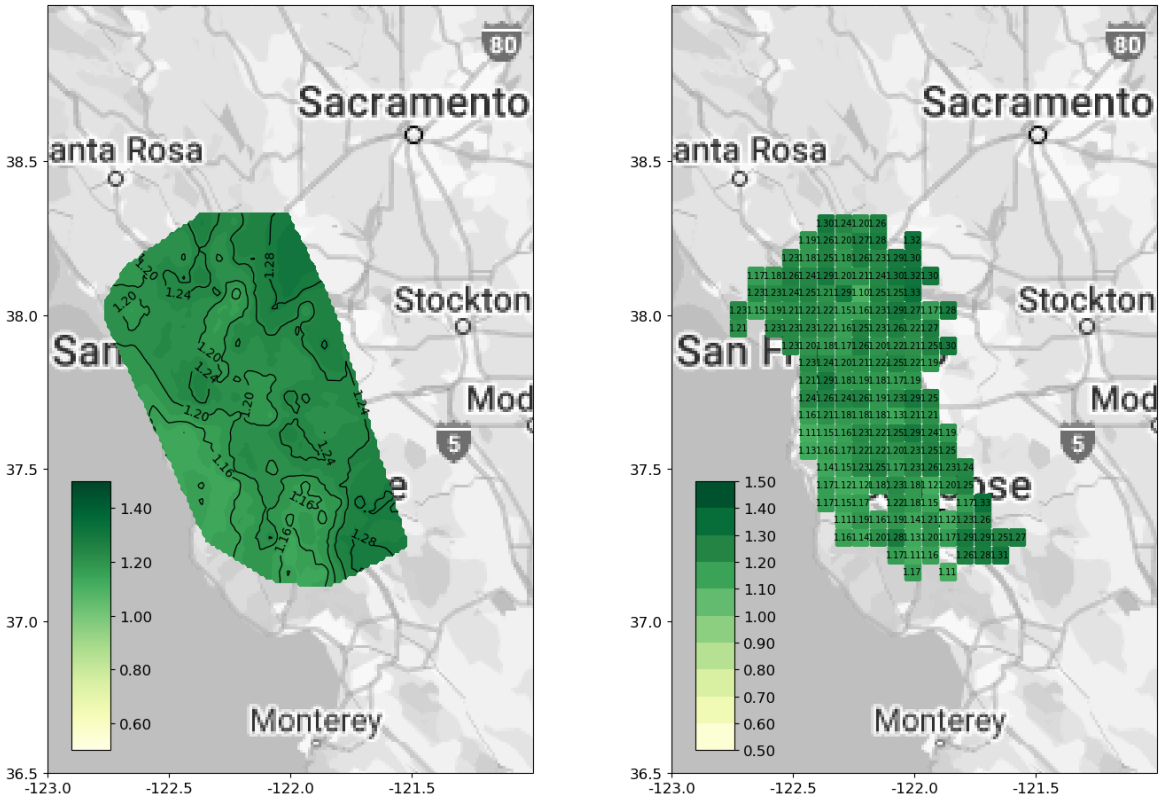

Figure 8-27 φ_L for Bay Area, 975-yr, Site Class D

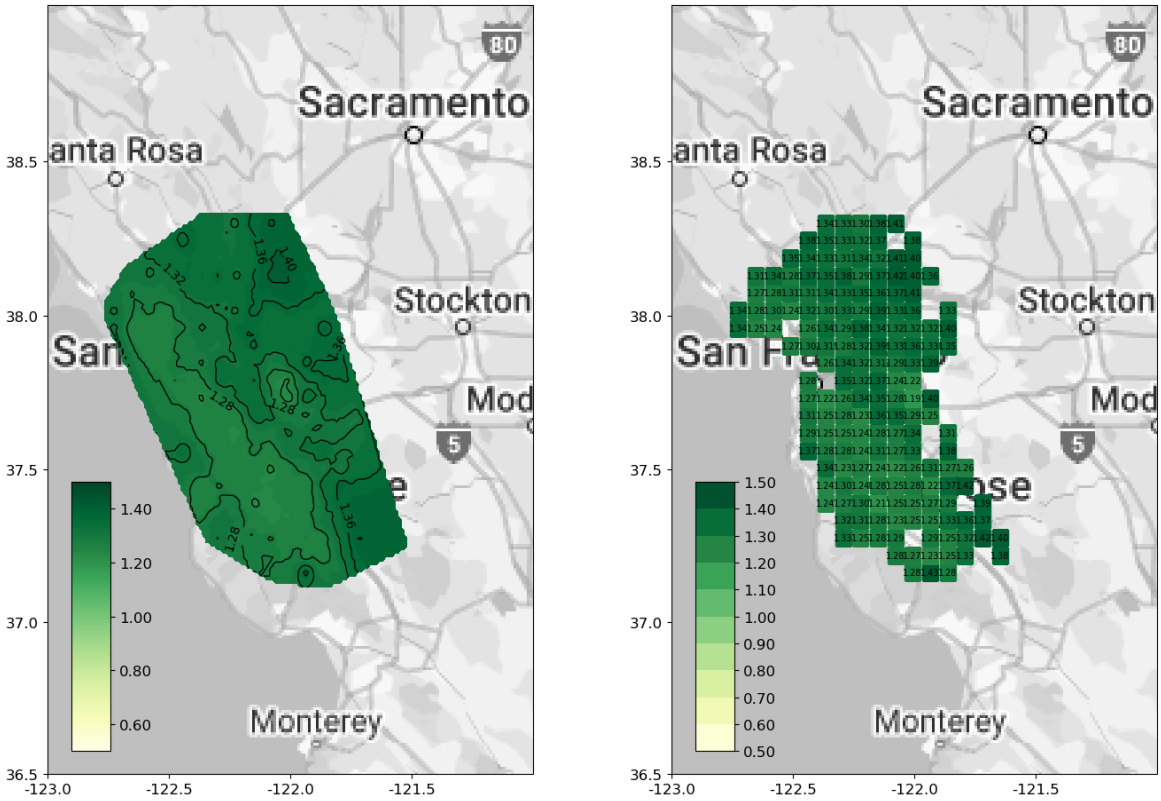

Figure 8-28 φ_L for Bay Area, 2475-yr, Site Class D

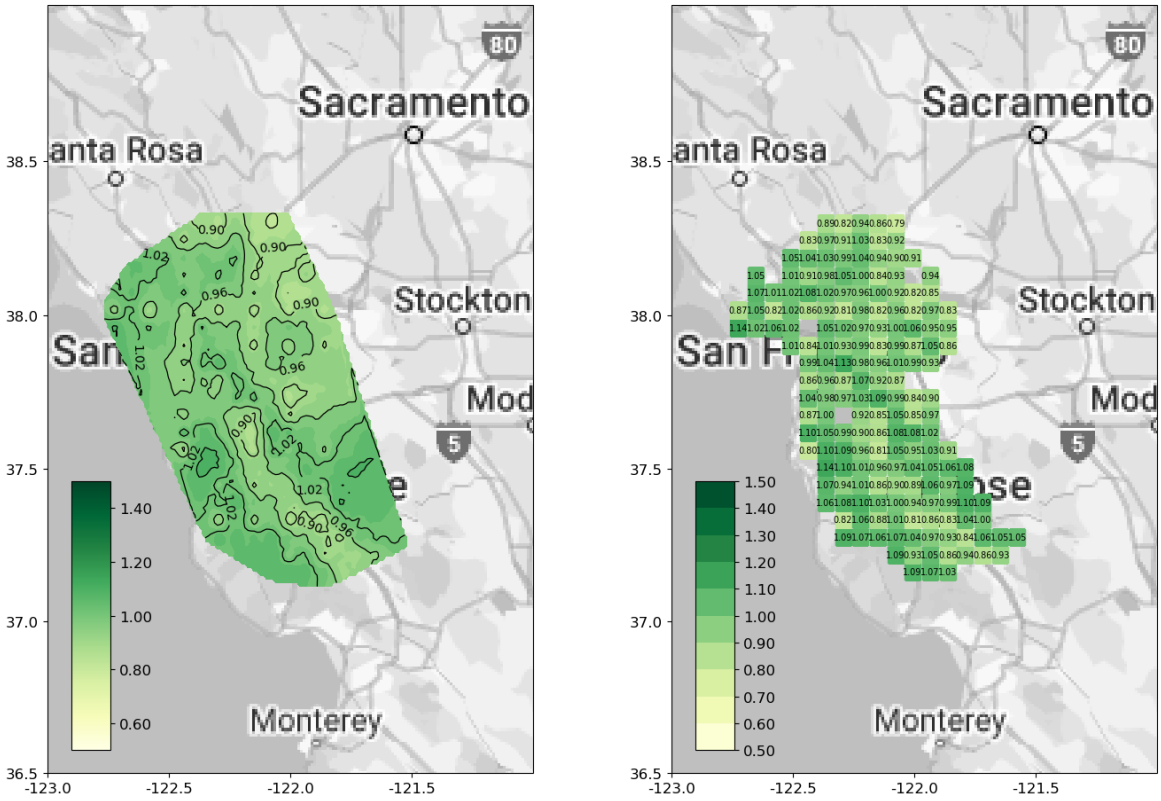

Figure 8-29 φ_L for Bay Area, 225-yr Site Class C

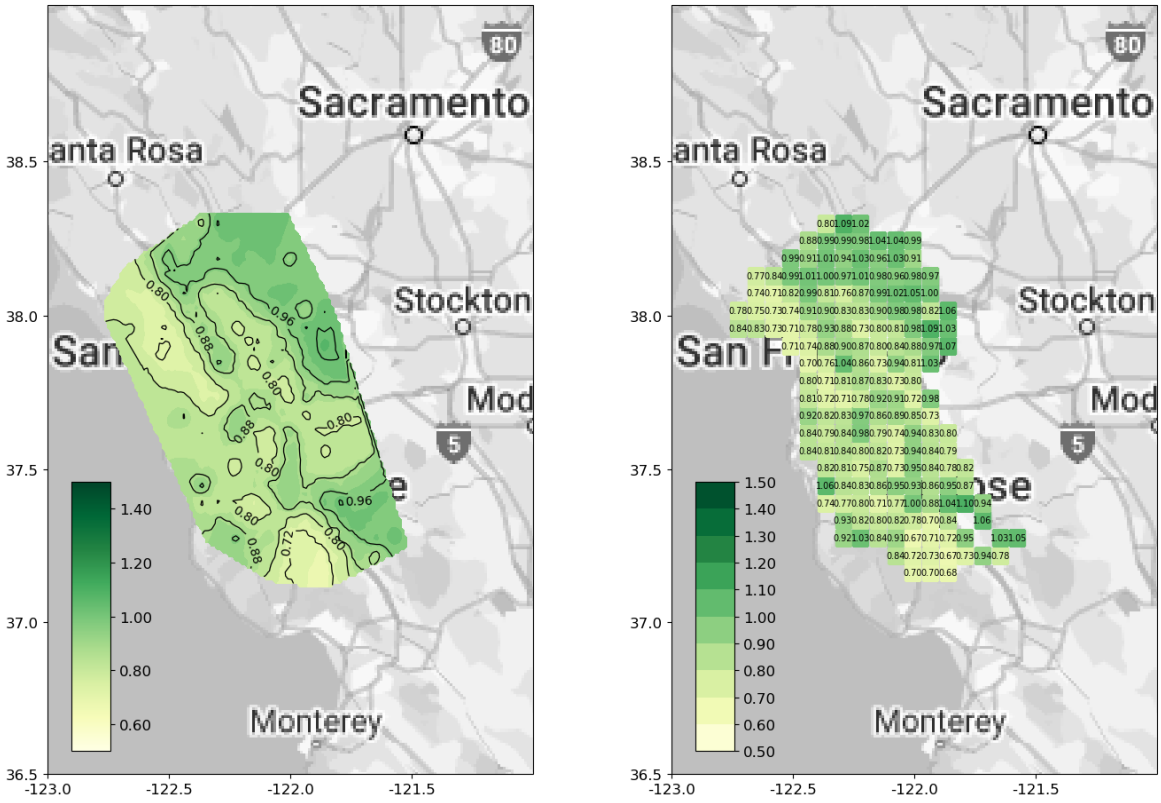

Figure 8-30 φ_L for Bay Area, 975-yr, Site Class C

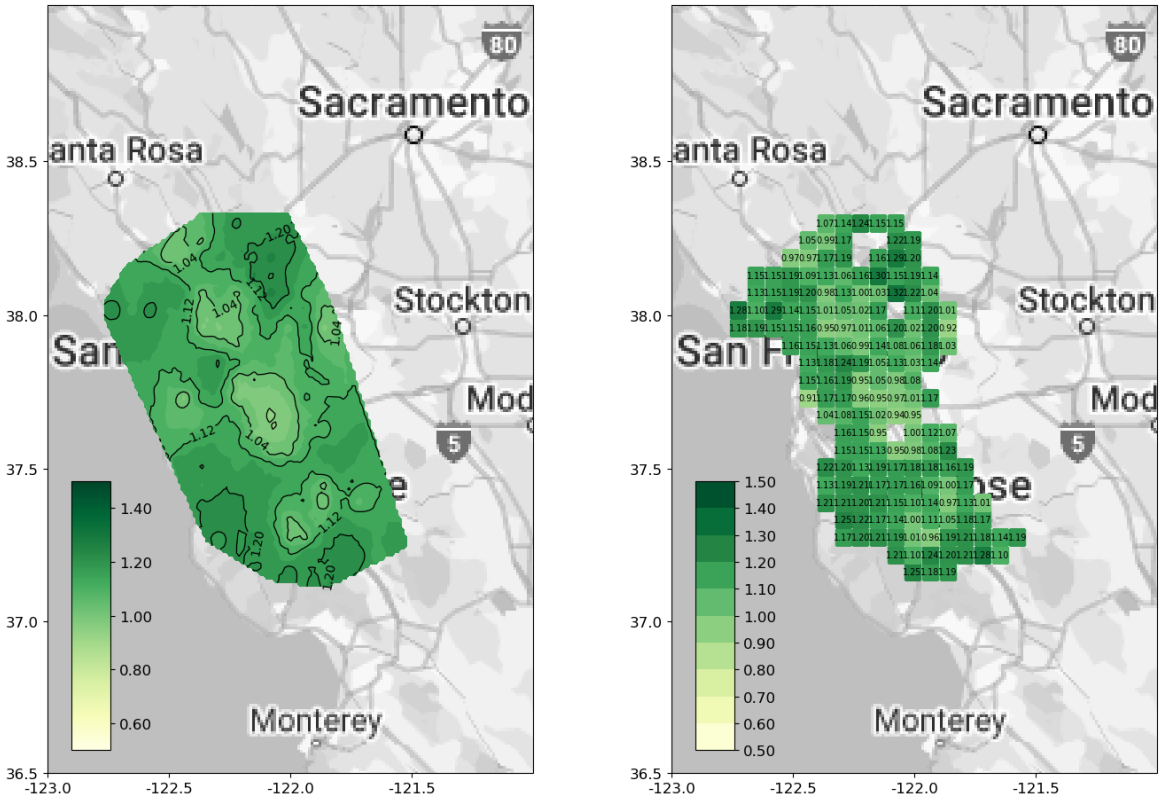

Figure 8-31 φ_L for Bay Area, 2475-yr, Site Class C

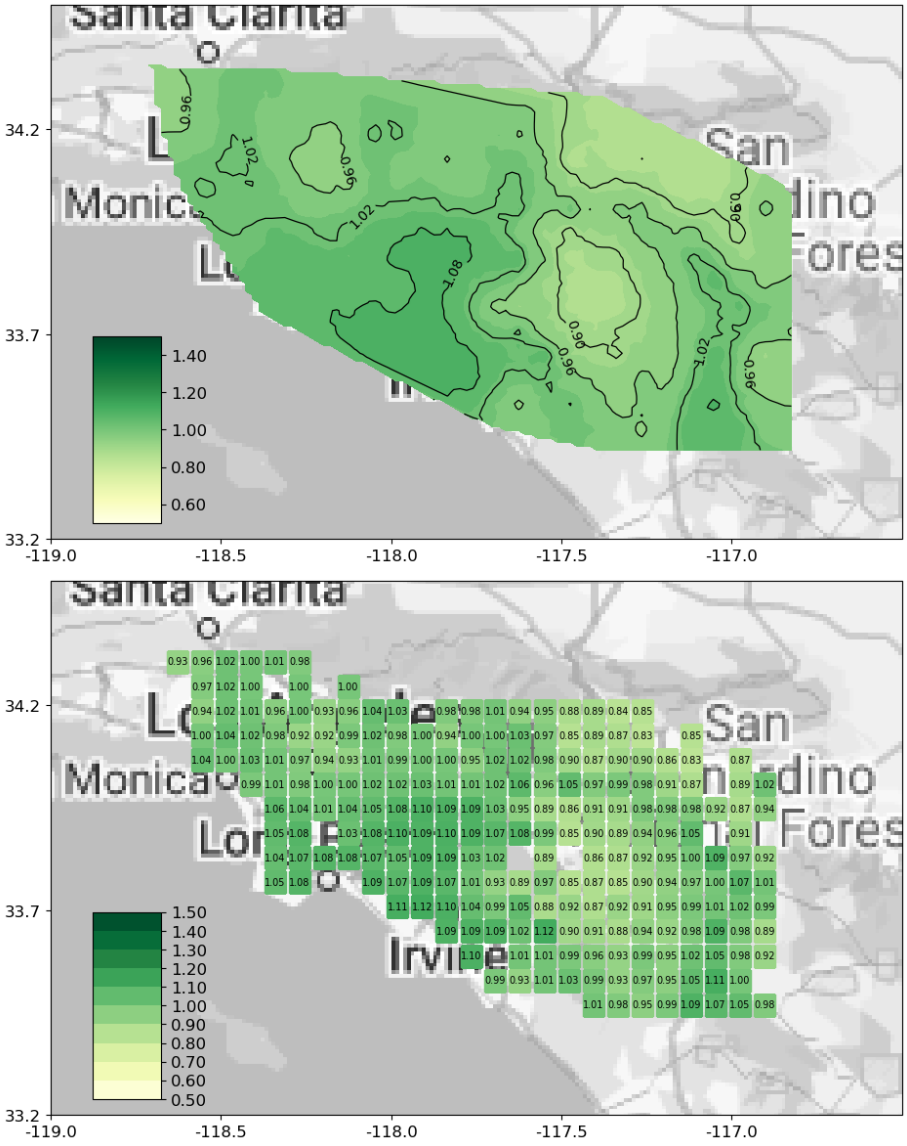

Figure 8-32 φ_L for LA Area, 225-yr, Site Class D

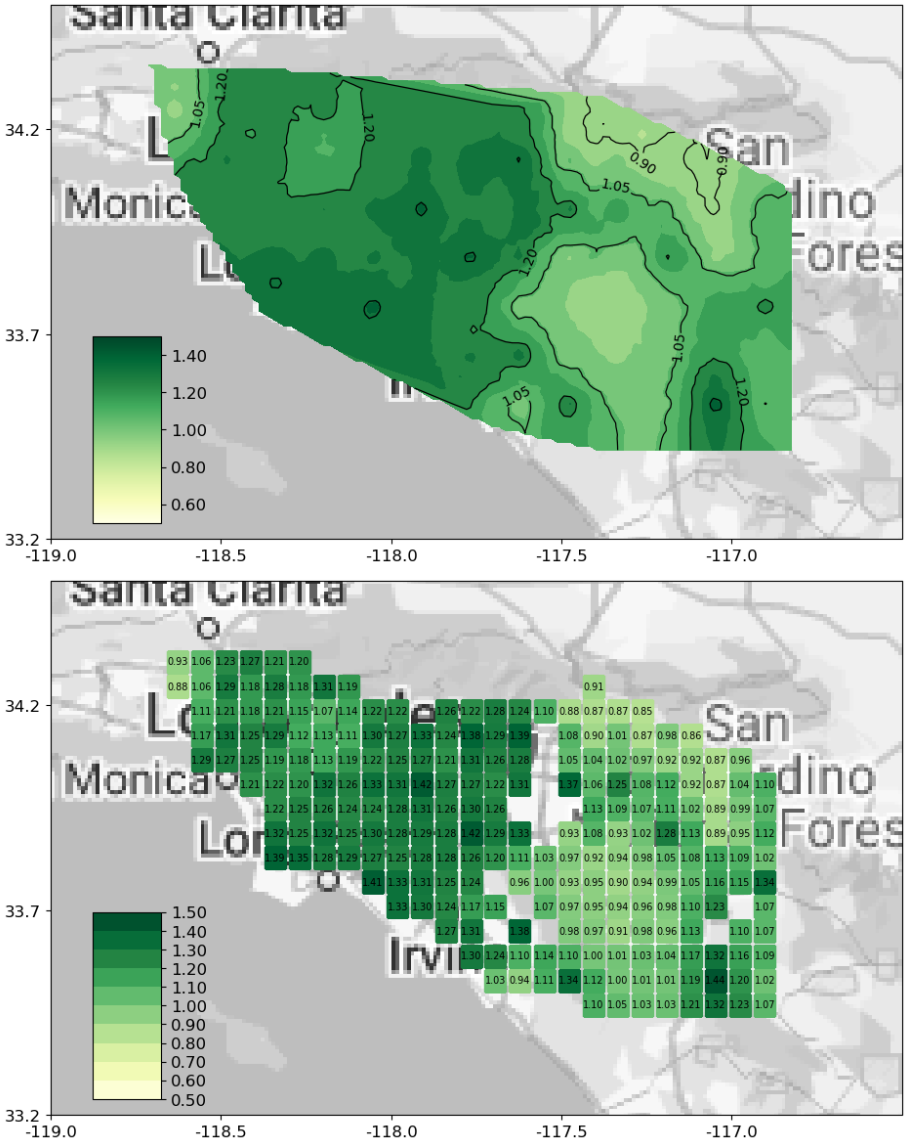

Figure 8-33 φ_L for LA Area, 975-yr, Site Class D

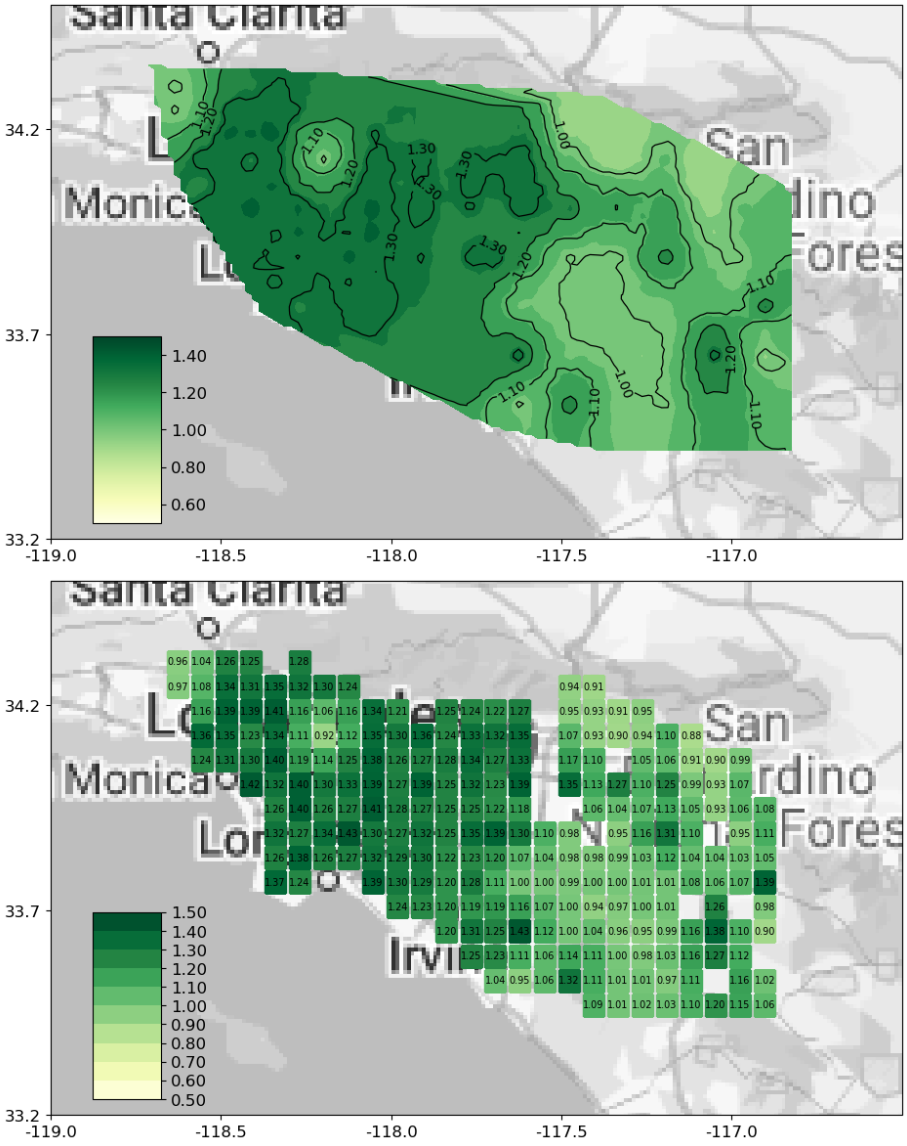

Figure 8-34 φ_L for LA Area, 2475-yr, Site Class D

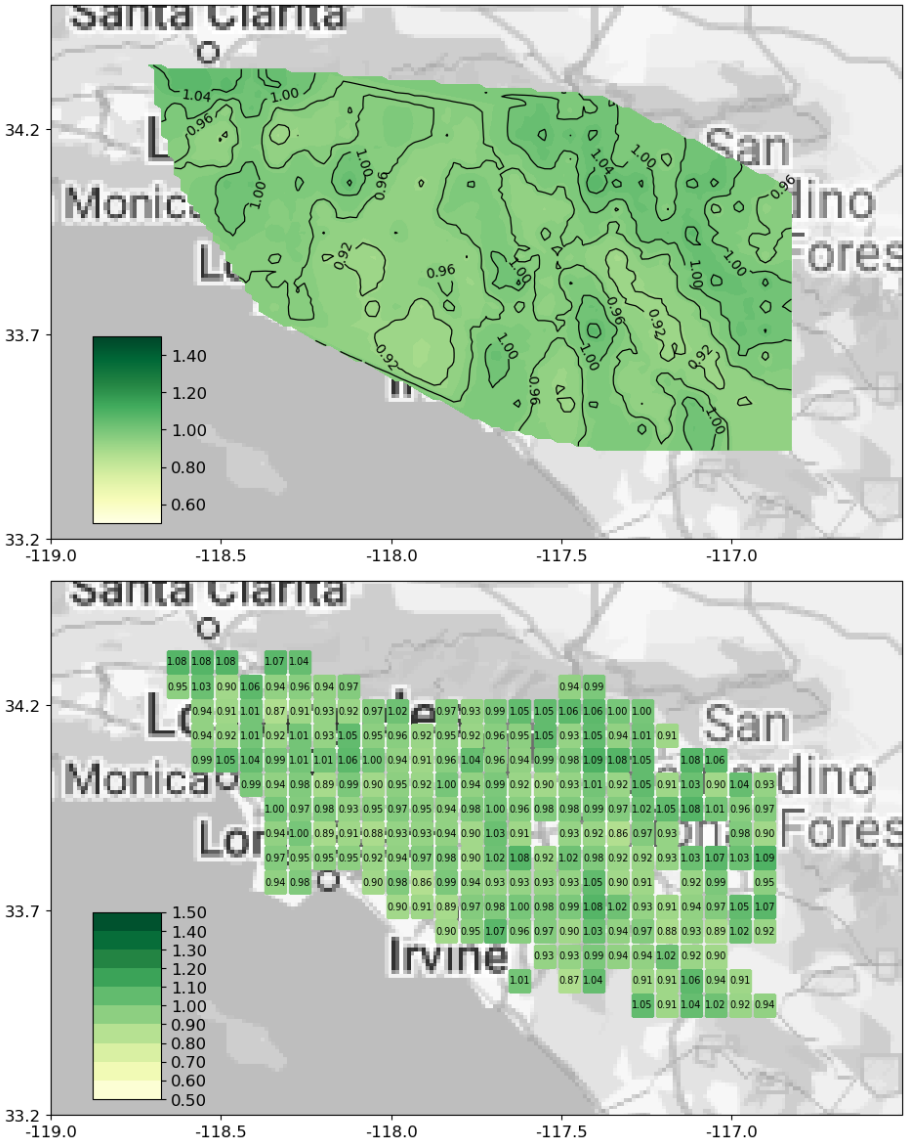

Figure 8-35 φ_L for LA Area, 225-yr, Site Class C

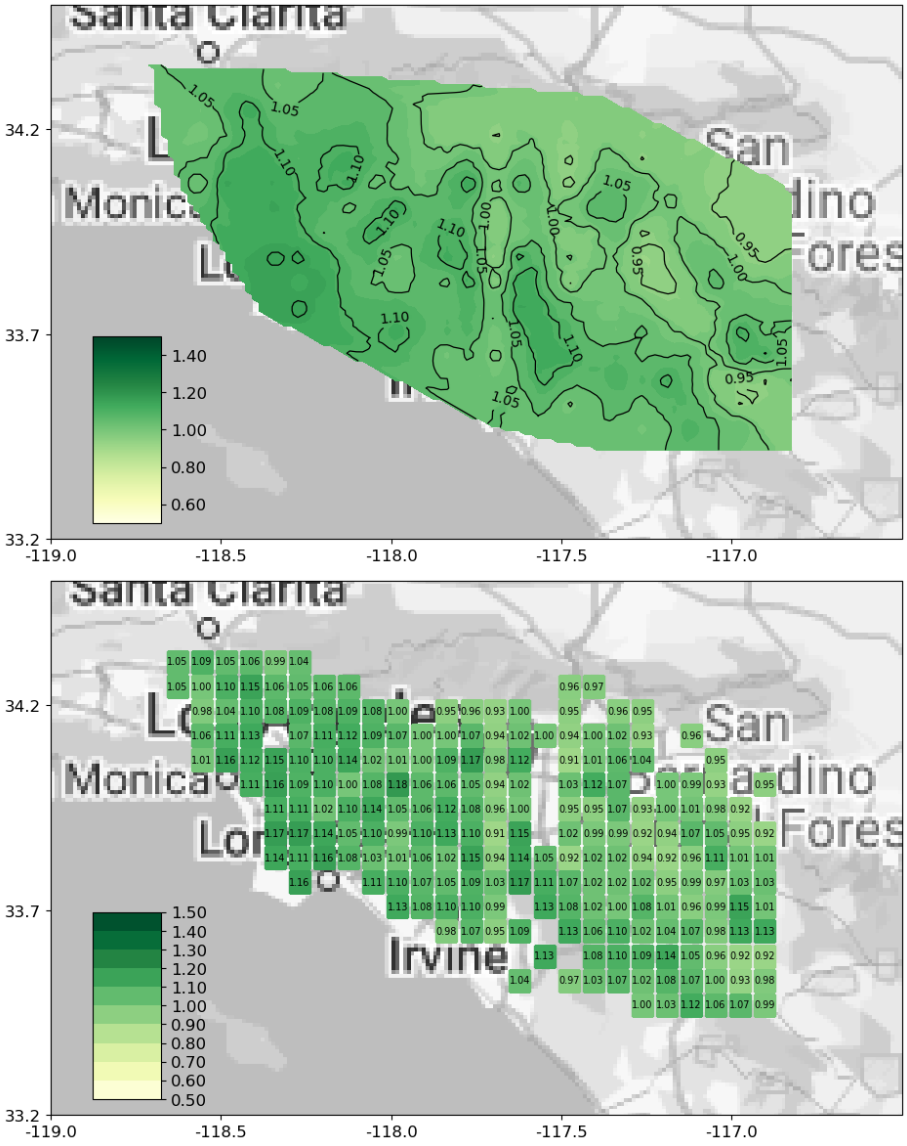

Figure 8-36 φ_L for LA Area, 975-yr, Site Class C

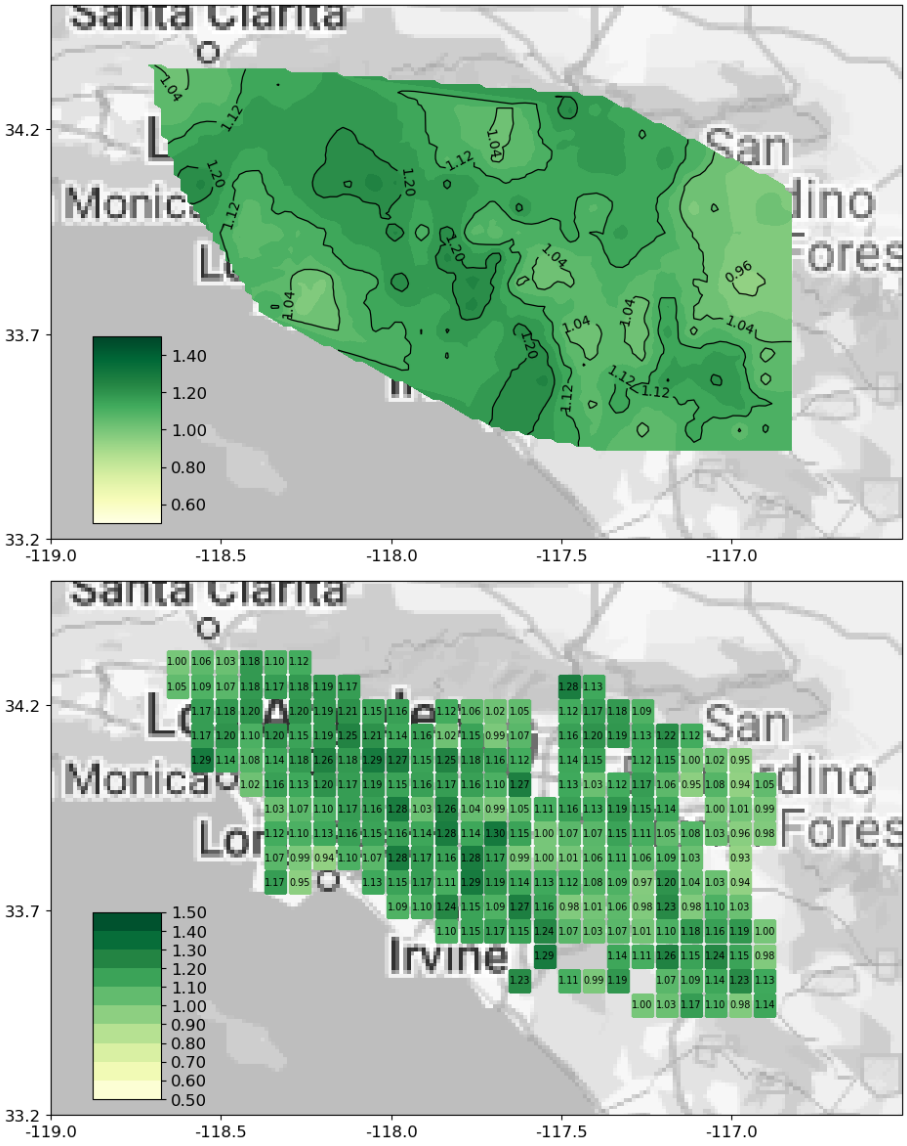

Figure 8-37 φ_L for LA Area, 2475-yr, Site Class C

REFERENCES

AASHTO (2017) AASHTO LRFD Bridge Design Specifications. 8th Edition, American Association of State Highway and Transportation Officials, Washington DC.

Abrahamson, C., Shi, M., & Yang, B. (2016). Ground-motion prediction equations for Arias intensity consistent with the NGA-West2 ground motion models, PEER 2016/05 Report.

Abrahamson, N. A., & Bhasin, S. (2020). Conditional ground-motion model for peak ground velocity for active crustal regions. Journal of Earthquake Engineering.

Abrahamson, N. A., Silva, W. J., & Kamai, R. (2013). Update of the AS08 ground-motion prediction equations based on the NGA-West2 data set. Pacific Earthquake Engineering Research Center.

American Association of State Highway and Transportation Officials. (2017). AASHTO LRFD Bridge Design Specifications, 8th Edition.

Baker, J. W., & Jayaram, N. (2008). Correlation of spectral acceleration values from NGA ground-motion models. Earthquake Spectra, 24(1), 299-317.

Bozorgnia, Y., Abrahamson, N. A., Atik, L. A., Ancheta, T. D., Atkinson, G. M., Baker, J. W., & Youngs, R. (2014). NGA-West2 research project. Earthquake Spectra, 30(3), 973-987.

Caltrans .(2019). Seismic Design criteria for bridges. Version 2.0.

Campbell, K. W., & Bozorgnia, Y. (2014). NGA-West2 ground motion model for the average horizontal components of PGA, PGV, and 5% damped linear acceleration response spectra. Earthquake Spectra, 30(3), 1087-1115.

Chiou, B. S. J., & Youngs, R. R. (2014). Update of the Chiou and Youngs NGA model for the average horizontal component of peak ground motion and response spectra. Earthquake Spectra, 30(3), 1117-1153.

Dabaghi, M. N. (2014). Stochastic modeling and simulation of near-fault ground motions for performance-based earthquake engineering. University of California, Berkeley.

Hamburger, R. O., Rojahn, C., Heintz, J., & Mahoney, M. G. (2012, September). FEMA P58: Next-generation building seismic performance assessment methodology. In 15th world conference on earthquake engineering (Vol. 10, No. 10).

Krawinkler, H., and Miranda, E. (2006). Performance-based earthquake engineering. Chapter 9: *Earthquake engineering: From engineering seismology to performance-based engineering*, Y. Borzognia and V. Bertero, eds., 1st Ed., CRC, Boca Raton, FL, 9-1–9-59.

Kaklamanos, J., Baise, L. G., & Boore, D. M. (2011). Estimating unknown input parameters when implementing the NGA ground-motion prediction equations in engineering practice. Earthquake Spectra, 27(4), 1219-1235.

Lehman, D. E., & Moehle, J. P. (1998). Seismic Performance of Well-Confined Concrete Bridge Columns, PEER Report 1998-01. Pacific Earthquake Engineering Research Center, University of California, Berkeley, CA.

Lin, T., Harmsen, S. C., Baker, J. W., & Luco, N. (2013). Conditional spectrum computation incorporating multiple causal earthquakes and ground-motion prediction models. Bulletin of the Seismological Society of America, 103(2A), 1103-1116.

Mackie, K. R., & Stojadinović, B. (2007). Performance-based seismic bridge design for damage and loss limit states. Earthquake engineering & structural dynamics, 36(13), 1953-1971.

Macedo, J., Abrahamson, N., & Liu, C. (2021). New scenario-based cumulative absolute velocity models for shallow crustal tectonic settings. Bulletin of the Seismological Society of America, 111(1), 157-172.

Mander, J. B., Priestley, M. J., & Park, R. (1988). Theoretical stress-strain model for confined concrete. Journal of Structural Engineering, 114(8), 1804-1826.

McKenna, F., Scott, M. H., & Fenves, G. L. (2010). Nonlinear finite-element analysis software architecture using object composition. Journal of Computing in Civil Engineering, 24(1), 95-107.

Nowak, A. S., and Collins, K. R. (2000). Reliability of Structures. McGraw-Hill, New York.

Petersen, M. D., Shumway, A. M., Powers, P. M., Mueller, C. S., Moschetti, M. P., Frankel, A. D., ... & Zeng, Y. (2020). The 2018 update of the US National Seismic Hazard Model: Overview of model and implications. Earthquake Spectra, 36(1), 5-41.

Petersen, M. D., Moschetti, M. P., Powers, P. M., Mueller, C. S., Haller, K. M., Frankel, A. D. & Olsen, A. H. (2015). The 2014 United States national seismic hazard model. Earthquake Spectra, 31, S1-S30.

Petersen, M. D., Frankel, A. D., Harmsen, S. C., Mueller, C. S., Haller, K. M., Wheeler, R. L., ... & Rukstales, K. S. (2008). Documentation for the 2008 update of the United States national seismic hazard maps (No. 2008-1128). US Geological Survey.

Porter, K. A. (2003, July). An overview of PEER's performance-based earthquake engineering methodology. In Proceedings of ninth international conference on applications of statistics and probability in civil engineering (pp. 1-8).

Ruiz-García, Jorge, and Eduardo Miranda. "Inelastic displacement ratios for evaluation of existing structures." Earthquake Engineering & Structural Dynamics 32, no. 8 (2003): 1237-1258.

Saini, A., & Saiidi, M. (2014). Probabilistic damage control approach for seismic design of bridge columns. California Department of Transportation.

Shantz, T., & Merriam, M. (2009). Development of the Caltrans deterministic PGA map and Caltrans ARS online.

Shahi S.K., Baker J.W. (2011). An empirically calibrated framework for including the effects of near-fault directivity in probabilistic seismic hazard analysis, Bull. Seismol. Soc. Am., 101(2):742-755.

Silva, W. J., Abrahamson, N., Toro, G., & Costantino, C. (1997). Description and validation of the stochastic ground motion model. Submitted to Brookhaven National Laboratory, Associated Universities, Inc. Upton, New York.

Vosooghi, A., & Saiidi, M. S. (2012). Experimental fragility curves for seismic response of reinforced concrete bridge columns. ACI Structural Journal, 109(6), 825.

Wills, C. J., Gutierrez, C. I., Perez, F. G., & Branum, D. M. (2015). A Next Generation V_{S30} Map for California Based on Geology and Topography: A Next Generation V_{S30} Map for California Based on Geology and Topography. Bulletin of the Seismological Society of America, 105(6), 3083-3091.

Wills, C. J., Weldon II, R. J., & Bryant, W. A. (2008). California fault parameters for the National Seismic Hazard Maps and Working Group on California Earthquake Probabilities 2007 (No. 2007-1437-A). US Geological Survey.

Yoon, Y.H., Ataya, S., Mahan, M., Malek, A., Abrahamson, N., Zokaie, T., Ong, R. and Ahmed, A., 2022. Total risk model and loss analysis of probabilistic damage control application in seismic design of highway bridges. Journal of Bridge Engineering, 27(5), p.04022020.

Yoon, Y. H., Ataya, S., Mahan, M., Malek, A., Saiidi, M. S., & Zokaie, T. (2019). Probabilistic Damage Control Application: Implementation of performance-based earthquake engineering in seismic design of highway bridge columns. Journal of Bridge Engineering, 24(7), 04019068.

APPENDIX A AMPLIFICATION FACTORS AND ACCELERATION SPECTRUM TOOLS

The Seismic Design Criteria (SDC 2.0) by Caltrans incorporates Near-Fault and Basin factors as additional amplifications to the design spectral acceleration, which is initially estimated using the USGS Unified Hazard Tool. This same amplification methodology and hazard spectrum estimation are implemented in ARS Online (Version 3.0.2), a tool developed by Caltrans for use by bridge designers. SDC 2.0 recommends using Caltrans' ARS Online tool to estimate spectral acceleration for bridge design in accordance with seismic hazard analysis. However, the ongoing CT-RBSD study does not apply this hazard amplification approach and instead relies solely on spectral acceleration values produced directly by the USGS tool (i.e., without any additional amplification). This research investigates the root causes of this methodological disparity, analyzes its implications for the CT-RBSD study, and provides recommendations to enhance the inclusion of near-fault and basin effects within the study framework..

Amplification factors in ARS Online tool and USGS tool

The ARS Tool was first released in 2008 following the introduction of the USGS 2008 National Seismic Hazard Model (NSHM) maps and the corresponding USGS Hazard Tool. It was later updated to the ARS Online tool (v3.0.2) (https://arsonline.dot.ca.gov/) after the release of the USGS 2014 NSHM.

As documented by Shantz et al. (2009), the ARS tool was developed to provide Caltrans engineers with spectral acceleration estimates based on probabilistic seismic hazard analysis (PSHA), enabling them to evaluate bridge performance over its lifespan. The tool generates spectral acceleration values along with near-fault factors, basin factors, and spectral acceleration estimates from the USGS Unified Hazard Tool (2014). The USGS Unified Hazard Tool (UHS) (2014) (https://earthquake.usgs.gov/hazards/interactive/) is an update to the 2008 USGS Hazard Tool and incorporates the latest 2014 NSHM maps for seismic hazard estimation.

Near-Fault amplification factor

The ARS tool calculates the near-fault amplification factor based on the mean rupture distance (R_{mean}) obtained for the 1-second spectral period and a 975-year return period hazard. When provided with location coordinates (latitude, longitude) and the expected shear-wave velocity at 30m depth (V_{S30}), the ARS tool connects to the USGS Unified Hazard Tool (UHS) to retrieve the hazard spectrum for acceleration and the corresponding mean source-to-rupture distance (R_{mean}).

Using this mean rupture distance, the ARS tool applies an amplification factor to each spectral acceleration value based on the criteria defined in SDC 2.0. Specifically, SDC 2.0 recommends a 20% increase in spectral acceleration for sites where R_{mean} is less than 15 km and the spectral period exceeds 1 second. This amplification gradually tapers off to zero for sites with R_mean greater than 25 km and for spectral periods of 0.5 seconds or less (Figure A-1).

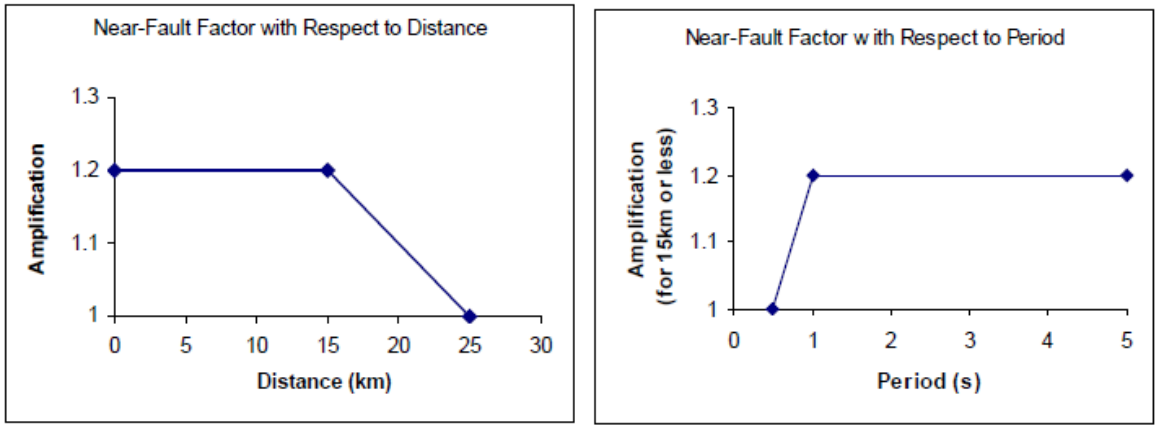

Figure A-38 Near-Fault Amplification Factor in SDC2.0 (Caltrans 2019)

Basin amplification factor

The ARS tool calculates the basin amplification factor by averaging amplification factors from two Ground Motion Models (GMMs)—Campbell-Bozorgnia 2013 (CB13) and Chiou-Young 2013 (CY13). These factors are based on the basin depths (Z1.0 or Z2.5) at a given location, which are derived from local hazard databases. For example, Caltrans' SDC 2.0 provides Z1.0 and Z2.5 contour maps for basins in Los Angeles, Ventura, and the Bay Area.

The NGA-WEST2 GMMs determine basin amplification either by using the actual basin depth or a differential basin depth, which represents the difference between the actual depth and the empirically estimated depth from the GMM. This estimation depends on the spectral period and the V_S30 value used for hazard estimation. A similar methodology is applied across multiple GMMs for estimating basin amplification.

While the ARS tool follows the GMM-recommended approach, it tends to overestimate basin amplification because it relies on only two GMMs (CB13 and CY13) rather than considering all five NGA GMMs, as specified in the 2014 NSHM documentation.

To obtain the most accurate estimate of basin amplification at a given location, field-measured shear wave velocity (V_{S30}) and basin depth (Z1.0 or Z2.5) from local velocity models should be used. However, in the CT-RBSD study, seismic demand is estimated using assumed V_{S30} values of 259 m/s and 537 m/s (termed Pseudo V_{S30}) to account for site effects in seismic hazard estimation. Combining these assumed V_{S30} values with basin depths results in inconsistent amplification estimates, rather than a realistic site-specific estimate. This suggests that assuming

a uniform V_{S30} across California does not allow for the proper incorporation of basin effects and could introduce unintended hazard inflation if an additional amplification factor were applied.

Since the 2014 NSHM maps and the 2014 USGS tool are based on 2013 GMMs, one would expect them to account for basin amplification in seismic hazard estimation. However, basin amplification was not introduced into the USGS tool until the 2018 update to the NSHM maps. Currently, a new USGS tool is under development (available as a Beta version), integrating these updated NSHM maps with basin amplification effects.

For this study, the new 2018 USGS tool (https://earthquake.usgs.gov/nshmp/) was evaluated by comparing the hazard spectra obtained from different tools. The results indicate that the USGS 2018 tool produces a hazard spectrum more consistent with expectations compared to the ARS tool. Based on this evaluation, the USGS 2018 tool is recommended for use in the CT-RBSD study. More details on this comparison are provided in the later sections.

Hazard estimation in CT-RBSD study

The ultimate goal of the CT-RBSD study is to provide seismic demand estimates in terms of COV (coefficient of variation) and a scaling factor for μ_L, specific to a given location and hazard level. The study aims to quantify variations in seismic demand by analyzing bridge column performance for the most probable earthquake events, as determined through hazard aggregation and deaggregation. Based on currently available resources, the USGS tool is the most suitable tool for identifying probable earthquake events for a given hazard level. Its aggregation and deaggregation methods rely on the widely recognized NGA-WEST2 database, providing a comprehensive list of significant earthquake events for hazard assessment. The CT-RBSD study utilizes this event list to generate ground motions using the stochastic model for ground motion generation developed by Dabaghi (2014). These simulated motions are subsequently used in Nonlinear Time History Analysis (NTHA) of bridge columns. Additionally, when generating ground motions for near-fault scenarios, the Dabaghi tool incorporates a fraction of ground motions with pulse characteristics, following the methodology of Shahi and Baker (2011).

The μ_L factor is defined as the ratio of μ_L estimated from the CT-RBSD study to the demand parameter (DI_{ESA}) obtained from the Equivalent Static Analysis (ESA) method in SDC 2.0. The CT-RBSD methodology recommends that bridge designers begin their assessment by estimating the Design DI based on the mean spectral acceleration obtained from the ARS tool. Since spectral acceleration only affects the Design DI computed via ESA—and does not alter the core properties of the bridge column (e.g., confined concrete backbone curve)**—the bridge designer has the flexibility to use either the ARS Online tool or the USGS tool to determine the Design DI. For example, a bridge column with a 6 ft diameter, 30 ft height, 1% longitudinal reinforcement, #6 hoops at 4-inch spacing, and an axial load of 10% $f'_c A_g$ will maintain the same structural properties, regardless of whether its Design DI is estimated to be 0.3 or 0.35. The Design DI serves as a reference point, allowing the bridge designer to compute the COV and Mean DI factor for the column under consideration.

Comparison of hazard spectrums from the ARS tool, 2014 USGS tool, and 2018 USGS tool

To evaluate variations in spectral acceleration hazard spectra across different tools, 16 locations across California were analyzed (Table A-1). For each location, we assessed whether near-fault and basin effects, as defined by SDC 2.0 (the same criteria used in the ARS tool), were applicable. Additionally, the in-situ shear wave velocity (V_{S30}) was determined using V_{S30} maps from the California Geological Survey (CGS), based on the work of C.J. Wills et al. (2015).

Hazard spectra for three return periods—225-year, 975-year, and 2475-year—were obtained from three tools: ARS Online (v3.0.2), the 2014 USGS tool, and the 2018 USGS tool. For a more detailed comparison, the ARS Online tool was further divided into two cases:

1. Including both near-fault and basin amplification factors
2. Considering only near-fault amplification (to isolate its effects)

The analysis was conducted for the two V_{S30}values used in the CT-RBSD study—259 m/s and 537 m/s. Among the three tools, only the 2018 USGS tool allows hazard estimation for any user-specified V_{S30}. To leverage this capability, an additional case was included where the hazard spectrum was estimated using the in-situ V_{S30} from the CGS maps. The results from all these analyses were plotted on log-log plots for comparison (Figures A-3 to A-18).

For location 10535, neither near-fault nor basin effects apply, and the in-situ V_{S30} is 552 m/s, which is close to 537 m/s, resulting in a similar hazard estimate. Consequently, we expect all three tools to yield identical spectral acceleration values for the same V_{S30} and hazard level. This hypothesis was confirmed in Figure A-4, where the hazard spectra from the three tools overlap. This also validates that the 2018 USGS tool uses the same GMMs as the 2014 USGS tool, confirming its reliability for hazard estimation.

For locations 11026 and 13290, near-fault effects are present, but basin effects are not (per SDC 2.0). At these sites, the 2018 USGS tool produces spectral acceleration values slightly higher than the 2014 USGS tool, but lower than those from the ARS tool. The difference between the 2018 USGS tool and the ARS tool is minor and can be attributed to differences in how near-fault events are accounted for in each tool.

For locations 13058, 13062, 13278, and 13281, both near-fault and basin amplification effects are present. Here, spectral acceleration values from the 2018 USGS tool closely match those from the ARS tool. However, the ARS tool produces higher spectral acceleration estimates, which is attributed to its inflated basin amplification factor. This inflation arises because the ARS tool relies on only two GMMs (CB13 and CY13), whereas the USGS tool incorporates all five NGA GMMs, following the weighting criteria outlined in the 2014 NSHM documentation.

Review Team Recommendations

The primary objective of this study is to characterize seismic demand in terms of the coefficient of variation (COV) and a median displacement demand adjustment factor, which bridge designers can use to estimate the probability of exceeding a given damage state. This is achieved by

evaluating the performance of a bridge column under the most probable earthquake events, identified through hazard aggregation and deaggregation for a specific location and hazard level.

To simulate realistic ground motions, the event parameters obtained from hazard deaggregation are used as inputs to the stochastic ground motion generation model developed by Dabaghi et al. Among the available tools, the USGS tool is the most suitable option for identifying probable earthquake events corresponding to a given hazard level. Its aggregation and deaggregation processes are based on the widely accepted NGA-WEST2 database, ensuring a comprehensive and reliable list of significant earthquake events.

While the 2014 USGS tool does not incorporate basin amplification, this feature was introduced in the updated 2018 USGS tool. Additionally, although explicit near-fault amplification factors are not applied in USGS tools, they accommodate a broader range of near-fault events in spectral acceleration estimation, capturing the effect through an increased spread of results. Furthermore, the Dabaghi ground motion generation algorithm inherently incorporates pulse-like ground motions, ensuring that higher hazard levels for near-fault events are adequately represented.

Given these considerations, the CT-RBSD team recommend continuing to use the USGS tool for hazard estimation, as it remains the most robust and appropriate option for this study.

Table A-1 Evaluated Location Across California to Assess Basin Amplification Factors

LID	Latitude	Longitude	In-Situ V_{S30} (m/s)	Near Fault Effect from SDC2.0 (Yes/No)	Basin Effect from SDC2.0 (Yes/No)
10167	40.6838	-124.018	405	Yes	No
10535	41.4963	-122.94	552	No	No
11172	38.6932	-122.293	237	Yes	No
11031	38.1301	-121.934	341	Yes	Yes
11026	38.1301	-122.293	237	Yes	No
12455	39.1962	-122.149	623	No	No
13134	34.0671	-118.125	468	Yes	No
13129	34.0671	-118.484	416	Yes	No
13028	33.7689	-117.047	244	Yes	No
13290	34.3642	-118.484	443	Yes	No
13058	33.8883	-118.197	259	Yes	Yes
13062	33.8883	-117.909	354	Yes	Yes
13281	34.3642	-119.131	446	Yes	Yes
13278	34.3642	-119.346	392	Yes	Yes
12304	38.7492	-122.006	623	No	Yes
12109	38.243	-121.862	978	No	Yes

Figure A-39 Evaluated Location Across California to Assess Basin Amplification Factors

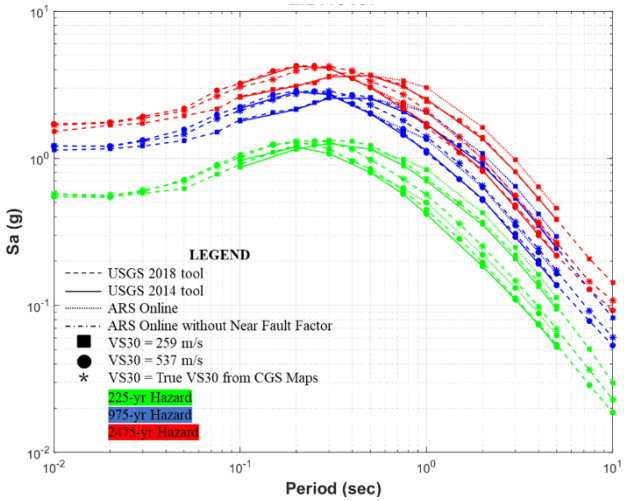

Figure A-40 UHS for Location 10167

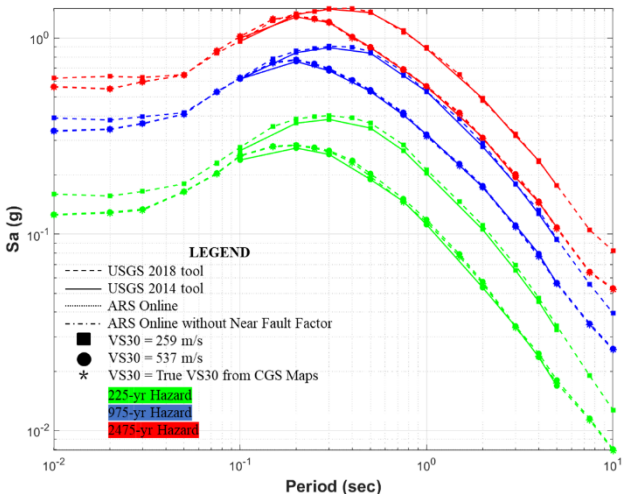

Figure A-41 UHS for Location 10535

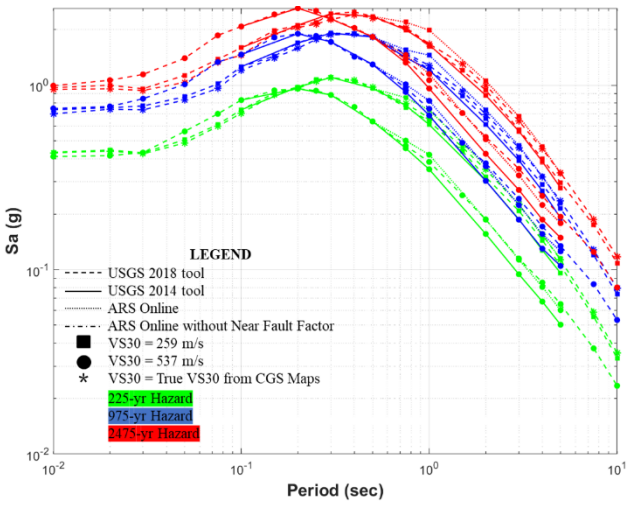

Figure A-42 UHS for Location 11026

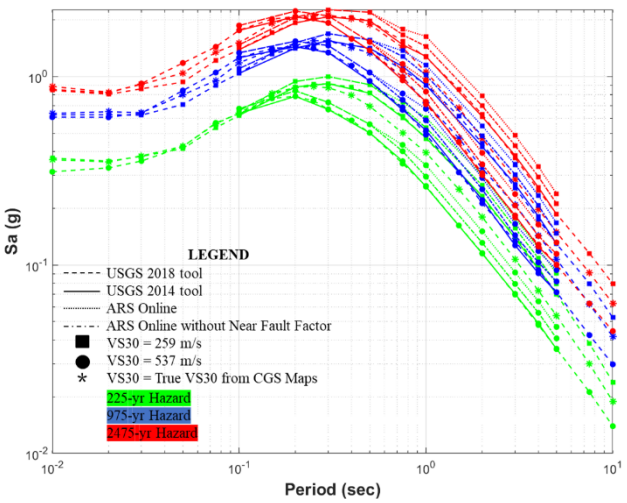

Figure A-43 UHS for Location 11031

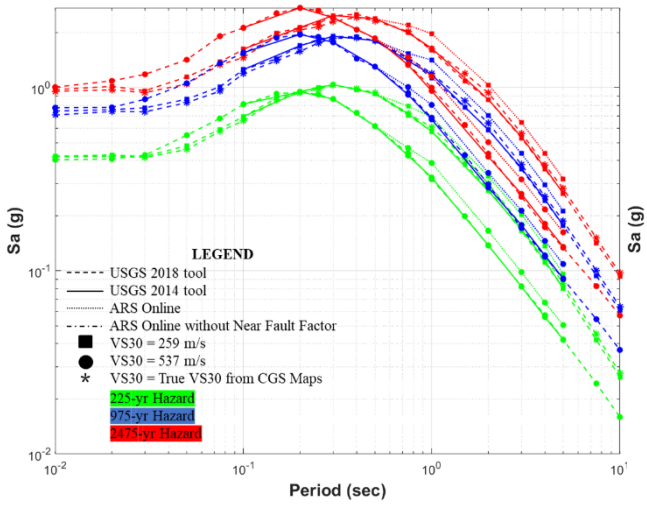

Figure A-44 UHS for Location 11172

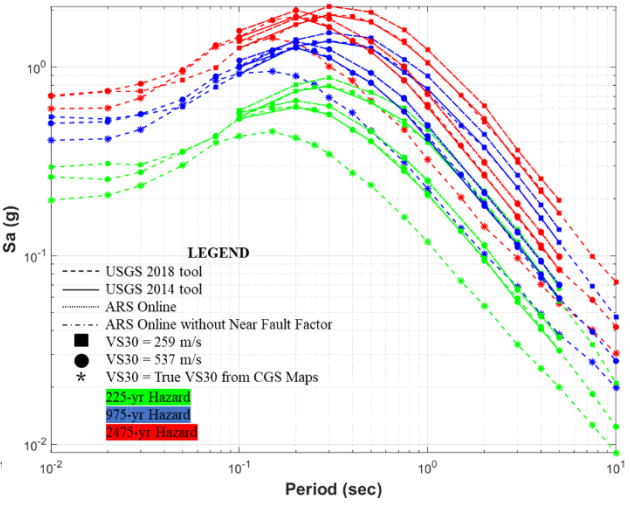

Figure A-45 UHS for Location 12109

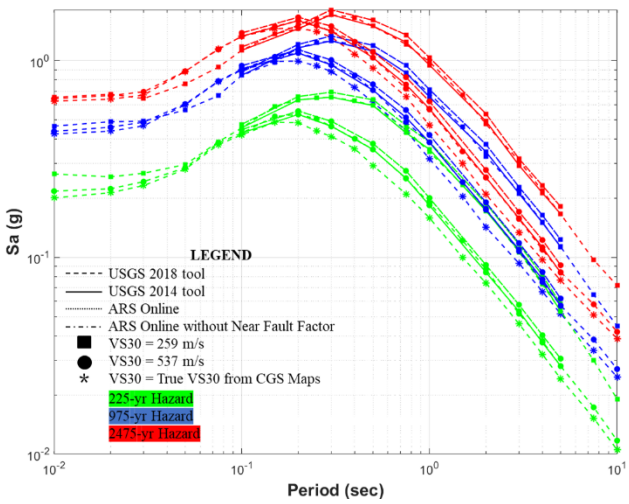

Figure A-46 UHS for Location 12304

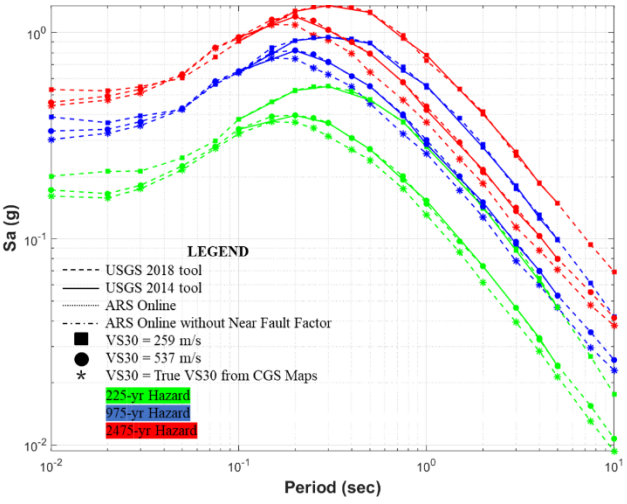

Figure A-47 UHS for Location 12455

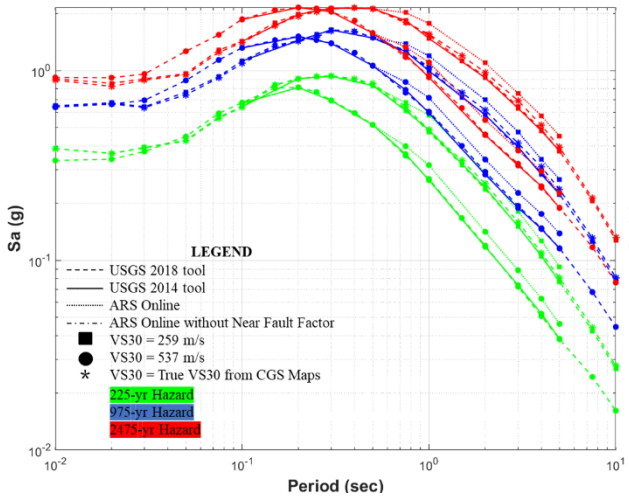

Figure A-48 UHS for Location 13028

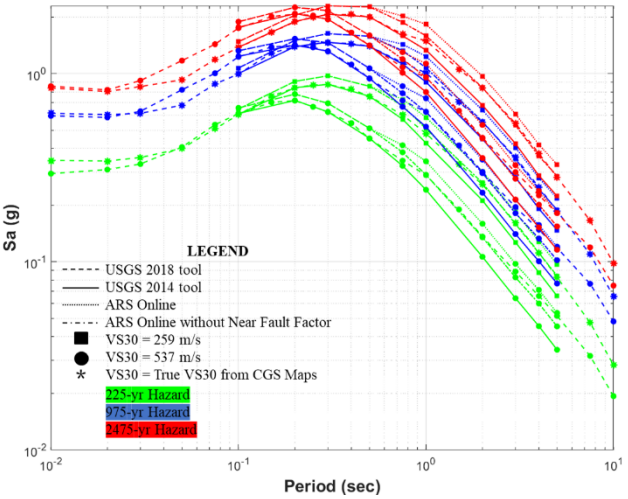

Figure A-49 UHS for Location 13058

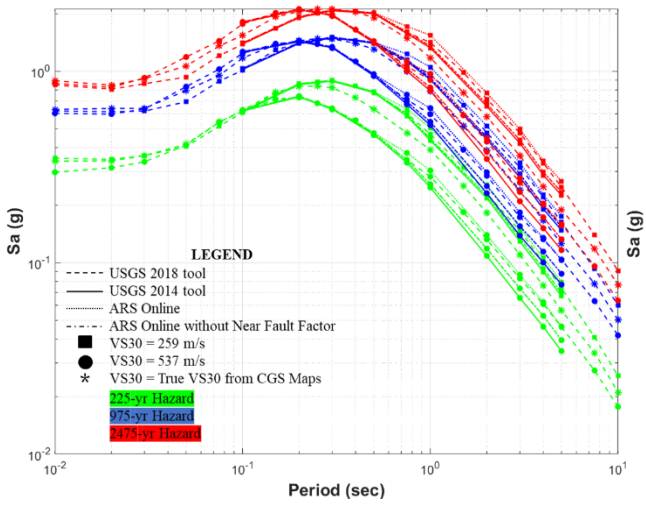

Figure A-50 UHS for Location 13062

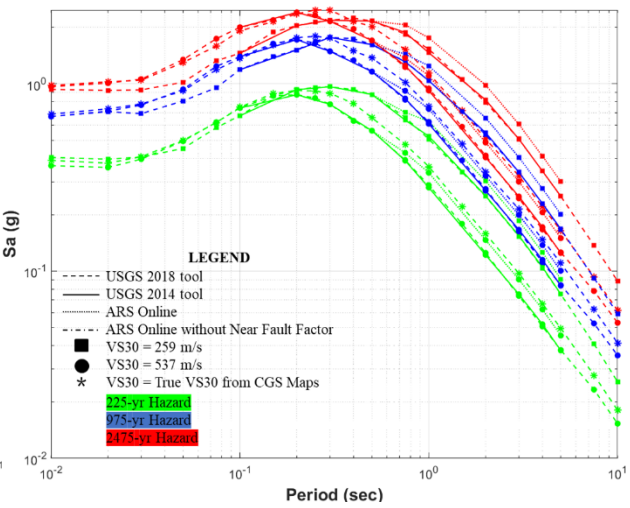

Figure A-51 UHS for Location 13129

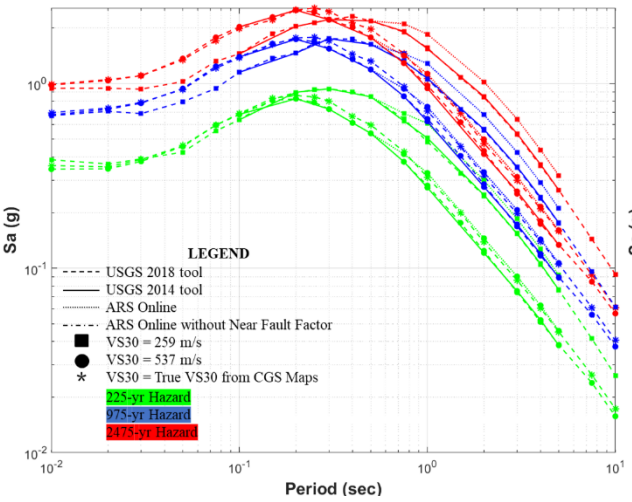

Figure A-52 UHS for Location 13134

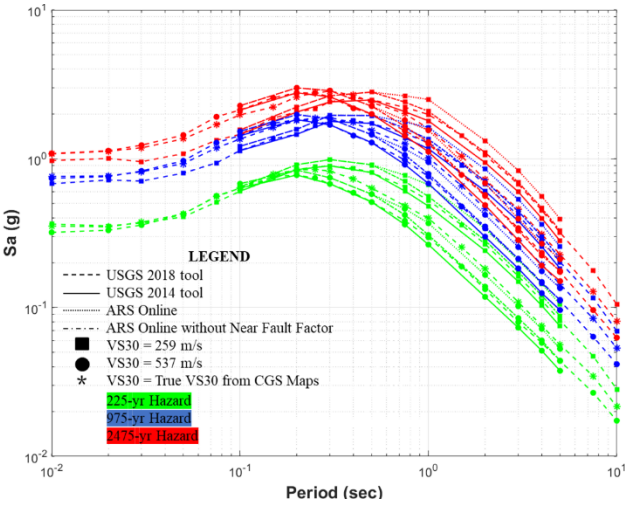

Figure A-53 UHS for Location 13278

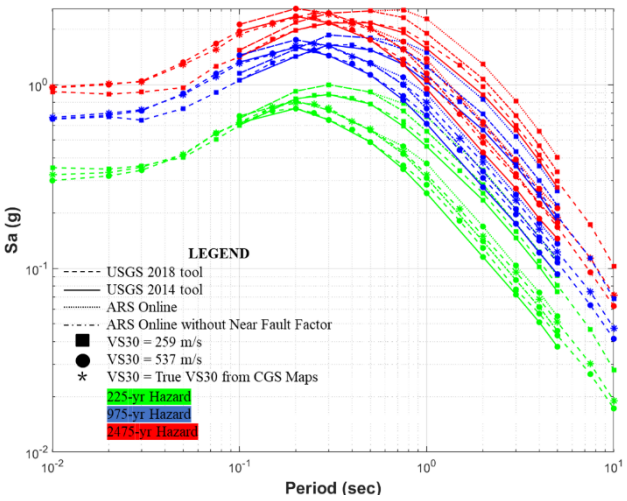

Figure A-54 UHS for Location 13281

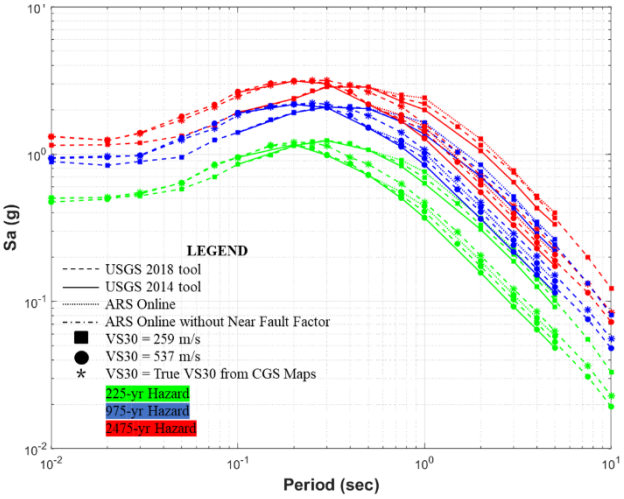

Figure A-55 UHS for Location 13290

APPENDIX B GROUND MOTION DIRECTIONALITY AND DISPLACEMENT RESPONSE

The seismic performance of a bridge is typically assessed based on its lateral deformation capacity in the transverse direction, as its movement is restrained by abutments in the longitudinal direction. This same approach is applied in seismic analysis, where the transverse response from ground motion excitation serves as the demand parameter for performance evaluation. However, the actual direction of ground movement during an earthquake is unpredictable, making it challenging to directly determine the critical displacement demand. To address this, researchers have developed a rotation-based approach, in which the two horizontal components of the ground motion are rotated at regular intervals, and the median (RotD50) or maximum (RotD100) transverse response is extracted as the displacement demand. For map generation in the CT-RBSD methodology, the displacement demand should reflect the maximum deformation the bridge might experience during an earthquake event. Therefore, RotD100 is the appropriate demand parameter to be used in this study.

In seismic bridge analysis, ground motion excitation is typically defined along two horizontal directions, denoted as X and Y (Figure B-1a), while structural responses are recorded in the longitudinal (L) and transverse (T) directions. Since the actual direction of earthquake shaking is unknown, a common approach is to rotate the two horizontal components at regular intervals and extract either the median (RotD50) or maximum (RotD100) transverse response as the displacement demand for analysis. However, in this study, the bridge model is simplified using a circular concrete column with a dead load on top, leading to uniform behavior in all horizontal directions. As a result, regardless of the rotation angle, the vector sum of the two horizontal displacements ($\overrightarrow{d_X}$ and $\overrightarrow{d_Y}$) remains constant and inherently captures the maximum response. This eliminates the need for ground motion rotation since the maximum response can be obtained directly. Instead of applying rotations, the two ground motion components can simply be assigned to the longitudinal and transverse directions, and the vector sum of the displacements can be taken as the total response ($\overrightarrow{d}$) (Equation B.1). This method provides the maximum response without additional computational steps, significantly reducing computational effort by a factor equal to the number of rotations that would otherwise be required.

$$\overrightarrow{d} = \overrightarrow{d_X} + \overrightarrow{d_Y} \tag{B.1}$$

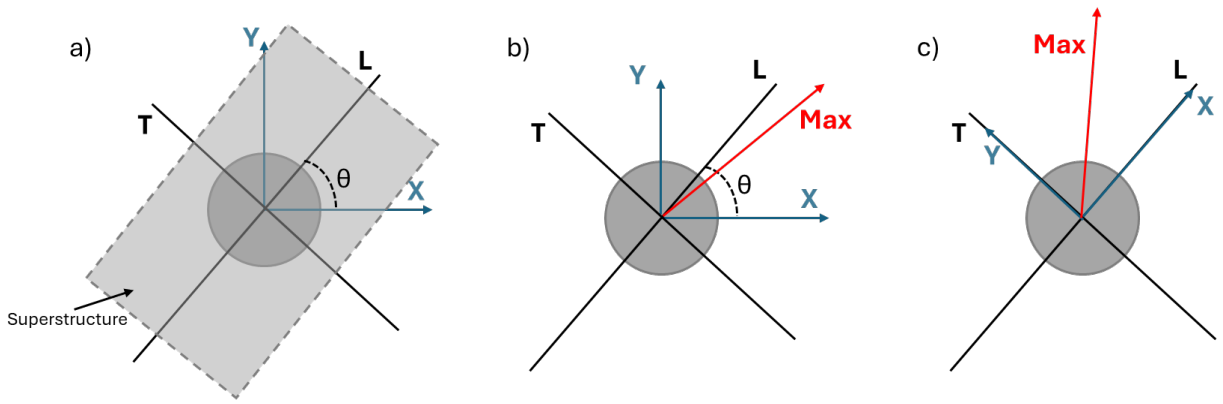

Figure B-56 Ground Motion Directivity and Model Orientation During Analysis

The proposed method was verified by extracting a specific case of a column at a given location, along with all the applicable ground motions (all hazard levels, 153 in total), from the data inventory of this study. The location and column details are provided in Table B-1, while ground motion spectrums are shown in Figure B-2.

Table B-7 Verification Locations for the Proposed Ground Motion Directionality Analysis and Associated Bridge Column Characteristics

Site Class (V_{S30})	D (259 m/s)
Latitude	40.137
Longitude	-124.018
Column Height (ft)	30
Dead Load ($\%f'_cA_g$)	5
Number of Long. Rebars	50
Long. Rebars Size	#9
Column Diameter (ft)	5
Hoop Size	#5
Hoop Spacing (in)	3
Natural Time-Period (sec)	0.8
Ultimate/Capacity Displacement (in)	30.47
Yield Displacement (in)	2.64
Design DI	0.28

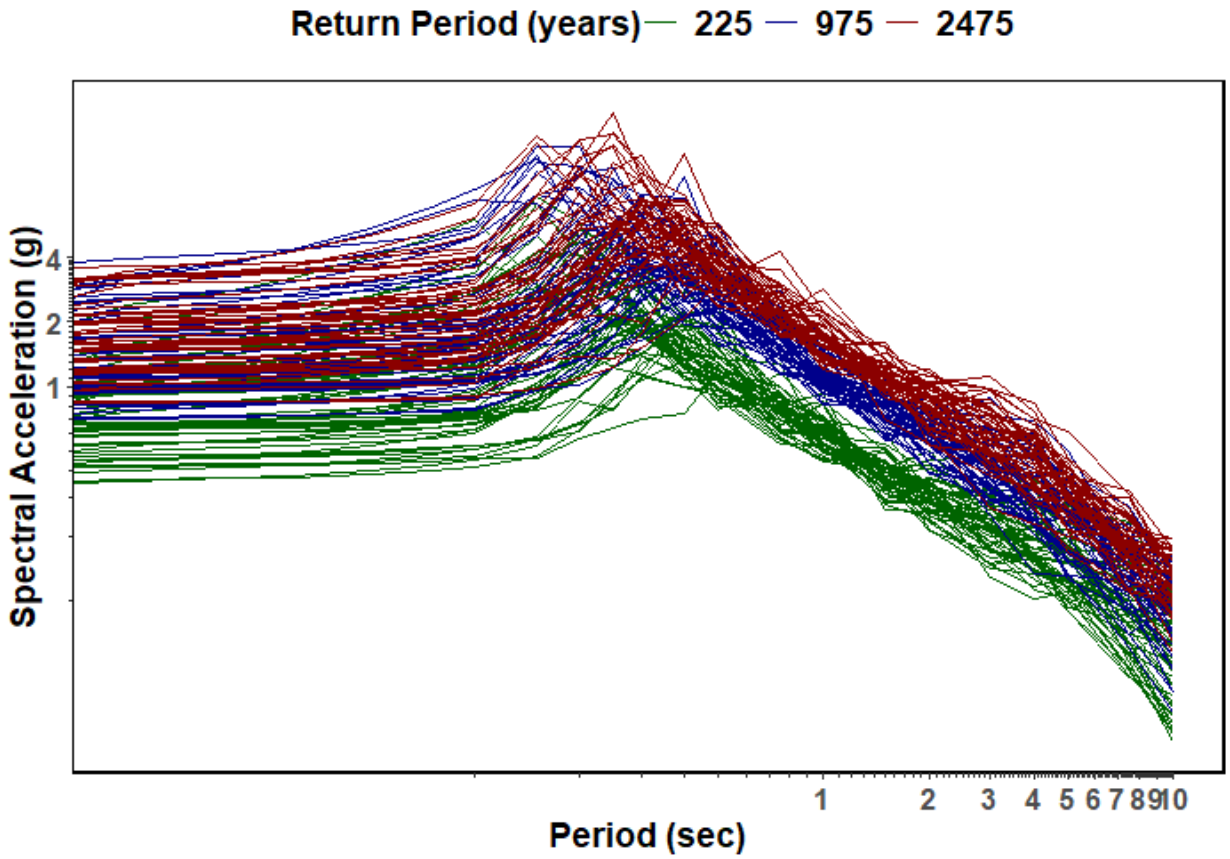

Figure B-57 Ground Motion Spectra for the Proposed Ground Motion Directionality Analysis

The OpenSees column model was analyzed individually for each ground motion, with the two horizontal components applied along the longitudinal and transverse directions, as illustrated in Figure B-1c. The two responses in terms of displacement time series were extracted in longitudinal ($\overrightarrow{d_X}$) and transverse ($\overrightarrow{d_Y}$) directions and were also combined at each time step to get the resultant vector ($\overrightarrow{d}$). The absolute maximum of each displacement time series is taken as the maximum in that direction, i.e., the maximum of $\overrightarrow{d_X}$ is $d_{X,max}$, the maximum of $\overrightarrow{d_Y}$ is $d_{Y,max}$ and the maximum of $\overrightarrow{d}$ is d_{max}. The hypothesis states that rotating the ground motion will not alter the vector sum of the two responses. To test this, the same ground motion was rotated by an angle θ, ranging from 20° to 180° in 20° increments, and the corresponding responses ($\overrightarrow{d_\theta}$, $\overrightarrow{d_{X|\theta}}$, $\overrightarrow{d_{Y|\theta}}$) were recorded following the previously outlined methodology. The maximum responses for each rotation were denoted as $d_{\max|\theta}$, $d_{X,\max|\theta}$ and $d_{Y,\max|\theta}$, respectively. To get a better perspective, $d_{\max|\theta}$, $d_{X,\max|\theta}$ and $d_{Y,\max|\theta}$ were normalized (to $\hat{d}_{\max|\theta}$, $\hat{d}_{X,\max|\theta}$ and $\hat{d}_{Y,\max|\theta}$) by dividing them with $d_{\max|\theta}$ as shown in Equations B.2 to B.4. By logic, the $\hat{d}_{\max|\theta}$ should come out to be 1, while $\hat{d}_{X,\max|\theta}$ and $\hat{d}_{Y,\max|\theta}$ would show the trend of user-interested maximum responses.

$$\hat{d}_{\max\,|\theta} = \frac{d_{\max|\theta}}{d_{\max|\theta}} \qquad (B.2)$$

$$\hat{d}_{\mathrm{X,max}\,|\theta} = \frac{d_{\mathrm{X,max}|\theta}}{d_{\mathrm{max}|\theta}} \qquad (B.3)$$

$$\hat{d}_{\mathrm{Y,max}\,|\theta} = \frac{d_{\mathrm{Y,max}|\theta}}{d_{\mathrm{max}|\theta}} \qquad (B.4)$$

The comparison between $\hat{d}_{\mathrm{max}|\theta}$, $\hat{d}_{X,\mathrm{max}|\theta}$ and $\hat{d}_{Y,\mathrm{max}|\theta}$ as a function of rotation angle is shown in Figure B-3, with each line representing a different ground motion. As expected, the $\hat{d}_{\mathrm{max}\,|\theta}$ value remains constant at 1 even when the ground motion is rotated. However, $\hat{d}_{X,\mathrm{max}|\theta}$ and $\hat{d}_{Y,\mathrm{max}|\theta}$ are observed to be less than 1 across all rotation angles, confirming that the vector sum of the two horizontal components remains unchanged regardless of the ground motion rotation.

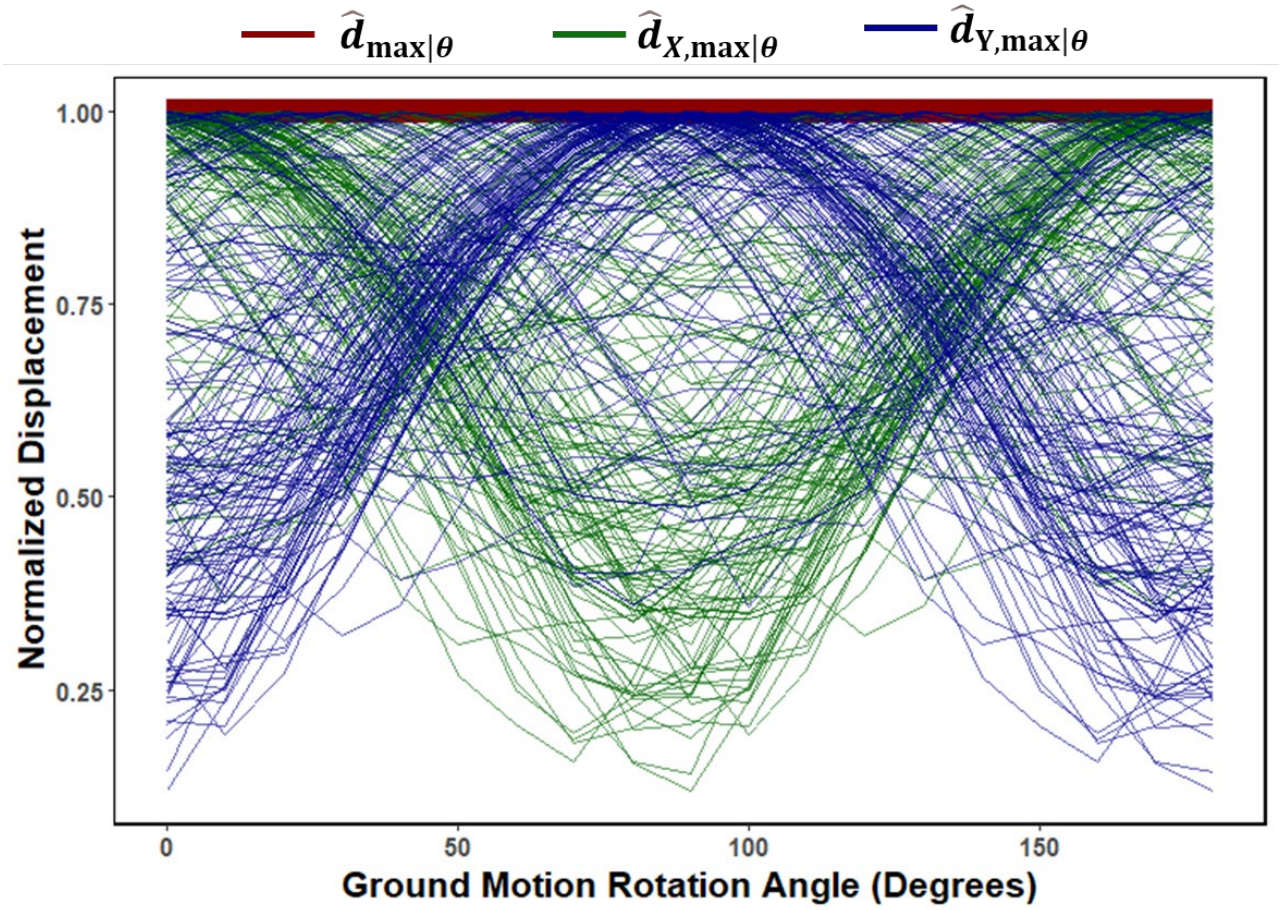

Figure B-58 Response Displacement Response vs. Ground Motion Orientation